

## Response to Editor

We would like to thank the Editor for his comments helping us to improve furthermore our paper. Below, you can find our comment-by-comment replies.

*“Thank you for your efforts in improving the initial version of your manuscript. I recommend that you submit a revised version considering the new comments made by referee #2 (see initial report #4), and the additional comments in my initial report that were not yet considered.”*

We would like to clarify that many comments (e.g. statistical significance, potential reasons of DD episodes' misclassification) from the Editor's initial report were already included in the submitted document. Here, in the revised manuscript, we have added a short text (Lines 499-505) referring to the comparison of the old (Gkikas et al., 2013) and new version (present analysis) satellite algorithm outputs versus AERONET retrievals, as it has been suggested by the Editor. This was done in order to investigate the benefits of using QA-weighted level-3 MODIS AOD data (present analysis) in contrast to non-weighted QA ones (Gkikas et al., 2013). Note that the utilization of QA-weighted MODIS retrievals constitutes an improvement of our algorithm and for this reason any possible impacts on its performance must be evaluated.

*“I share with this referee the feeling that a number of clarifications given in your reply letter in response to our comments on the initial version would be useful to the readers and need to appear in the paper itself. One example concerns your reply on the use of the cloud fraction (CF) test. The main text (line 342) still presents the use of this test as an improvement of the methodology, when your reply indicates that this filter is only performed for a sensitivity test. Please clarify.”*

The majority of the comments made by the Reviewer-4 were primarily related to the applied methodology (satellite algorithm) and secondarily to data description and are more linked to our published paper in ACP (Gkikas et al., 2013). In the submitted manuscript, despite the disagreement of many of the authors to accept all the argumentation without any cited work to back it up, we have included as many as possible of our replies, addressing issues raised by the Reviewer-4, to the text resulting thus in an extension of its length. Moreover, the extension of the manuscript parts related to the satellite algorithm and data (both discussed thoroughly in our previous papers) induces an unbalance and inhomogeneity making hard to a potential reader to focus on our primary scientific target, which is the description of dust outbreaks' vertical structure. This is clearly reflected by the fact that half of the Results section is dedicated on the relevant discussion (Sections 4.3 and 4.4). For this reason, we have selected to insert to the document the most important replies, to our opinion, and not all of them. As it concerns the second part of the Editor's comment, we agree with him and we have modified the relevant part of the manuscript accordingly (Lines: 419-424).

*“I also believe an effort must be made on the structuration of the paper which is long, trying to decrease the number of sub-titles levels. I invite you to reconsider the referee and my own initial comments on the structure of the paper. For instance, I recommend that the methodological points that I listed in my initial report are not left in the results section. For instance what concerns AERONET*

*can come in the description of AERONET data (e.g., derivation of AERONET AOD at 550nm) or in a small additional paragraph at the end of section 3 (e.g., the detection of dust episodes with AERONET data). I also follow the referee suggestion to present first in section 4 the comparisons/“evaluation” of the algorithm before going to main results on the horizontal and vertical distribution of dust episodes. For this, I think that the section 4.2 would better come as a sub-section of present section 3 or make a distinct section (4) before the Results section (5) itself. Furthermore, I suggest to have two distinct main sections discussing results, a first one (5) made of the geographical distributions (present section 4.1) with 2 sub-sections on frequencies and intensities, and a second one (6) on the vertical distribution including present sub-sections 4.3 and 4.4, the last one being presented as a series of case studies without reference to PM in its title.”*

We agree with the Editor that the length of the manuscript is long but consider that, to our opinion, we are providing the information which is required in order to support our findings helping thus the reader to follow our approach. It is evident, that the length of the text has been grown due to the inclusion of our responses to the Reviewer-4 comments as well as to the added Section 4.4 which has been suggested by the Reviewers 2 and 3. In addition, during the second round of comments, new questions have been raised by the Reviewer-4 and the inclusion of our responses to the revised document will cause a further extension of its length. Trying to compensate this, we had removed from the initial document submitted to the ACPD, three figures related to AERONET (now available in the supplementary material, Figs. S2-S4) and the obtained results are briefly (less than one page) discussed in Section 4.1.1.3. Also, we would like to point out that through the review phases (your initial report, the four reviews, your second report and the second round of reviews) we have modified the text accordingly trying to address all the reviewers' proposals which in some cases were contradictory. The most outstanding example is that the Section 4.4, suggested by the Reviewers 2 and 3, should be removed according to the opinion of the Reviewer-4.

As it concerns the structure of the paper, in the revised manuscript we have changed the order of Sections 4.1 and 4.2 as it has been proposed by the Editor. More specifically, the comparison of the satellite algorithm's outputs against AERONET/PM<sub>10</sub> comes first, then the geographical distributions of DD episodes' frequency/intensity are drawn while in Sections 4.3 and 4.4 are discussed the results for the vertical structure and the level of agreement between MODIS-PM, respectively. Nevertheless, we would like to clarify the reasons why we have not fully adopted the Editor's suggestions. We believe that is better to keep Section 3 as is since it is described the identification of the desert dust episodes based on the satellite algorithm, which is the main tool used in the present analysis. In addition, we believe that the evaluation of the satellite algorithm must be a sub-section in Results and not in a separate section since useful information, based on AERONET retrievals (e.g. volume size distribution), is provided. Moreover, we think that it is not necessary to split the section where the geographical distributions of the DD episodes' frequency and intensity are presented in two subsections in order to avoid adding new subtitles levels. As it concerns the “methodological” parts of the manuscript, we strongly believe that the existing serial order which we have decided helps the reader to understand our approach in each phase of the analysis. We are aware that this issue was raised in your initial review but still we prefer to sustain the existing structure of the paper. We believe that is quite important considering that a potential reader will not be forced to go back and forth throughout the

manuscript. For this reason, in Section 4.1.1.1 we are discussing briefly how the AERONET AOD<sub>870</sub> retrievals are converted to AOD<sub>550</sub>, through the implementation of the Ångström formula, in order to match with the corresponding MODIS data. For the same reasons, in Section 4.1.1.4 (identification of DD episodes based on AERONET), Section 4.3 (satellite algorithm – CALIOP) and Section 4.4 (specific dust cases) the reader can find all the relevant information gathered (followed methodology – obtained results). Summarizing, we think that it is a matter of personal point of view and we would like to keep ours. Our argument is also supported by the fact that the Reviewers 1-2-3 agree that the presentation of our results is clear and the paper is well structured. Finally, we have removed from the titles the PM sites' names as it has been asked by the Editor.

*“I also follow referee 2 on the fact that the PM stuff has no major input for the main purpose of this study and could be removed for shortening and better focusing the revised paper.”*

We disagree with this comment for the following reasons. The part of the manuscript referring to the comparison between satellite algorithm's outputs and PM<sub>10</sub> concentrations occupies less than 1.5 pages. This means that its omission will not reduce significantly the length of the manuscript. On the contrary, apart from the results which are presented here (success scores, dust contribution, mean and median levels) and not in Gkikas et al. (2013), thanks to this analysis we are investigating the level of agreement between columnar (MODIS) and surface-based (PM<sub>10</sub>) measurements across the Mediterranean. In a further step, the obtained results trigger the analysis which is presented in Section 4.4 where it is investigated (through the CALIOP-CALIPSO lidar retrievals) how the desert dust outbreaks' vertical distribution affects the level of agreement between columnar (MODIS AOD) and ground (PM<sub>10</sub>) observations. For the aforementioned reasons, we believe that the omission of Section 4.1.2 will cause a discontinuity, not helping us to clarify to a potential reader why/how we have selected the specific desert dust episodes which are analyzed in Section 4.4. Moreover, considering the extension of Section 3, by adding to the revised manuscript our old/new responses to the Reviewer 4, the removal of Section 4.1.2 will induce an unbalance (in terms of text length and focus) between the obtained results and the discussion about the applied methodology. In addition, if we follow the Editor's suggestion then the additional information of the present analysis with respect to Gkikas et al. (2013) will be minor to our opinion and we would like to avoid it. Of course, we can remove Section 4.1.2 from the revised manuscript just citing the obtained results from Gkikas et al. (2013) but in this case someone easily can raise a question if the aforementioned findings are similar for the extended period (almost double years) considered in the present analysis.

*“Results on the horizontal distribution need to appear in the abstract.”*

The results about DD episodes' frequency of occurrence and intensity were already appeared in the abstract. Please, see lines 32-41.

#### Other technical remarks:

*“-Fig.1 is almost identical to Fig. 2 published in the same journal by Gkikas et al. (2013). Please specify “(after Gkikas et al., 2013)” in the figure legend.”*

We have decided to remove Figure 1 from the manuscript following your initial proposal in the uploaded comment to the ACPD (1<sup>st</sup> March). In the revised manuscript, we are directing the reader to Figure 2 (in Gkikas et al., 2013) where the flowchart of our methodology is depicted.

*“-Please check the systematic use of the italic style for abbreviations, especially SSA and AOD.”*

We have changed to italic format all the SSA and AOD abbreviations.

*“-add missing doi numbers in the reference list (especially verify J. Geophys. Res. papers).”*

We have added the doi numbers which were missing from the reference list.

*“-Abbreviate “Remote Sens. Lett.” in line 1189, “Ocean.” in line 1347, “Technol.” in lines 1400, 1463 and 1609, “Trans. Inst. Br. Geogr.” in lines 1433-1434, and “Adv. Meteorol.” in lines 1442-1443.”*

Done.

*“-Also check missing or incorrect journal name in the references Matthias et al., 2004 (“J. Geophys. Res.”), and Papayannis et al., 2014 (“Sci. Total Environ., 500-501,”...); check also the spelling of the 2nd author “Nicolae” in Papayannis et al., 2014.”*

Done.

*“-no italic in line 1521.”*

Done.

## Response to Reviewer-4

We would like to thank the Reviewer for his/her second round of comments, which we tried to take into account in order to further revise and improve our manuscript. Our responses (in regular format) to the comments (in italic format) are listed below.

### General

*“Many answers to my questions are given as ‘reply to the reviewer’, but not (or only partly) inserted into the body of the manuscript itself. It was obviously the intent of my revision to provide hints to strengthen the manuscript, and make it more legible. I did not need ‘personal’ answers, my comments were rather oriented to make the authors provide any potential reader with all the needed/useful information and to show/demonstrate the robustness of the methodology proposed to achieve the results. Thus, some of my comments were not fully understood/addressed in the text and this intent of mine was therefore not achieved within the revised version submitted. My personal impression in reading the revised version is that all the efforts done by the authors in revising the text translated at last into some additional material inserted within the original manuscript in a rather ‘patchy’ way, with no substantial improvement of its structure and no real embedding of the given suggestions in its core concept. The overall result is a long text, focusing on (too) many different aspects. The authors should make an effort to decide which is the core objective of the manuscript and limit the length of the other sections. Some suggestions on which parts could be removed (and possibly addressed in a companion study) were already given in my first review, and are further indicated below.”*

First of all, we would like to kindly remind that this Reviewer is and has been not solely reviewing our manuscript, and that there are and have been three others. Thus, our revision was based on the comments of all of them, which not always were in line with this Reviewer comments. This could at least partly respond the Reviewer’s statements referring to the improvement and re-structure of the paper according to his/her indications. In addition, we would also like to kindly remark that our responses in the previous round and the associated modified manuscript were not supposed to just show that every comment of this Reviewer has been adopted and inserted in the manuscript; it is our opinion that this is an important principle in the review/revision procedure of a paper. Of course, we believe that whenever responding to a Reviewer comments, authors must show that all of them are considered, not just adopted, while efforts should be made to either implement them in the revised manuscript when adopted or appropriate replies and arguments are given in the answer when not endorsed.

In this line, we believe that we have made a strong effort to give detailed answers to all of the Reviewer’s questions and to insert as many as possible of them to the revised manuscript. However, we also took care not to extend the paper length with information that is either already provided in our previous papers or it is not critical, to our opinion, for a potential reader. We would like to remind the employed methodology in this paper does not appear for the first time but has been introduced to a few previous evaluated and published papers in other ISI journals or to ACP.

The majority of the Reviewer's comments in his/her first report were mainly focused on the applied methodology (satellite algorithm) and to the data description. Trying to address and implement the Reviewer's old and current raised issues we were and still are forced to extend the aforementioned parts of the manuscript, sometimes risking to make it probably unbalanced and inhomogeneous. If we are to follow the Reviewer's suggestion to remove from the paper the PM analysis as well as Section 4.4 (which has been suggested by the Reviewers 2 and 3) then indeed the length of the paper would be shortened, but on the other hand this may result in a much similar paper with that by Gkikas et al., (2013) and focused on discussing issues related to the applied methodology. This was/is not the main objective of this paper, in which we really intend to improve our methodology but also emphasize the vertical structure of the Mediterranean desert dust outbreaks. According to this strategy, first an analysis is undertaken to ensure that the satellite algorithm's outputs are reliable, also highlighting the possible differences between the current geographical distributions and the corresponding ones obtained by Gkikas et al. (2013). Next, the CALIOP vertical resolved dust retrievals are used to investigate the Mediterranean dust outbreaks' annual and seasonal characteristics (in Section 4.3) as well as to give a better insight of how the vertical distribution of dust loads affects the level of agreement between columnar (MODIS) and ground (PM<sub>10</sub>) measurements (in Section 4.4). We believe that the present manuscript is organized in the best possible way to fulfill the afore-mentioned priorities in this paper.

More specific answers to the Reviewer's comments referring to methodological and datasets problems, as well as to the presentation of results are given below. As it has been mentioned above, we have decided to sustain the PM<sub>10</sub> analysis as well as Section 4.4 in the revised document in contrast to the Reviewer's suggestion for the reasons which will be discussed later.

## **1. METHODOLOGICAL PROBLEMS**

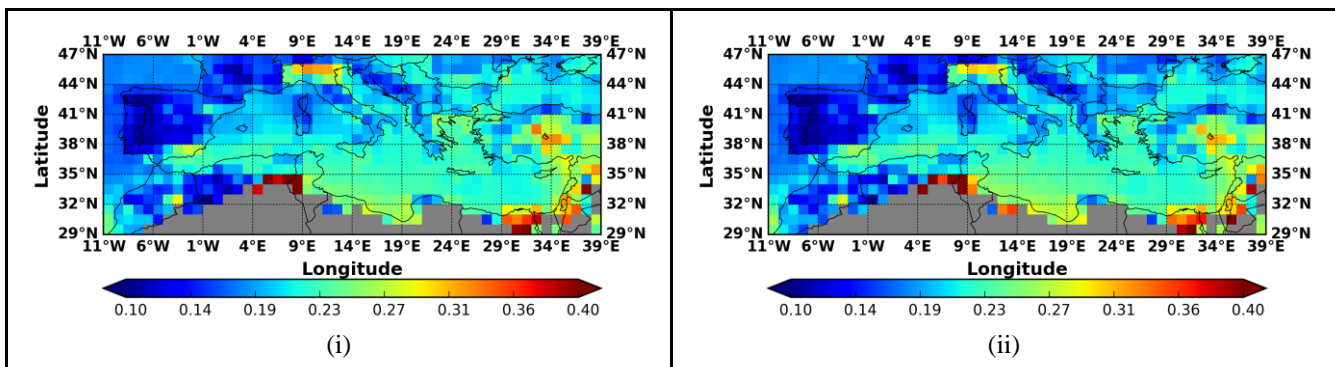
*“An unequal distribution of AOD data within the whole dataset considered DOES HAVE A CRITICAL IMPACT on the pixel-resolved ‘AOD Mean values’ being derived and THEREFORE on the final outcome of their algorithm. Proving there is a rather uniform distribution of the number of single, daily-resolved AOD data points in the dataset is essential to demonstrate your method builds on robust basis. Should this not be the case, i.e., should the number of AOD data-points be unbalanced (in the different months or in the different years within the long-term period covered), other strategies should be adopted to compute reasonable ‘AOD Mean values’ (i.e., the threshold values used to drive the empirical algorithm).”*

The applied methodology which is followed in the present analysis for the calculation of the mean AOD levels has been used in numerous studies in the past dealing with satellite or AERONET data at local, regional or global scale. It is well known that the satellite and ground aerosol retrievals are characterized by an unequal distribution of available data (in spatial and temporal terms). We agree with the Reviewer that this temporal inhomogeneity can affect the calculated threshold levels but their definition as well as the identification of DD episodes is simply done based on the available data. However, following the Reviewer's thinking then we have to reject thousands of papers dealing with AOD climatologies/trends studies just because satellite (e.g. MODIS) or ground (e.g. AERONET) data

are utilized which are unequal distributed on monthly, seasonal, annual or other possible temporal scale.

This “loss” of data would lead to lower mean AOD levels (based on our default methodology) if for example a dust outbreak had occurred during the missing day/s. In addition, the calculated mean AOD levels will be positive or negative biased depending on the seasonal availability of AOD retrievals. We can understand the Reviewer’s argument if the obtained results are going to be used for health impact studies but we disagree as it concerns the climatic effects. In his/her initial report he/she suggested to compute the mean AOD levels from monthly values (weighted equally) instead of daily ones as we are doing in our methodology. In case of radiative forcing studies (related to climatic impacts) the direct radiative effects on a monthly basis, in all studies to our knowledge, are calculated according to the available daily measurements of each month. Following the Reviewer’s suggestion, the normalization of AOD requires at the same time the normalization of the identified dust events on a monthly scale which is not feasible due to the variation of AOD retrievals’ availability (attributed to clouds, retrieval algorithm assumptions) as well as by the seasonal variation of dust events. Moreover, it is not clear why the mean AOD levels should be calculated by monthly values and not from seasonal or annual ones or other temporal scales (e.g. weekly).

However, in order to be more specific and dispel any concern, we proceeded as suggested by the Reviewer, namely we calculated the mean AOD levels (on which are based the AOD thresholds) based on monthly values (calculated by any available daily retrievals) and we have compared them against the corresponding ones calculated based on our default methodology (daily retrievals). According to our results, depicted in Figure R1, the two sets of AOD mean values have almost identical spatial patterns and magnitudes. The differences are smaller than 0.1 in absolute or 5% in relative terms. More specifically, the monthly-based mean AODs over land are smaller than the daily-based ones by less than 10 % (observed in northern parts of the study region where dust outbreaks have less impact) while the opposite is found over sea. This finding reveals thus that the unequal temporal distribution of daily AOD retrievals does not have a critical impact on the computed mean AODs (Lines: 372-381) utilized in this manuscript. Therefore, also taking into account the common practice and for reasons of consistency with our and others’ previous studies we prefer to keep using the daily-based AOD mean and threshold levels.



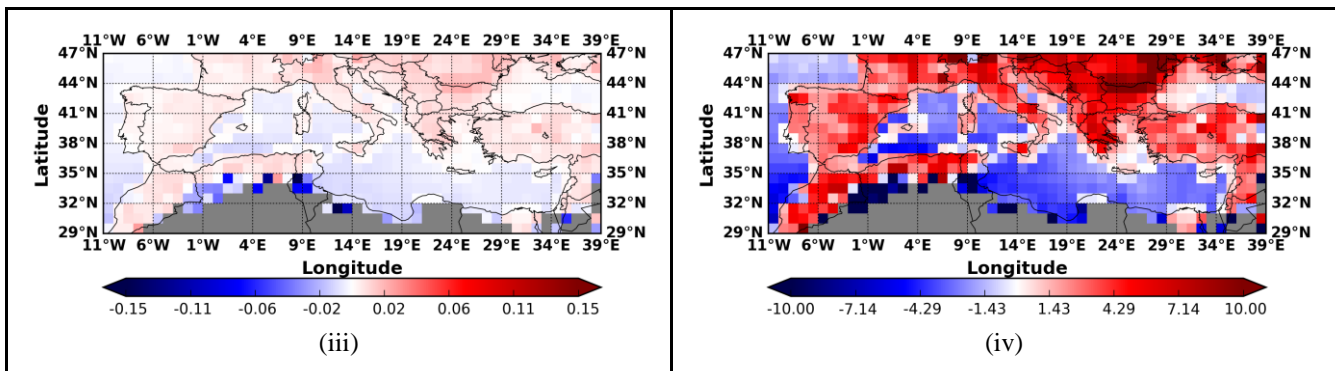


**Figure R1:** Geographical distributions of the: (i) long-term averaged  $AOD_{550nm}$  based on daily MODIS-Terra, (ii) long-term averaged  $AOD_{550nm}$  based on monthly MODIS-Terra, (iii) absolute daily-monthly differences and (iv) percentage daily-monthly differences. The calculations for the broader Mediterranean area have been made over the period 1 Mar. 2000 - 28 Feb. 2013.

Summarizing, this point, looking at any published AOD map of any satellite product, someone can argue that the map has no meaning since it is produced by an unequal distribution of AOD data over different days/months/years for different grids. To take this even further, even the 1 by 1 degree daily MODIS AOD could be considered in general, inhomogeneous since it is the average of 10 by 10 Km AODs that represent different areas during different days due to the day to day random presence of clouds in the 1 by 1 degree pixel. Does this mean that any AOD time series by any satellite in any 1 by 1 grid has no scientific importance before a spatial homogenization/normalization?

Continuing the normalization discussion for CALIPSO data, things get much worse as a CALIPSO daily/monthly profile in any publication is a sum of a number of parts of vertical profiles in a specific grid. In this case in addition to the temporal and the 2D spatial inhomogeneity, a 3D inhomogeneity is included.

Our definition of the AOD mean calculated with only available data is based on answering the main question of the work which is if at a certain day and a certain grid we have a strong or an extreme dust event.

*“In fact, in Figure R1-to-R4 the authors show the data in terms of ‘percentages’, without reporting the formula these percentages represent. Anyway, if I understand correctly, this ‘percentage’ means that for example in the month of January (Figure R1) a 100% value (dark red) is obtained in pixels when they get 31/31 daily data points for each year of the period considered (i.e., they get (31 days x 13 years)/(31 days x 13 years) values, covering all days of January 2001-2002-2003-2004-2005-2006-2007-2008-2009-2010-2011-2012-2013). Is this interpretation correct? If no, the authors should please define what’s the meaning of ‘percentage’ here. If yes, then by similarity your Figure R2 shows that in winter they get more than 85% of the data over sea and less than about 50% over land (excluding bright areas having no data), while the opposite occurs in summer. This clearly reveals the seasonal unbalance I suspected, plus a land/sea unbalance in data availability I did not expect. This does critically affect their results.”*



Yes. The calculated percentages refer to the availability of the daily MODIS-Terra AOD retrievals depending on the temporal scale (i.e., months, seasons, years and whole study period). As shown in the previous response, the seasonal unbalance does not critically affect our results.

*“Why should cloud cover in winter affect land and not sea (Mediterranean) areas? Are the two different MODIS retrievals over land and ocean playing a role in this land/ocean difference in the number of data availability? It is true that the DD impact in winter at higher latitudes is expected to be low, but what about the different data availability over the Med sea among seasons? This clearly affects the results over the Med areas closest to the North African coasts where the maximum impact of dust is rather expected. The authors should comment on that.”*

The data availability varies between land and sea surfaces due to the different applied MODIS retrieval algorithms. During warm seasons, across the Mediterranean Sea, a large amount of retrievals is masked out from the dataset due to Sun glint, which varies with season and gets less important in winter and autumn. As it concerns the variability of the MODIS retrievals availability throughout the year, the main driving factor is the clouds since AOD is measured by satellites under clear skies conditions. In the broader Mediterranean basin, the cloud coverage increases from south to north (spatial variability) and from warm to cold seasons (temporal variability). Therefore, both aforementioned reasons (Sun glint, clouds), either solely or combined, can explain the spatial patterns of MODIS-Terra AOD availability displayed in Figures R1-R4 of our previous response. We have modified the relevant part of the manuscript accordingly (Lines: 368-372).

*“In brief, although I’m aware the same methodology has been used in several other publications, to my opinion the different data coverage in time and space is a major critical element not properly addressed by the algorithm currently adopted.”*

See our responses to previous comments.

*“[Further comment: good that this unbalance of Figure R1 and R2 somehow ‘compensates’ in the annual Figure R3 and that this compensation keeps similar for the different years considered (Figure R4). I believe Figure R5 I suggested to produce is indeed interesting and useful. I think the authors should insert it at least in the supplementary material].”*

We have added the geographical distributions of the calculated statistics (for both study periods) namely the mean value and the associated standard deviation as well as both threshold levels in the revised supplementary material (Figure S1). A sentence has been added to the manuscript (Lines: 339 - 342) directing the reader to the obtained results.

*“Does this mean in METHOD-B the identification of ‘pure’ DD cases uses the thresholds for Ångström exponent, Fine Fraction, Aerosol Index and Effective radius BUT NO threshold for AOD? The authors should please clarify this point, as the same ambiguity is found in the text added to the revised manuscript (lines 371-383).”*

Yes, this is stated clearly in our manuscript (Lines: 399-410). Only the defined criteria for Ångström exponent, fine fraction, effective radius and Aerosol index are used in order to mask out the “pure” dust

AOD retrievals. Then, from the remaining non-dust AOD retrievals the threshold levels (Mean + 2\*Std and Mean+4\*Std) are calculated for each pixel. Finally, the DD episodes' frequency of occurrence and intensity are calculated based on the defined thresholds.

## 2. DATASET PROBLEMS

*“I understand the authors reasons to keep a different time range for AQUA and TERRA, exploiting the longer TERRA dataset. Still, I think showing the results I asked for (Figures R7 and R8) in the supplementary is important because then (and only then) the authors can substantiate the statement that differences between TERRA and AQUA are likely due to daily cycle effects rather than to the different long-term period addressed.”*

In the revised supplementary material we have added both figures (Figures S5 and S6).

*“A similar text is inserted in the revised manuscript (lines 211-214). Given the ‘uncertainties’ on the accuracy of these parameters, some ‘sensitivity’ on the use of the relevant thresholds in the algorithm would have been opportune, as well as on the real need for such a multi-parameter dataset.”*

In the submitted document (Lines: 366-368) we were stating that the defined thresholds for  $\alpha$ , FF, reff and AI have been selected based on raw data availability, literature findings and several sensitivity tests directing the reader to Gkikas et al. (2013). In the revised document, we have added a short description about the obtained results concerning the sensitivity tests (Lines: 391-396).

*“This was the information I was asking for in my question. This information needs to be added to the text, together with the explanation on how these 23% and 12.8% percentages are obtained. This information is very interesting, and it is indeed a bit strange no mention to that Gkikas et al. 2016 paper (or manuscript in press) was done in the first version of the manuscript nor in the current revised one (the paper is now published). It should obviously be included in the reference list and mentioned in the introduction to put the present study into a more general prospective.”*

We have added in the revised manuscript that the algorithm which is used here is a branch of a unified algorithm presented in Gkikas et al. (2016) but we are not discussing other details (available in Gkikas et al. 2016) (See lines 331-335).

*“As mentioned in my general comment at the beginning, this manuscript addresses a lot of different aspects of DD events (DD algorithm issues, horizontal scale, vertical scale, comparison to AERONET, comparison to PM10) and seems to lack a main focus. This also translates into a very long and inhomogeneous text that does not help the reading. In my former comment 3.2, I suggested to leave the comparison with PM10 data to a further (interesting) investigation. I'm still convinced of this, and even more now that the revised version further added a 3 pages-section (4.4) on this aspect, with the study of specific ‘desert-dust cases’.”*

We disagree with the Reviewer's proposal for the following reasons. Section 4.4, which has been added in the submitted manuscript following the recommendations made by the Reviewer 3 and the acceptance of the Editor, discusses how the vertical distribution of dust outbreaks affects the level of agreement between columnar (MODIS) and ground (PM) observations. It is apparent that the obtained results (Section 4.4) are directly related to the scientific target of our analysis which is the description of the Mediterranean desert dust outbreaks' vertical structure. In addition, the analysis in Section 4.4 is triggered by the obtained results in Section 4.1.2 where it is investigated the agreement between columnar AODs (MODIS) and ground concentrations (PM) across the Mediterranean. Hence, these two sections are linked together and we believe that should be presented in the manuscript. Moreover, omitting the parts of the analysis related to PM (Sections 4.1.2 and 4.4) and extending those related to the applied methodology would result in an unbalanced manuscript providing little additional information with regards to that of Gkikas et al. (2013).

### **Some minor comments**

*“- Some of the information provided in your answers to my minor comments needs to be inserted in the text to improve its clarity and completeness.”*

We have inserted to the manuscript as many as possible of our responses to the Reviewer's minor comments trying also not to extend further the length of the manuscript (see also our response to the Reviewer's general comment).

*“- Declared aim of the study in the abstract is now ‘to describe the vertical structure of the intense Mediterranean dust outbreaks’ but this is just a part of the work, the horizontal structure over the basin, although less original, is also important within the manuscript and should be also emphasized in the abstract (see also my general comment on the need to better clarify which is the focus of the work and to re-arrange the whole text accordingly).”*

The aim of the study, as stated in the first two sentences of the Abstract, is the description of the Mediterranean dust outbreaks and their vertical structure. This already implies that features of their horizontal distribution are examined, as it is immediately understood/realized by the reader when reading about the obtained results of the DD episodes' frequency of occurrence and intensity in the following sentences of the Abstract (lines 32-41). Also note that adding Section 4.4 (specific dust outbreaks) in the revised manuscript resulted in a strengthened part of the analysis related to the vertical extension of dust outbreaks.

*“- The authors use the two metrics DD ‘episode frequency’ and ‘intensity’ to characterize DD over the Mediterranean. From their description (Section 3), it seems that an ‘episode’ (per pixel) is a single day of dust, while quite often in the literature the term ‘episode’ is used for a dust event lasting more than 1 day. This is quite important to clarify, also to allow comparison with other literature data. For example Pey et al., 2013 show a dust frequency (% over annual days) over Southern Europe up to about 37% in Sicily (Italy), and about 30% in Southern Spain and Greece. Note that these percentages in Pey et al. (2013) are obtained ONLY limiting to the cases in which Saharan dust is observed at the ground, thus*

*should correspond to a subset of the DD statistics from columnar measurements as in the present work. Here Gkikas et al get maximum frequencies for ‘strong’ events of about 10 episodes/year (i.e. less than 3% over annual days) close to the African coasts. How do the authors reconcile these numbers? Could they please comment on that? Note that this aspect is somehow connected to the definition of the ‘AOD thresholds’, from which all the subsequent analysis and definition of ‘strong’ and ‘extreme’ events derives.”*

We agree with the Reviewer that in literature the term “episodes” usually refers to unusually high concentrations recorded persistently for consecutive days but this does not mean that it cannot be used also for single days, as defined in the present and our previous papers. Yet, and based on this definition, the duration of DD episodes is easily understood and quantified, as done in Gkikas et al. (2013). We have added a brief clarification in Lines: 95-96. As it concerns the second part of the Reviewer’s comment, we would like to mention that it is normal to obtain different numbers (frequencies) because of the different approaches taken in different studies, as stated by the Reviewer himself/herself. In Pey et al. (2013), dust occurrences are identified when dust is recorded at stations regardless its concentration while in our analysis we are identifying intense dust episodes when AOD levels are higher/equal than mean plus two times standard deviation. Hence, these differences are attributed to the different “thresholds” definition. We have added the relevant information in the revised document (Lines: 685-691).

*“- Figure 1: The authors can keep it if adding a second panel showing the equivalent scheme for the METHOD-B, this making the figure different from the one in their former publication.”*

We have decided to remove Figure 1 from the revised manuscript following the initial suggestion made by the Editor.

*“- Figures 9 and 10 are not very much readable and should be improved.”*

We have increased furthermore the size of Figures 9 and 10.

*“- I did not have the opportunity to fully read the Gkikas et al (2016) paper on Atmospheric Environment, but why are the Figures 2 and 3 in this manuscript different from Figures 4 and 5 in that paper (for those plots referring to the same DD analysis on the same MODIS Terra dataset)? It would also be important to comment on these differences, given that this manuscript follows that other one from the authors.”*

The analysis in Gkikas et al. (2016) covers the period Mar. 2000 – Feb. 2007 while in the present paper the study period extends from March 2000 to February 2013. Moreover, in Gkikas et al. (2016) the satellite algorithm operates with non-weighted QA retrievals in contrast to the present analysis (QA weighted). For the aforementioned reasons, the obtained results from both studies are not identical. Note that the DD episodes presented in Gkikas et al. (2016) are obtained with the same previous version of algorithm utilized in Gkikas et al. (2013). Therefore, in this study we discuss the differences between the present analysis (improved algorithm) and Gkikas et al. (2013, previous algorithm).

*“- I noticed the following reference is reported twice in the reference list, with two different years of publication:*

*- Gkikas, A., Houssos, E. E., Lolis, C. J., Bartzokas, A., Mihalopoulos, N. and Hatzianastassiou, N.: Atmospheric circulation evolution related to desert-dust episodes over the Mediterranean. Q.J.R. Meteorol. Soc., 141: 1634–1645. doi: 10.1002/qj.2466, 2015.*

*- Gkikas, A., Houssos, E. E., Lolis, C. J., Bartzokas, A., Mihalopoulos, N. and Hatzianastassiou, N.: Atmospheric circulation evolution related to desert-dust episodes over the Mediterranean. Q.J.R. Meteorol. Soc., doi: 10.1002/qj.2466, 2014.”*

We would like to thank the Reviewer for noticing our mistake. In the revised manuscript we have kept the first reference which is the correct one.

1 **Mediterranean intense desert dust outbreaks and their vertical structure based on**  
2 **remote sensing data**

3  
4 A. Gkikas<sup>1</sup>, S. Basart<sup>1</sup>, N. Hatzianastassiou<sup>2</sup>, E. Marinou<sup>3,9</sup>, V. Amiridis<sup>3</sup>, S. Kazadzis<sup>4,5</sup>, J. Pey<sup>6</sup>, X.  
5 Querol<sup>7</sup>, O. Jorba<sup>1</sup>, S. Gasso<sup>8</sup> and J.M. Baldasano<sup>1,8</sup>

- 6  
7 <sup>1</sup>Earth Sciences Department, Barcelona Supercomputing Center, Barcelona, Spain  
8 <sup>2</sup>Laboratory of Meteorology, Department of Physics, University of Ioannina, Ioannina, Greece  
9 <sup>3</sup>Institute for Astronomy, Astrophysics, Space Applications and Remote Sensing, National Observatory of Athens, Athens,  
10 15236, Greece  
11 <sup>4</sup>Physikalisch-Meteorologisches Observatorium Davos, World Radiation Center, Switzerland  
12 <sup>5</sup>Institute of Environmental Research and Sustainable Development, National Observatory of Athens, Athens, Greece  
13 <sup>6</sup>Spanish Geological Survey. Zaragoza IGME Unit, Zaragoza, Spain  
14 <sup>7</sup>Institute of Environmental Assessment and Water Research, IDAEA-CSIC C/Jordi Girona, 18–26, 08034 Barcelona, Spain  
15 <sup>8</sup>Environmental Modelling Laboratory, Technical University of Catalonia, Barcelona, Spain  
16 <sup>9</sup>Laboratory of Atmospheric Physics, Department of Physics, Aristotle University of Thessaloniki, Thessaloniki, Greece  
17  
18

19 Corresponding author: Antonis Gkikas ([antonis.gkikas@bsc.es](mailto:antonis.gkikas@bsc.es))

20  
21 **Abstract**

22 The main aim of the present study is to describe the vertical structure of the intense Mediterranean  
23 dust outbreaks, based on the use of satellite and surface-based retrievals/measurements. Strong and  
24 extreme desert dust (DD) episodes are identified at 1° x 1° spatial resolution, over the period Mar. 2000  
25 – Feb. 2013, through the implementation of an updated objective and dynamic algorithm. According to  
26 the algorithm, strong *DD* episodes occurring at a specific place correspond to cases in which the daily  
27 aerosol optical depth at 550nm ( $AOD_{550nm}$ ) exceeds or equals the long-term mean  $AOD_{550nm}$  (*Mean*)  
28 plus two standard deviations (*Std*) value being smaller than  $Mean+4*Std$ . Extreme *DD* episodes  
29 correspond to cases in which the daily  $AOD_{550nm}$  value equals or exceeds  $Mean+4*Std$ . For the  
30 identification of *DD* episodes additional optical properties (Ångström exponent, fine fraction, effective  
31 radius and Aerosol Index) derived by the MODIS-Terra & Aqua (also *AOD* retrievals), OMI-Aura and  
32 EP-TOMS databases are used as inputs. According to the algorithm using MODIS-Terra data, over the  
33 period Mar. 2000 – Feb. 2013, strong *DD* episodes occur more frequently (up to 9.9 episodes yr<sup>-1</sup>) over

Formatted: Font: Italic

Formatted: Font: Italic

Formatted: Font: Italic

Formatted: Font: Italic

Formatted: Font: Italic

Formatted: Font: Italic

34 the western Mediterranean while the corresponding frequencies for the extreme ones are smaller (up to  
35 3.3 episodes  $\text{yr}^{-1}$ , central Mediterranean Sea). In contrast to their frequency, dust episodes are more  
36 intense (*AODs* up to 4.1), over the central and eastern Mediterranean Sea, off the northern African  
37 coasts. Slightly lower frequencies and higher intensities are found when the satellite algorithm operates  
38 based on MODIS-Aqua retrievals, for the period 2003–2012. The consistence of the algorithm is  
39 successfully tested through the application of an alternative methodology for the determination of *DD*  
40 episodes, which produced similar features of the episodes' frequency and intensity, with just slightly  
41 higher frequencies and lower intensities. The performance of the satellite algorithm is assessed against  
42 surface-based daily data from 109 sun-photometric (AERONET) and 22 *PM<sub>10</sub>* stations. The agreement  
43 between AERONET and MODIS *AOD* is satisfactory ( $R=0.505-0.750$ ) improving considerably when  
44 MODIS level 3 retrievals with higher sub-grid spatial representativeness and homogeneity are  
45 considered. The CALIOP vertical profiles of pure and polluted dust observations and the associated  
46 total backscatter coefficient at 532 nm ( $\beta_{532nm}$ ), indicate that dust particles are mainly detected between  
47 0.5 and 6 km, though they can reach 8 km between the parallels 32° N and 38° N in warm seasons,  
48 while an increased number of CALIOP dust records at higher altitudes is observed with increased  
49 latitude, northwards to 40° N, revealing an ascending mode of the dust transport. However, the overall  
50 intensity of *DD* episodes is maximum (up to  $0.006 \text{ km}^{-1} \text{ sr}^{-1}$ ) below 2 km and at the southern parts of  
51 the study region (30° N - 34° N). Additionally, the average thickness of dust layers gradually decreases  
52 from 4 to 2 km moving from south to north. In spring, dust layers of moderate-to-high  $\beta_{532nm}$  values (~  
53  $0.004 \text{ km}^{-1} \text{ sr}^{-1}$ ) are detected over the Mediterranean (35° N - 42° N), extending from 2 to 4 km. Over  
54 the western Mediterranean, dust layers are observed between 2 and 6 km, while their base height is  
55 decreased down to 0.5 km for increasing longitudes underlying the role of topography and thermal  
56 convection. The vertical profiles of CALIOP  $\beta_{532nm}$  confirm the multilayered structure of the  
57 Mediterranean desert dust outbreaks on both annual and seasonal basis, with several dust layers of  
58 variable geometrical characteristics and intensities. A detailed analysis of the vertical structure of  
59 specific *DD* episodes using CALIOP profiles reveals that consideration of the dust vertical structure is  
60 necessary when attempting comparisons between columnar MODIS *AOD* retrievals and ground *PM<sub>10</sub>*  
61 concentrations.

Formatted: Font: Italic

Formatted: Font: Italic

Formatted: Font: Italic

Formatted: Font: Italic

Formatted: Font: Italic

Formatted: Font: Italic

## 62 1. Introduction

63 The Mediterranean basin, due to its proximity to the major dust source arid areas of Northern  
64 Africa and Middle East (Middleton and Goudie, 2001; Prospero et al., 2002; Ginoux et al., 2012) is  
65 frequently affected by transported high dust loads referred to as episodes or events. The suspension and

66 accumulation of mineral particles into the atmosphere over the Saharan and Arabian Peninsula's  
67 deserts are determined by various factors such as the enhanced turbulence, soil conditions (reduced  
68 vegetation cover and soil moisture), reduced precipitation amounts, latitudinal shift of the Intertropical  
69 Convergence Zone (*ITCZ*) as well as by small scale meteorological processes (e.g. haboobs). However,  
70 dust particles can be transported far away from their sources, mainly towards the Atlantic Ocean (e.g.  
71 Prospero and Lamb, 2003; Ben-Ami et al., 2010; Huang et al., 2010) and Europe (e.g. Mona et al.,  
72 2006; Mona et al., 2012; Papayannis et al., 2008; Basart et al., 2012; Bègue et al., 2012; Pey et al.,  
73 2013), favored by the prevailing atmospheric circulation patterns, from planetary to synoptic scales.  
74 Due to their frequent transport in the Mediterranean, mineral dust particles, constitute the predominant  
75 aerosol type there (Barnaba and Gobbi, 2004; Basart et al., 2012), as shown by the good agreement, in  
76 spatial terms, between the geographical distributions of dust episodes' *AOD* (Gkikas et al., 2013) and  
77 average *AOD* conditions (Papadimas et al., 2008).

Formatted: Font: Italic

78 Dust particles play an important role for the shortwave (*SW*) and longwave (*LW*) radiation budget  
79 (e.g. Kaufman et al., 2002; Tegen et al., 2003; Heinold et al., 2008) and climate (IPCC, 2013). They  
80 affect atmospheric heating/cooling rates (e.g. Mallet et al., 2009) while they can also result in a  
81 modification of atmospheric dynamics and large atmospheric circulations like monsoons (e.g. Lau et  
82 al., 2006; Bollasina et al., 2011), cloud properties and precipitation (e.g. Huang et al., 2006; Solmon et  
83 al., 2008). Moreover, it has been shown that the consideration of their radiative impacts in numerical  
84 simulations can improve the forecasting accuracy of weather models (Pérez et al., 2006). Dust particles  
85 also affect air quality in urban areas (Basart et al., 2012) causing adverse health effects (Díaz et al.,  
86 2012; Karanasiou et al., 2012; Pérez García-Pando et al., 2014). All these consequences of dust aerosol  
87 are relevant and maximize under maximum dust loads, namely dust episodes, highlighting thus the  
88 significance of analyzing the spatial and temporal characteristics of such events. To this aim, many  
89 studies have been carried out using either surface (e.g. Cachorro et al., 2006) or satellite (e.g. Moulin et  
90 al., 1998) observations, as well as modelling techniques (e.g. Heinold et al., 2007) focusing on the  
91 broader Mediterranean area. These studies have been done either for specific cases (e.g. Kubilay et al.,  
92 2003; Balis et al., 2006) or for extended periods at specific locations (e.g. Meloni et al., 2007; Toledano  
93 et al., 2007a; Gobbi et al., 2013; Mona et al., 2014). Recently, Gkikas et al. (2013) developed an  
94 objective and dynamic algorithm relying on satellite retrievals, which enabled an overall view of dust  
95 episodes over the entire Mediterranean and the characterization of their regime (*i.e., frequency of*  
96 *occurrence, intensity and duration*).

Formatted: Font: Italic

Formatted: Font: Italic



97 Extensive research has been also carried out on the mechanisms of Mediterranean dust outbreaks.  
98 Therefore, several mechanisms and processes of transport, apart from dust emissions in source areas,  
99 have been proposed as controlling factors. Moulin et al. (1997) showed that the exported dust loads  
100 from Northern Africa towards the Atlantic Ocean and the Mediterranean are controlled by the phase of  
101 the North Atlantic Oscillation (*NAO*). Other studies, focused on the description of atmospheric  
102 circulation characteristics favoring the occurrence of desert dust outbreaks over the central (Barkan et  
103 al., 2005; Meloni et al., 2008) or western (Querol et al., 1998; Rodriguez et al., 2001; Salvador et al.,  
104 2014) Mediterranean, but on a synoptic scale. An objective classification, based on multivariate  
105 statistical methods, of the atmospheric circulation patterns related to dust intrusions over the  
106 Mediterranean, has been presented by Gkikas et al. (2015) and Varga et al. (2014).

Formatted: Font: Italic

107 The concentration of dust aerosols in the Mediterranean is characterized by strong spatial and  
108 temporal variability, associated with the seasonal variability of cyclones dominating or affecting the  
109 broader Mediterranean basin (Trigo et al., 2002). According to Moulin et al. (1998), dust *AOD* levels  
110 are higher in spring and summer compared to the wet seasons of the year. Moreover, dust intrusions are  
111 mainly recorded over the southeastern Mediterranean in spring and winter, over the western parts in  
112 summer and over the central ones in autumn (Gkikas et al., 2013).

113 Dust transport over the Mediterranean is characterized by a multi-layered structure (Hamonou et  
114 al., 1999; Papayannis et al., 2008) in contrast to the Atlantic Ocean, which is well confined to the  
115 Saharan Air Layer (*SAL*, Karyampudi et al., 1999). The vertical distribution of dust load into the  
116 troposphere as well as the profile of dust aerosols' optical properties at different altitudes, control the  
117 impacts on atmospheric dynamics induced by the mineral particles (Zhang et al., 2013). In order to  
118 describe the geometrical features of dust transport, many researchers have used ground lidar  
119 measurements, model simulations (Alpert et al., 2004; Kishcha et al. 2005) or they have relied on a  
120 synergistic use of satellite observations and ground lidar profiles (Berthier et al., 2006). The vertical  
121 extension of the Saharan dust intrusions over Europe, during the period 2000-2002, was the subject of a  
122 comprehensive study by Papayannis et al. (2008), who used lidar measurements from the EARLINET  
123 (European Aerosol Research Lidar Network, Bösenberg et al., 2003). Over the Mediterranean stations,  
124 the mean base, top and thickness of dust layers was found to vary from 1356 to 2980 m, 3600 to 5900  
125 m and 726 to 3340 m, respectively. According to the obtained results, tracers of dust particles can be  
126 detected up to 10 km, as also reported by Gobbi et al. (2000), who studied a Saharan dust event in  
127 Crete (south Greece) during spring of 1999.

Formatted: Font: Italic

128 Several similar studies have been also performed for specific Mediterranean locations based on  
129 EARLINET lidar measurements. For example, Mona et al. (2006) analyzed the vertical structure of 112  
130 Saharan intrusions that occurred over Potenza (Italy), from May 2000 to April 2003. The authors found  
131 that these outbreaks are confined between 1.8 and 9 km while their mass center is located at 3.5 km  
132 above sea level (a.s.l.). A similar analysis for Athens and Thessaloniki over the period 2000-2002, was  
133 conducted by Papayannis et al. (2005) who demonstrated that dust layers are recorded mainly between  
134 2 and 5 km while their thicknesses vary from 0.2 to 3 km. The geometrical characteristics of dust layers  
135 over Athens, during the period 2004 – 2006, have been also presented by Papayannis et al. (2009), who  
136 pointed out that the center of mass of dust layers is located at 2.9 km being in a very good agreement  
137 with Kalivitis et al. (2007) findings (around 3 km) for the eastern Mediterranean. Additionally, the  
138 authors reported that the dust layers mainly extend from 1.6 to 5.8 km while mineral particles can be  
139 detected, at very low concentrations, up to 8 km a.s.l.. Gobbi et al. (2013) found that dust plumes, over  
140 Rome, mainly extend from 0 to 6 km while their center of mass is located at around 3 km. In the  
141 southern parts of Italy (Potenza), dust layers' base is found between 2 and 3 km, their geometrical  
142 height extends from 2.5 to 4 km while tracers of dust particles can be detected up to 10 km, based on a  
143 dataset of 310 dust events analyzed by Mona et al. (2014). Finally, Pisani et al. (2011) stated that the  
144 mean base and top of dust layers is found at 1.5 km and 4.6 km a.s.l., respectively, while their mean  
145 thickness is equal to 3.1 km, based on a statistical analysis of 45 desert dust episodes observed over  
146 Naples (Italy), from May 2000 to August 2003.

147 Surface-based lidar measurements like those used in the aforementioned studies provide useful  
148 information about the geometrical and optical properties of dust layers, but they are representative only  
149 for specific locations. Yet, a more complete knowledge about the vertical structure of dust outbreaks is  
150 necessary in order to adequately understand and determine their possible effects. The limitation  
151 imposed by the use of surface-based lidar observations can be overcome by utilizing accurate satellite  
152 retrievals, as a complementary tool, which provide extended spatial coverage. Since 2006, vertical  
153 resolved observations of aerosols and clouds from space were made possible thanks to the CALIOP  
154 (Cloud-Aerosol Lidar with Orthogonal Polarization) lidar flying onboard the CALIPSO (Cloud-  
155 Aerosol Lidar and Infrared Pathfinder Satellite Observations) satellite (Winker et al., 2009). Based on  
156 CALIOP observations, Liu et al. (2008) analyzed the global vertical distribution of aerosols for one  
157 year, while other studies focused on the vertical structure of dust outflows towards the Atlantic Ocean  
158 (e.g. Ben-Ami et al., 2009; Adams et al., 2012; Tsamalis et al., 2013) and the Pacific Ocean (e.g.  
159 Eguchi et al., 2009; Hara et al., 2009). On the contrary, over the broader Mediterranean area, only a

160 small number of studies has been made aiming at describing the vertical distribution of dust aerosols  
161 (Amiridis et al., 2013) or specifying the vertical structure of dust events (Amiridis et al., 2009).  
162 Nevertheless, they only dealt with a single dust event (18-23 May 2008, Amiridis et al., 2009) and thus  
163 cannot satisfy the need to know the general vertical structure of Mediterranean dust episodes.

164 The main target of the present study is to describe the Mediterranean desert dust outbreaks' vertical  
165 structure. For this purpose, satellite retrievals derived by the MODIS-Terra/Aqua, ~~Earth Probe~~EP-  
166 TOMS, OMI-Aura and CALIOP-CALIPSO databases (Section 2) are used in a synergistic way. The  
167 dust outbreaks are identified with an objective and dynamic algorithm, which uses appropriate aerosol  
168 optical properties representative of suspended particles' load, size and nature (Section 3). ~~First, the~~  
169 ~~outputs of the default version of the satellite algorithm are compared versus surface measurements~~  
170 ~~provided by AERONET or  $PM_{10}$  stations, located within the study region (Section 4.2).~~ Additionally,  
171 ~~useful information about various optical and physical properties under intense dust episodes conditions~~  
172 ~~is also derived from the aforementioned analysis.~~ Then, ~~Based on its outputs,~~ the primary  
173 characteristics of the intense Mediterranean desert dust (*DD*) episodes, namely their frequency and  
174 intensity, are described in Section 4.2. Just in order to assess the consistency of the algorithm'  
175 concept, an alternative methodology for the determination of *DD* episodes is also applied and the  
176 obtained results are inter-compared with the basic methodology. ~~The outputs of the default version of~~  
177 ~~the satellite algorithm are compared versus surface measurements provided by AERONET or  $PM_{10}$~~   
178 ~~stations, located within the study region (Section 4.2).~~ Additionally, ~~useful information about various~~  
179 ~~optical and physical properties under intense dust episodes conditions is also derived from the~~  
180 ~~aforementioned analysis.~~ For the identified *DD* episodes, collocated CALIOP-CALIPSO vertical  
181 feature mask and total backscatter coefficient at 532 nm retrievals are used in order to describe the  
182 annual and seasonal variability of dust outbreaks' vertical extension over the Mediterranean (Section  
183 4.3). Moreover, in Section 4.4, a thorough analysis of ~~few~~-specific Mediterranean *DD* episodes is  
184 made, in order to examine how the vertical distribution of desert dust outbreaks can affect the  
185 agreement between MODIS *AOD* and  $PM_{10}$  data. Finally, the summary and conclusions are drawn in  
186 Section 5.

187

## 188 2. Satellite and surface-based data

189 The different types of satellite retrievals that have been used as inputs to the objective and dynamic  
190 satellite algorithm are described below, namely the MODIS (Section 2.1.1), EP-TOMS and OMI-Aura

Formatted: Font: Italic

Formatted: Font: Italic

Formatted: Font: Italic

Formatted: Font: Italic

Formatted: Font: Italic

Formatted: Font: Italic

191 (Section 2.1.2) databases. Also, CALIOP-CALIPSO vertically resolved satellite data, coincident with  
192 the identified desert dust outbreaks by the satellite algorithm, are described in Section 2.1.3. Finally,  
193 surface-based sun-photometric AERONET retrievals and  $PM_{10}$  concentrations, both used for the  
194 comparison against the satellite algorithm's outputs, are described in Sections 2.2.1 and 2.2.2,  
195 respectively.

Formatted: Font: Italic

196

## 197 2.1 Satellite data

### 198 2.1.1 MODIS

199

200 MODerate resolution Imaging Spectroradiometer (MODIS) onboard the Terra and Aqua satellites –  
201 with daytime local equator crossing time at 10:30 and 13:30 UTC, respectively, and 2330 km viewing  
202 swath – acquires measurements at 36 spectral bands between 0.415 and 14.235  $\mu\text{m}$  with varying spatial  
203 resolution of 250, 500 and 1000 m. Observations from Terra and Aqua are made continuously since  
204 February 2000 and July 2002, respectively, and are available from the LAADS website  
205 (<ftp://ladsweb.nascom.nasa.gov/>). Aerosol optical properties are retrieved through the Dark Target (*DT*)  
206 algorithm (see e.g. Kaufman et al., 1997, 2001; Tanré et al., 1997; Levy et al., 2003; Remer et al.,  
207 2005) where different assumptions are considered depending on the underlying surface type (land or  
208 ocean). Several evaluation studies (e.g. Remer et al., 2008; Papadimas et al., 2009; Levy et al., 2010;  
209 Nabat et al., 2013) have shown that aerosol optical depth (*AOD*) can be retrieved satisfactorily by  
210 MODIS, nevertheless its performance is better over sea (uncertainty equal to  $\pm 0.03 \pm 0.05 \times AOD$ ,  
211 Remer et al., 2002) than over land ( $\pm 0.05 \pm 0.15 \times AOD$ , Levy et al., 2010).

Formatted: Font: Italic

212 The following daily MODIS-Terra and MODIS-Aqua Collection 051 (C051) level 3 satellite data  
213 (MOD08\_D3 and MYD08\_D3 files) provided at  $1^\circ \times 1^\circ$  latitude-longitude spatial resolution are used:  
214 (i)  $AOD_{550\text{nm}}$ , (ii) Ångström exponent over land ( $\alpha_{470-660\text{nm}}$ ), (iii) Ångström exponent over ocean  
215 ( $\alpha_{550-865\text{nm}}$ ), (iv) fine-mode fraction (*FF*) of *AOD* over land and ocean and (v) Effective radius over  
216 ocean ( $r_{\text{eff}}$ ). It must be mentioned that the size parameters ( $\alpha$ , *FF*) over land are less reliable compared  
217 to the corresponding ones over sea, since they are highly sensitive to spectral dependent factors such as  
218 errors in the surface model or sensor calibration changes. Over sea, the accuracy of size parameters is  
219 strongly dependent on wind conditions.

220 Similar data have been used by Gkikas et al. (2013), however, in the present study we have  
221 improved data quality by using the quality assurance-weighted (QA) level 3 data ([http://modis-](http://modis-atmos.gsfc.nasa.gov/docs/QA_Plan_2007_04_12.pdf)  
222 [atmos.gsfc.nasa.gov/docs/QA\\_Plan\\_2007\\_04\\_12.pdf](http://modis-atmos.gsfc.nasa.gov/docs/QA_Plan_2007_04_12.pdf)) derived from the level 2 retrievals (10 km x 10  
223 km spatial resolution). Each level 2 retrieval, is flagged with a bit value (from 0 to 3) corresponding to  
224 confidence levels (No confidence: 0, Marginal: 1, Good: 2 and Very Good: 3). Based on this, the level  
225 3 QA-weighted spatial means are obtained by the corresponding level 2 retrievals considering as  
226 weight their confidence level (bit value). In addition, the day cloud fraction as well as the number of  
227 level 2 counts, which are both relevant to the performance of the satellite algorithm, are also used in  
228 this study. The time series of daily MODIS aerosol data cover the 13-yr period March 2000-February  
229 2013 (Terra) and the 10-yr period January 2003-December 2012 (Aqua).

### 230 2.1.2 EP/TOMS and OMI-Aura

231 The selected retrievals from MODIS provide information about particles' load (*AOD*) and size ( $\alpha$ ,  
232  $FF$ ,  $r_{eff}$ ), which are both necessary to identify dust episodes. However, since dust is not the only coarse  
233 aerosol, for example sea-salt can be so as well, another optical property indicative of particle  
234 absorption efficiency is also required by the algorithm. To address this issue, the Absorption Aerosol  
235 Index (*AI*) daily data were also used, derived from measurements taken by the Total Ozone Mapping  
236 Spectrometer (TOMS) instrument onboard the NASA's Earth-Probe satellite (2000-2004) and the  
237 Ozone Monitoring Instrument (OMI) onboard the NASA's Aura satellite (2005-2013). *AI* is the  
238 primary TOMS aerosol product (Herman et al., 1997) based on a spectral contrast method in a *UV*  
239 region (331-360 nm) where ozone absorption is very small and can be used for the distinction between  
240 scattering (e.g. sea-salt) and absorbing (e.g. desert dust, smoke) aerosols. The retrieval algorithm (fully  
241 described by Torres et al., 1998; 2002; 2005) takes advantage of the low surface albedo in the *UV*  
242 spectrum range, even in arid and semi-arid areas, making thus possible the estimation of the *AOD* over  
243 highly reflecting desert surfaces, where the major dust sources are located. Since the late 70's, the  
244 TOMS sensor onboard Nimbus-7 (1978 – 1993) and Earth Probe (1996 – 2005) has been providing  
245 global aerosol measurements. With the deployment of the EOS-Aura OMI (Ozone Monitoring  
246 Instrument) in mid-2004 (Torres et al., 2007) the near *UV* aerosol record continues to be extended into  
247 the foreseeable future. OMI is a hyperspectral sensor, covering the 270-500 nm range, launched  
248 onboard the EOS-Aura satellite on July 15, 2004 (1:38 pm equator crossing time, ascending mode)  
249 providing almost daily global coverage thanks to its wide viewing swath (2600 km with 13 km x 24 km  
250 nadir resolution). Apart from *AI* measurements, OMI aerosol products include also the total and  
251 absorption *AOD* and the single scattering albedo at 388 and 500 nm (Torres et al., 2007). Both EP-

Formatted: Font: Italic

Formatted: Font: Italic

Formatted: Font: Italic

252 TOMS and OMI-Aura retrievals are available via the Mirador ftp server (<http://mirador.gsfc.nasa.gov/>)  
253 of the Goddard Earth Sciences Data and Information Services Center (GES DISC). OMI-Aura data, as  
254 MODIS, are provided at 1° x 1° spatial resolution while the EP-TOMS retrievals have been regridded  
255 from their raw spatial resolution (1° x 1.25°) in order to match with the other two datasets (OMI,  
256 MODIS).

257

### 258 2.1.3 CALIOP-CALIPSO

259

260 The Cloud-Aerosol Lidar with Orthogonal Polarization (CALIOP) onboard the NASA's satellite  
261 CALIPSO (Cloud-Aerosol Lidar and Infrared Pathfinder Satellite Observations), launched in April  
262 2006, provides vertical resolved aerosol and cloud observations (Winker et al., 2009) since June 2006.  
263 CALIPSO is flying in the A-Train constellation (Stephens et al., 2002; <http://atrain.nasa.gov/>) in a sun-  
264 synchronous polar orbit at 705 km over the surface, with a 16-day repeat cycle, crossing the equatorial  
265 plane at about 13:30 local solar time (Winker et al., 2009). CALIOP is an active sensor measuring the  
266 backscatter signal at 532 nm and 1064 nm as well as the polarization at 532 nm (Winker et al., 2009).  
267 These level 1 retrievals are further processed (calibration and range corrections) passing to Level 2 in  
268 order to retrieve the backscatter and extinction coefficients, at 532 nm and 1064 nm, for aerosol and  
269 cloud layers. The identification of cloud and aerosol layers within the atmosphere (Vaughan et al.,  
270 2009) is made through the cloud aerosol discrimination (*CAD*) algorithm (Liu et al., 2009), which is  
271 based on the probability distribution functions (*PDFs*) of altitude-and-latitude-dependent parameters  
272 (integrated color ratio, layer-integrated volume depolarization ratio, mean attenuated backscatter  
273 coefficient). *CAD* scores vary mainly from -100 to 100 indicating the presence of aerosols and clouds  
274 when are negative and positive, respectively, while bins of confidence levels, both for aerosols and  
275 clouds, are defined based on their absolute values  
276 ([https://eosweb.larc.nasa.gov/sites/default/files/project/calipso/quality\\_summaries/CALIOP\\_L2VFMPr  
278 oducts\\_3.01.pdf](https://eosweb.larc.nasa.gov/sites/default/files/project/calipso/quality_summaries/CALIOP_L2VFMPr<br/>277 oducts_3.01.pdf)). More specifically, the performance of the classification scheme in the *VFM*  
279 algorithm, either for aerosols or clouds, is more reliable for increasing *CAD* scores in absolute terms.  
280 Aerosols are categorized in 6 primary types namely: (i) clean marine, (ii) dust, (iii) polluted  
281 continental, (iv) clean continental, (v) polluted dust and (vi) smoke (Omar et al., 2009).

281 In the present analysis, we use the Version 3 (3.01 and 3.02) of the Level 2 Vertical Feature Mask  
282 (*VFM*) and Aerosol Profile Products (*APro*) files, available from June 2006 to February 2013, both  
283 derived from the NASA's Earth Observing System Data and Information System

Formatted: Font: Italic

Formatted: Font: Italic

Formatted: Font: Italic

Formatted: Font: Italic

Formatted: Font: Italic

284 (<http://reverb.echo.nasa.gov/>). The aerosol profile products are generated at a uniform horizontal  
285 resolution of 5 km ([http://www-calipso.larc.nasa.gov/products/CALIPSO\\_DPC\\_Rev3x6.pdf](http://www-calipso.larc.nasa.gov/products/CALIPSO_DPC_Rev3x6.pdf)), while the  
286 vertical resolution varies from 60 to 180 m depending on the altitude range and the parameter. The  
287 scientific data sets which have been analyzed are the following: (i) aerosol subtype, (ii) *CAD* score and  
288 (iii) Total Backscatter Coefficient at 532 nm ( $\beta_{532nm}$ ), reported at several tropospheric and stratospheric  
289 levels above mean sea level (Hunt et al., 2009).

290

## 291 2.2 Surface-based data

292

### 293 2.2.1 AERONET

294 The AEROSOL ROBOTIC NETWORK (AERONET, Holben et al., 1998) is a worldwide network of  
295 installed CIMEL sun-sky radiometers obtaining sun-photometric observations in more than 1000  
296 locations of the planet (<http://aeronet.gsfc.nasa.gov>). The solar irradiances received by the photometer  
297 are inverted to columnar aerosol optical and microphysical properties through the implementation of  
298 retrieval algorithms (e.g. Dubovik and King, 2000; O' Neill et al., 2003). The followed standardized  
299 methods concerning instrument maintenance, calibration, cloud screening and data processing allow  
300 aerosol monitoring and comparison between different study periods and areas (Smirnov et al., 2000).  
301 From the global AERONET stations, 109 are located within the geographical limits of our study  
302 region. For each station, the daily averages of cloud-screened and quality assured data (Level 2.0) of  
303 direct sun and almucantar retrievals are used for: (i) *AOD* at 7 wavelengths from 340 to 1020 nm, (ii)  
304 size distribution retrieved for 22 logarithmically equidistant discrete points ( $r_i$ ) in the range of sizes  
305  $0.05 \mu\text{m} \leq r \leq 15 \mu\text{m}$ , (iii) Ångström exponent between 440 and 870 nm ( $\alpha_{440-870nm}$ ), (iv) total effective  
306 radius ( $r_{eff}$ ), and (v) single scattering albedo (*SSA*) and asymmetry parameter ( $g_{aer}$ ) both retrieved at 440  
307 nm, 675 nm, 870 nm and 1020 nm. The uncertainty in the estimation of *AOD* depends on technical  
308 (e.g. calibration method) factors and inversion assumptions, both described in detail in Holben et al.  
309 (1998). Moreover, the accuracy of the retrieved *AOD* by the CIMEL radiometer is spectrally  
310 dependent, being higher ( $< \pm 0.01$ ) for wavelengths longer than 440 nm and lower ( $< \pm 0.02$ ) for the *UV*  
311 wavelengths (Eck et al., 1999). It should be also noted that the AERONET Level 2.0 inversion products  
312 (e.g. *SSA*) are provided when *AOD* at 440 nm is higher than 0.4 ensuring the minimization of the  
313 inversion uncertainties, which are also determined by other factors (e.g. scattering angle, particles'  
314 sphericity) as stated in detail by Dubovik et al. (2000).

315

Formatted: Font: Italic

316 2.2.2  $PM_{10}$

317 Daily total and dust surface  $PM_{10}$  concentrations, over the period 2001-2011 from 22 regional  
318 background and suburban background sites were used in this study. The monitoring sites are distributed  
319 as follows: 10 in Spain; 2 in southern France; 5 in Italy; 3 in Greece; 1 in southern Bulgaria and 1 in  
320 Cyprus.  $PM_{10}$  concentrations were obtained in most cases from gravimetric determinations on filters,  
321 whereas in few cases they were determined by real time instruments (Querol et al., 2009b; Pey et al.,  
322 2013) but corrected against gravimetric measurements carried out in annual field campaigns. The  
323 disaggregation of the dust component to the total amount is made based on a statistical approach which  
324 has been applied in several past studies (e.g. Rodríguez et al., 2001; Escudero et al., 2007; Querol et al.,  
325 2009b; Pey et al., 2013). A full description of the methodology which is followed for the calculation of  
326 dust particles' contribution to the total  $PM_{10}$  is presented in Escudero et al. (2007). Briefly, the net dust  
327  $PM_{10}$  amount is calculated through the subtraction of the regional background  $PM_{10}$ , which is obtained  
328 by applying a monthly moving 30<sup>th</sup> percentile to the  $PM_{10}$  timeseries excluding days of dust transport,  
329 from the corresponding values of the total  $PM_{10}$  concentrations. Most of the derived data were obtained  
330 from the AirBase (<http://acm.eionet.europa.eu/databases/airbase/>) database, while for the stations  
331 Finokalia (Crete) and Montseny (NE Spain) the relevant measurements have been acquired from the  
332 EUSAAR (<http://www.eusaar.net/>) database.

333

334 **3. Identification of desert dust episodes**

335

336 ~~Following the methodology proposed by Gkikas et al. (2013), desert dust (DD) episodes are~~  
337 ~~identified based on an objective and dynamic algorithm (see Figure 2 in Gkikas et al., 2013) which~~  
338 ~~consists a branch of a unified algorithm able to identify not only DD episodes, but also four other types~~  
339 ~~of aerosol episodes, namely biomass urban (BU), dust/sea salt (DSS), mixed (MX) and undetermined~~  
340 ~~(UN). The unified algorithm has been applied by Gkikas et al. (2016) in order to characterize aerosol~~  
341 ~~episodes in the greater Mediterranean Sea area, over the period Mar. 2000 – Feb. 2007. Following the~~  
342 ~~methodology proposed by Gkikas et al. (2013), desert dust (DD) episodes are identified based on an~~  
343 ~~objective and dynamic algorithm, which is depicted in the flowchart of Figure 1.~~

344 ~~The present (“dust”) algorithm operates~~The algorithm operates in three steps and is applied in each  
345 ~~individual 1° x 1° geographical cell within the geographical limits of the study domain (29° N – 47° N~~  
346 ~~and 11° W – 39° E). Following the methodology proposed by Gkikas et al. (2013), desert dust (DD)~~  
347 ~~episodes are identified based on an objective and dynamic algorithm which consists a branch of a~~

Formatted: Font: Italic

Formatted: Font: Italic

Formatted: Font: Italic

Formatted: Font: Italic

Formatted: Font: Italic

Formatted: Font: Italic

Formatted: Font: Italic

Formatted: Font: Italic



348 unified algorithm (Gkikas et al., 2016) able to identify and characterize not only *DD* episodes, but also  
349 four other types of aerosol episodes, namely biomass-urban (*BU*), dust/sea-salt (*DSS*), mixed (*MX*) and  
350 undetermined (*UN*). The algorithm (see Figure 2 in Gkikas et al., 2013) operates in three steps and is  
351 applied in each individual 1° x 1° geographical cell within the geographical limits of the study domain  
352 (29° N - 47° N and 11° W - 39° E). First (~~Fig. 1, yellow box~~), the mean (*Mean*) and the associated  
353 standard deviation (*Std*) from the available  $AOD_{550nm}$  retrievals are calculated for the whole study  
354 period. These primary statistics are used for the definition of two threshold levels, which are equal to  
355  $Mean+2*Std$  and  $Mean+4*Std$ . The geographical distributions of the computed statistics (*Mean* and  
356 *Std*) as well as the corresponding spatial patterns of both threshold levels are displayed in Figures S1-a  
357 (MODIS-Terra, Mar. 2000 – Feb. 2013) and S1-b (MODIS-Aqua, 2003 – 2012) in the supplementary  
358 material. At the next step, the algorithm analyzes the daily  $AOD_{550nm}$  timeseries and classifies an  
359 episode as a strong one when  $AOD$  is between the two defined thresholds ( $Mean+2*Std \leq AOD_{550nm} <$   
360  $Mean+4*Std$ ) and as an extreme one when  $AOD$  is higher/equal than  $Mean+4*Std$  (~~cyan boxes~~). The  
361 same approach was undertaken by Gkikas et al. (2009) who classified the Mediterranean aerosol  
362 episodes over the period 2000-2007 according to their strength and described their frequency and  
363 intensity. It must be clarified that according to our methodology in areas frequently affected by dust  
364 episodes, both mean and standard deviation values are expected to be high resulting to high thresholds  
365 which means that cases with moderate-to-high  $AODs$ , also possibly relevant to radiative and health  
366 effects, are masked out from the dataset. In order to investigate the possible impact of this, “unbiased”  
367 mean, standard deviation and thresholds of  $AOD$  are also computed based on another methodology and  
368 the results are discussed comparatively to those of the primary methodology in a separate paragraph.  
369 Moreover, it must be mentioned that the satellite algorithm identifies only intense desert dust episodes  
370 since their  $AOD$  must be higher than  $Mean+2*Std$  which is considered as a high threshold level.

371 It should be noted that the representativeness of the calculated mean levels is possibly affected by  
372 the availability of the  $AOD$  retrievals and particularly by the way these data are distributed both at  
373 temporal and spatial-different temporal scales. Thus, a possible underrepresentation of winter  $AOD$  data  
374 in the long-term dataset, which is often the case in satellite retrievals of  $AOD$ , may result in a smaller  
375 mean  $AOD$  than what would be in case of complete and balanced seasonal availability. ~~It should be~~  
376 noted that ~~Moreover, the spatiotemporal availability of  $AOD$  is determined by the different satellite~~  
377 retrieval algorithm assumptions depending on the underlying surface type (land or sea) and clouds (i.e.  
378 satellite retrievals are possible only under clear skies conditions). In order to investigate the possible  
379 effect of temporal availability of daily  $AOD$  data, ~~To this aim~~, we have calculated the percentage

Formatted: Font: Italic

Formatted: Font: Italic

Formatted: Font: Italic

Formatted: Font: Italic

Formatted: Font: Italic

Formatted: Font: Italic

Formatted: Font: Italic

380 availability of *AOD* retrievals on a monthly, seasonal and year by year basis, over the period 2000-2013  
381 (results not shown here). Seasonal differences of *AOD* availability are mainly encountered in the  
382 northern most parts of the study region, attributed to the enhanced cloud coverage, with lower values  
383 (20 to 40 %) from December to February against 50-85% for the rest of the year. Differences of *AOD*  
384 availability ~~Bare also found between land and sea surfaces are also found differences of *AOD*~~  
385 ~~availability~~ which are more pronounced in winter and summer and less remarkable during the transition  
386 seasons. More specifically, across the Mediterranean Sea, in winter, the availability percentages range  
387 from 70 to 90 % while in summer the corresponding values are decreased, due to Sun glint, down to 60  
388 % and 80 %, respectively. Over land, for both seasons, the spatial patterns of *AOD* availability are  
389 reversed. ~~This is attributed to the enhanced cloud coverage prohibiting the satellite observations. In~~  
390 order to investigate furthermore how the spatiotemporal *AOD* variability and unbalanced seasonal  
391 distribution of MODIS *AOD* data can affect the calculated mean *AOD* levels (calculated by daily  
392 retrievals) we have repeated the calculations by utilizing monthly retrievals (calculated by the daily  
393 ones) thus removing the unequal seasonal contribution to the long-term mean *AOD* values. According  
394 to our results, only small differences are found, generally hardly exceeding 0.1-0.2-0.2 in absolute  
395 and 5% in relative percentage terms, with the mean *AOD*s over land ~~are~~ being higher by up to 10 % when  
396 these ~~ey~~ are computed from daily than monthly data, while the opposite is found over sea. This finding  
397 reveals ~~thus~~ that the unequal temporal distribution of *AOD* retrievals does not have critical impact on  
398 the computed mean *AOD*s and the resulting algorithm outputs presented in this study. The loss of  
399 satellite *AOD* retrievals in winter can affect the statistics and computed long-term *AOD* mean values  
400 and associated thresholds. According to performed computations, such losses of up to 70% daily values  
401 in winter months result in overestimated *AOD* thresholds by up to 4% and 3% for strong and extreme  
402 *DD* episodes. This is small overestimation does not affect essentially the outputs of the present  
403 algorithm, namely the computed frequency and intensity of *DD* episodes. The 4% and 3% are the  
404 maximum possible uncertainties of the algorithm which are encountered in the northernmost parts of  
405 the study region (e.g. Balkans), whereas in the rest of the area corresponding uncertainties are even  
406 much smaller. Nevertheless, this does not essentially affect the algorithm outputs since these regions,  
407 being far away from the dust sources, are not so frequently affected by dust outbreaks, especially given  
408 the significant wet removal of aerosols during this most rainy season of the year. On a year by year  
409 basis, the differences of the *AOD* data's availability are almost negligible.

410 In a further step of the methodology, the strong and extreme *DD* episodes are identified separately  
411 over land and sea surfaces of the study region. This is achieved through the usage of specific aerosol

Formatted: Font: Italic

Formatted: Font: Italic

Formatted: Font: Italic

Formatted: Font: Italic

Formatted: Font: Italic

Formatted: Font: Italic

Formatted: Font: Italic

Formatted: Font: Italic

Formatted: Font: Italic

Formatted: Font: Italic

Formatted: Font: Italic

Formatted: Font: Italic

Formatted: Font: Italic

412 optical properties, namely the Ångström exponent, effective radius, fine fraction and aerosol index,  
413 which provide information about particles' size and nature (~~black box, Figure 1~~). For each optical  
414 property, appropriate upper or lower thresholds have been set up (~~green boxes, Figure 1~~) which must be  
415 valid concurrently in order to certify the presence of dust particles in the atmosphere. Note that there  
416 are not any unanimously defined acknowledged thresholds in literature. Therefore, these cut-off levels  
417 have been selected here according to the literature findings, availability of raw data and several own  
418 sensitivity tests (more details are provided in Gkikas et al., 2013) which have been applied individually  
419 to the MODIS size parameters (i.e.,  $\alpha$ ,  $FF$  and  $r_{eff}$ ). Such analysis is essential when multi-parameter  
420 datasets are utilized and their variations can possibly modify the satellite algorithm's outputs. To this  
421 aim, we have applied the satellite algorithm altering/modifying by 0.1 the  $\alpha$ ,  $FF$  and  $r_{eff}$  values for/within  
422 the ranges 0.6 – 0.8, 0.1 – 0.4 and 0.4 – 0.8, respectively. Our results indicate that the geographical  
423 patterns remain similar and the total number of  $DD$  episodes is only slightly modified (less than 4 %)  
424 for the  $\alpha$  and  $r_{eff}$  retrievals, whereas it changes more for the  $FF$  retrievals (by up to 25% over sea for  
425 strong episodes). On the contrary, the highest sensitivity is found for the  $FF$  retrievals over sea where  
426  $DD$  episodes, particularly the strong ones, are decreased abruptly (> 25 %) even for a small decrease  
427 (0.1) of the  $FF$  cut off level. Here, the validity of these thresholds is further evaluated against  
428 AERONET measurements and the corresponding results are discussed in Section 4.2.1.4.

429 In order to address the issue of possible overestimation of the defined threshold levels, particularly  
430 in the most dust affected areas as it has been mentioned above, we have also applied the satellite  
431 algorithm using an alternative methodology (METHOD-B) in which dust-affected grid cells were  
432 excluded. In this case, from the raw  $AOD$  retrievals we have masked out the “pure” desert dust grid  
433 cells, which were identified based on the concurrent fulfillment of the defined criteria for dust  
434 occurrence in the algorithm (for Ångström exponent, fine fraction, aerosol index and effective radius;  
435 ~~green boxes of Figure 1~~). Then, from the remaining data (non-dust  $AOD$  retrievals), the mean, the  
436 associated standard deviation as well as the defined thresholds of  $AOD$  are computed for the whole  
437 study period, for each pixel, as also done in the primary methodology. Finally, also similarly to the way  
438 done in the primary methodology, the  $DD$  episodes were classified into strong and extreme ones. The  
439 obtained results, i.e. frequency of occurrence and intensity of  $DD$  episodes, based on the primary  
440 methodology and METHOD-B are discussed in Section 4.2. The frequency of occurrence and intensity  
441 of  $DD$  episodes determined with METHOD-B are provided in the supplementary material (Figures S12  
442 and S23) while their differences with regards to the primary methodology are discussed in Section  
443 4.12.

Formatted: Font: Italic

Formatted: English (U.S.)

Formatted: Font: Italic

Formatted: Font: Italic

Formatted: Font: Italic, Subscript

Formatted: Font: Italic

Formatted: Font: Italic

Formatted: Font: Italic

Formatted: Font: Italic, Subscript

Formatted: Font: Italic

Formatted: Font: Italic

Formatted: English (U.S.)

Formatted: Font: Italic

Formatted: Font: Italic, Subscript

Formatted: Font: Italic

Formatted: Font: Italic

Formatted: Font: Italic

Formatted: Font: Italic

Formatted: Font: Italic

444 As explained, a similar methodology and data were used in the study by Gkikas et al. (2013).  
445 Nevertheless, the present one is a significant extension mainly for five reasons: (i) *DD* episodes are  
446 identified here over an extended period of study and for both MODIS platforms, i.e. Mar. 2000 – Feb.  
447 2013 for MODIS-Terra and 2003–2012 – 2012 –for MODIS-Aqua, (ii) a second methodology  
448 (METHOD-B) for the identification of *DD* episodes is tested, (iii) the quality of the input data is  
449 improved by using QA-weighted level-3 data produced by weighting level-2 data based on their  
450 confidence flag instead of regular ones ( $QA \geq 1$ ), (iv) emphasis is given to the vertical structure of the  
451 intense *DD* episodes and (v) the role of the detailed dust outbreaks' vertical structure for the level of  
452 agreement between columnar MODIS *AOD* and ground *PM*<sub>10</sub> concentrations is investigated. Moreover,  
453 ~~the~~ In addition, in the present analysis, the satellite algorithm operates also an improvement of the  
454 methodology consists in the application of our satellite algorithm also using only *AODs* associated with  
455 cloud fractions (*CF*) lower/equal than 0.8, in order to investigate possible modifications of our results  
456 due to the cloud contamination effects on MODIS *AODs*. The critical value of 0.8 for *CF* has been  
457 defined according to Zhang et al. (2005) and Remer et al. (2008), who stated that under extended cloud  
458 coverage conditions *AOD* levels can be increased substantially.

459  
460

#### 461 4. Results

462 Before dealing with the horizontal patterns (sub-section 4.2) and the vertical structure of dust  
463 outbreaks (sub-sections 4.3 and 4.4), it is very important to ~~describe their horizontal patterns (sub-~~  
464 ~~section 4.1) and also to~~ compare the algorithm's outputs against quality AERONET and *PM*<sub>10</sub>  
465 observations (sub-section 4.2.1) in order to ensure an accurate three-dimensional view of the intense  
466 Mediterranean *DD* episodes. It must be clarified, that the comparison of the satellite algorithm's  
467 outputs versus AERONET/*PM*<sub>10</sub> is made only for its default version and not for the METHOD-B, since  
468 between the two methodologies are not found remarkable differences, as it will be presented in Section  
469 4.2. Accordingly, ~~For the same reason~~, the synergistic implementation of the CALIOP-CALIPSO lidar  
470 profiles is done only when the *DD* episodes are identified based on the primary methodology. The  
471 present section has been organized accordingly and the results are given below.

#### 472 4.2.1 Comparison of the satellite algorithm's outputs against AERONET and *PM*<sub>10</sub> measurements

473 The ability of the satellite algorithm to identify satisfactorily *DD* episodes, is tested against ground  
474 measurements from 109 AERONET (Fig. 4.1, orange squares) and 22 *PM*<sub>10</sub> (Fig. 4.1, green triangles)

Formatted: Font: Italic

Formatted: Font: Italic

Formatted: Font: Italic

Formatted: Font: Italic

Formatted: Font: Italic

Formatted: Font: Italic

Formatted: Font: Italic

Formatted: Font: Italic, Subscript

Formatted: Font: Italic

Formatted: Font: Italic

Formatted: Font: Italic

475 stations located in the broader Mediterranean area. This is an extended and thorough comparison which  
476 exceeds largely a similar one done for the outputs of the previous version of satellite algorithm (2000-  
477 2007, Gkikas et al., 2013), but only relying on 9 AERONET stations and using *AOD* and volume size  
478 distribution data. Here, the comparison is repeated for the improved algorithm, being extended over a  
479 longer time period, for a much larger number of AERONET stations, and an analysis of more optical  
480 properties, namely the Ångström exponent, effective radius, single scattering albedo and asymmetry  
481 parameter is made. The comparison is performed for both study periods and satellite platforms (Mar.  
482 2000 – Feb. 2013 for Terra and 2003-2012 – 2012 -for Aqua) while the issue of possible cloud  
483 contamination is also considered. However, since the obtained results revealed a very similar  
484 performance of the algorithm for both periods and platforms, only the results for the period Mar. 2000  
485 – Feb. 2013 are given here.

486 In 46 out of 109 AERONET stations, depicted with yellow triangles in Figure 41, we have found at  
487 least one strong or extreme dust episode, for which coincident satellite and ground measurements are  
488 available. For the specific AERONET stations and episode days, the mean values of the selected  
489 AERONET aerosol optical properties have been calculated separately for strong, extreme and all (both  
490 strong and extreme) *DD* episodes identified by the satellite algorithm. Subsequently, these values were  
491 compared to the corresponding ones calculated from all the available retrievals (climatological  
492 conditions, *clim*) collected from the 109 Mediterranean AERONET stations, during the period Mar.  
493 2000 – Feb. 2013, aiming at highlighting the effect of episodes on these optical properties.  
494 Additionally, in 7 AERONET stations (cyan circles in Figure 41) the intense *DD* episodes have been  
495 identified from ground (AERONET) and the corresponding results are compared with the satellite  
496 algorithm outputs (Section 4.21.1.4). Finally, the performance of the algorithm is also tested against  
497 surface *PM<sub>10</sub>* measurements from 22 stations (Section 4.21.2).

#### 499 4.21.1 AERONET

##### 500 4.12.1.1 Aerosol optical depth

501 During the period Mar. 2000 – Feb. 2013, 346 pixel level intense *DD* episodes have been identified  
502 by the satellite-based algorithm, in which coincident MODIS-Terra and AERONET retrievals are  
503 available. The selected dataset corresponds to 1.06 % of the overall (strong and extreme) *DD* episodes  
504 (32635) which have been identified during the study period. It should be noted that AERONET

Formatted: Font: Italic

Formatted: Font: Italic

Formatted: Font: Italic

Formatted: Font: Italic

Formatted: Font: Italic

Formatted: Font: Italic

Formatted: Font: (Default) Times New Roman, 12 pt

505  $AOD_{550nm}$  values have been calculated from available AERONET  $AOD_{870nm}$  and Ångström exponent  
506 data ( $\alpha_{440-870nm}$ ) by applying the Ångström equation (Ångström, 1929) to match the MODIS  $AOD_{550nm}$ .  
507 For these intense *DD* episodes, the comparison between the satellite and ground aerosol optical depths  
508 at 550 nm is given in Figure 52. Two similar scatterplots with matched MODIS-AERONET data pairs  
509 are given. The first one (Fig. 52 i-a) is resolved by the number of level 2 (*L2*) measurements of 10 km x  
510 10 km spatial resolution from which the compared 1° x 1° level 3 (*L3*) *AODs* in the figure are derived.  
511 The second scatterplot (Fig. 52 i-b) is resolved by the spatial standard deviation inside the 1° x 1°  
512 geographical cell (level 3 *AODs*). Both scatterplots address the issue of level 3 *AOD* sub-grid spatial  
513 variability, which is essential when attempting comparisons against local surface-based *AOD* data like  
514 the AERONET.

Formatted: Font: Italic

Formatted: Font: Italic

Formatted: Font: Italic

515 The overall correlation coefficient (*R*) between MODIS and AERONET *AODs* is equal to 0.505,  
516 with the satellite *AODs* being overestimated (bias=0.143). From the overall scatterplots, it is evident  
517 the existence of outliers associated with small number of level 2 retrievals (<20, blue color Fig. 52 i-a)  
518 and/or high standard deviations (>0.5, yellowish-reddish points, Fig. 52 i-b) inside the *L3* grid cell.  
519 This finding underlines the role of homogeneity and representativeness of *L3* retrievals for the  
520 comparison of MODIS *AODs* against AERONET. This role is better visualized in Fig. 52 ii-a, where  
521 are presented the computed *R* values between MODIS level-3 and AERONET *AODs* depending on the  
522 number of *L2* retrievals from which the *L3* products were derived. In general, it is known that the *L2*  
523 pixel counts range from 0 to 121 while in polar regions (typically around 82° latitude) the maximum  
524 count numbers can be even higher due to overlapping orbits and near nadir views intersect (Hubanks et  
525 al., 2008). It is clear from our results that the correlation coefficients are gradually and essentially  
526 improved, from 0.49 to 0.75, with increasing representativeness of MODIS *AODs*, i.e. increasing  
527 counts of *L2* retrievals attributed. A similar improvement has been reported by Amiridis et al. (2013)  
528 who found a better agreement between MODIS/AERONET and CALIOP aerosol optical depths  
529 applying similar spatial criteria. The agreement between MODIS and AERONET also improves when  
530 the former *AOD* products are more spatially homogeneous, i.e. when they are characterized by smaller  
531 *AOD* standard deviations at the grid-level (from <0.25 down to <0.05, Fig. 52 ii-b). However, our  
532 results also indicate that apart from increasing correlation coefficients (up to 0.7-0.8) with increasing  
533 level-2 counts and decreasing standard deviations, the number of intense *DD* episodes is decreased  
534 dramatically (about 40-50 for more than 50 counts and standard deviation smaller than 0.05).

Formatted: Font: Italic

Formatted: Font: Italic

Formatted: Font: Italic

Formatted: Font: Italic

Formatted: Font: Italic

Formatted: Font: Italic

Formatted: Font: Italic

Formatted: Font: Italic

Formatted: Font: Italic

535 In order to assess the performance of the satellite algorithm when operates with non- (Gkikas et al.,  
536 2013) and weighted QA (present analysis) MODIS-Terra retrievals we have compared its outputs (*DD*

Formatted: Font: Italic

537 episodes' AODs) of both versions versus the corresponding AERONET AODs for the period Mar. 2000  
538 – Feb. 2007 (Gkikas et al., 2013). Based on our results, the computed correlation coefficients are equal  
539 to 0.53 (135 DD episodes) and 0.59 (177 DD episodes) for the old and new version of the satellite  
540 algorithm, respectively, revealing thus a better performance when QA-weighted level 3 retrievals are  
541 utilized as inputs to the satellite algorithm.

Formatted: Font: Italic

Formatted: Font: Italic

Formatted: Font: Italic

Formatted: Font: Italic

542 ~~In addition~~Finally, the spectral variation of the AERONET AODs at 7 wavelengths, from 340 to  
543 1020 nm, in climatological and dust episodes conditions has been investigated (results given in Figure  
544 S3S2, supplementary material). The AOD boxplots produced for all the available daily AERONET  
545 measurements (orange) and for the corresponding retrievals during strong (cyan), extreme (red) and all  
546 DD (green) episodes identified by the satellite algorithm show that the spectral variation of aerosol  
547 optical depth decreases in cases of dust episodes, with respect to the “climatological” conditions. This  
548 is mainly attributed to the further increasing AOD levels at wavelengths longer than 500 nm (by about  
549 6 times) than in (or near) the visible.

Formatted: Font: Italic

550

#### 551 4.2.1.1.2 Aerosol volume size distribution

552 In Figure 63, are presented the mean aerosol volume size distributions (AVSDs) calculated from all  
553 available AERONET data (orange curve) as well as under strong (cyan curve), extreme (red curve) and  
554 all (green curve) DD episodes conditions. The results are given for Mar. 2000 – Feb. 2013 using  
555 MODIS-Terra (346 intense DD episodes) retrievals as inputs to the satellite algorithm. In the  
556 climatological curve, two modes are distinct centered at 0.15  $\mu\text{m}$  for the fine mode and 2.24  $\mu\text{m}$  for the  
557 coarse mode. There is an about equal contribution of both modes, indicating the coexistence of fine  
558 (e.g. urban aerosols) and coarse (e.g. dust aerosols) particles over the broader Mediterranean area. This  
559 result is in agreement with previous studies for the Mediterranean (e.g. Fotiadi et al., 2006; Mallet et  
560 al., 2013). However, under dust episodes conditions, although the AVSD still has two modes, there is a  
561 dramatic increase of the coarse mode, which strongly dominates. More specifically, the peak of the  
562 coarse mode (radius between 1.7 and 2.24  $\mu\text{m}$ ) is increased by factors of about 10, 15 and 11 for the  
563 strong, extreme and all DD episodes. The differences between the strong and extreme AVSDs are  
564 statistically significant (confidence level at 95 %) for almost all size bins (18 out of 22) except bin 1  
565 (0.050  $\mu\text{m}$ ), 2 (0.065  $\mu\text{m}$ ), 6 (0.194  $\mu\text{m}$ ) and 7 (0.255  $\mu\text{m}$ ). Moreover, it should be noted that the  
566 increment factors are slightly decreased when the algorithm operates only with AODs associated with  
567 cloud fractions less than 0.8 which is reasonable since possible “overestimated” retrievals are masked

Formatted: Font: Italic

Formatted: Font: Italic

Formatted: Font: Italic

Formatted: Font: Italic

568 out from the analysis. Similar modifications in the shape of *AVSD* during dust outbreaks have been  
569 pointed out by several studies in the past, either for the Mediterranean region (e.g. Kubilay et al., 2003;  
570 Lyamani et al., 2005; Córdoba-Jabonero et al., 2011) or for other dust affected areas of the planet (e.g.  
571 Alam et al., 2014; Cao et al., 2014).

#### 572 4.2.1.3 *Size optical properties, single scattering albedo and asymmetry parameter*

573 The accuracy of the *DD* episodes identification method was further assessed by also using other  
574 AERONET aerosol optical properties than *AOD*, namely the Ångström exponent ( $\alpha$ ) and the effective  
575 radius ( $r_{eff}$ ), able to provide information about particles' size. For both aerosol optical properties, the  
576 boxplots for all the available AERONET retrievals as well as for the corresponding data during strong,  
577 extreme and all *DD* episodes, have been produced and depicted in Figure S4-S36 (supplementary  
578 material).

579 Based on our results, the appropriateness of the applied methodology is confirmed by the drastic  
580 reduction of  $\alpha$  and increase of  $r_{eff}$  values when dust outbreaks occur. When all available AERONET  
581 retrievals are considered (*clim*), the majority (> 75%) of  $\alpha$  values is higher than 1.04 indicating the  
582 strong presence of fine particles in the study domain (Figure S3-i). On the contrary, during intense dust  
583 episodes the majority of the corresponding values for all and strong *DD* episodes are lower than 0.54  
584 while for the extreme ones are lower than 0.36. Such low Ångström exponent values, attributed to  
585 transported mineral particles from the northern African deserts (Pace et al., 2006), have been reported  
586 also in previous studies (e.g. Tafuro et al. 2006; Basart et al., 2009). The existence of coarse aerosols is  
587 also confirmed by the increase of  $r_{eff}$  values under intense *DD* conditions compared to the  
588 climatological levels (Figure S3-ii). For all *DD* episodes, the 75% of  $r_{eff}$  values is higher than 0.55  $\mu\text{m}$   
589 reaching up to 1.4  $\mu\text{m}$ , while the mean and the median values are equal to about 0.73, compared to  
590 about 0.37 for the climatological conditions. These values are even higher when extreme *DD* episodes  
591 are concerned.

592 Moreover, the spectral variations of the averaged AERONET single scattering albedo (*SSA*) and the  
593 asymmetry parameter ( $g_{aer}$ ) are also studied. During intense dust outbreaks the shape and magnitude of  
594 spectral *SSA* (Figure S574-i) and  $g_{aer}$  (Figure S574-ii) are modified compared to the climatological  
595 conditions. The spectral curves of both parameters become less and more flattened during dust episodes  
596 for *SSA* and  $g_{aer}$ , respectively. For *SSA*, the steepening results from decreasing values in the visible and  
597 increasing values in the near-infrared (by up to 0.04, reaching 0.97 at 1020 nm). The flattening for  $g_{aer}$   
598 arises from smaller and larger increments in visible and near-infrared values, by up to 0.04 and 0.0709,

Formatted: Font: Italic

Formatted: Font: Italic

Formatted: Font: Italic

Formatted: Font: Italic

Formatted: Font: Italic

Formatted: Font: Italic

Formatted: Font: Italic



599 | respectively. The differences between strong and extreme *DD* episodes *SSA* spectral curves are  
600 | statistically significant at 95 % confidence level only at 870 and 1020 nm. On the contrary, the  
601 | corresponding differences for the  $g_{aer}$  are statistically significant in all wavelengths. Our results are in  
602 | agreement with those presented for *SSA* by Mallet et al. (2013) in the Mediterranean and for  $g_{aer}$  by  
603 | Alados-Arboledas et al. (2008) during a dust episode over the southeastern parts of Spain.

Formatted: Font: Italic

604

605 | *4.2.1.4 Intercomparison of surface-based and satellite algorithms used for the identification of the*  
606 | *desert dust episodes*

607 | Despite their great usefulness, satellite aerosol retrievals still suffer from uncertainties, and  
608 | generally are considered as inferior to surface-based similar products, which are taken as the reference.  
609 | In order to examine this degree of uncertainty and to verify the successful performance of the  
610 | algorithm, we also tested using it along with AERONET retrievals. This has been made for 7  
611 | Mediterranean AERONET stations, depicted with cyan circles in Figure 41, during the periods for  
612 | which ground retrievals are available (Table 1). The selection of the AERONET stations was based on:  
613 | (i) data availability (see last column of Table 1), (ii) their location (i.e. near to the Northern African and  
614 | Middle East deserts) and (iii) the inclusion of sites where the aerosols' regime is complex (e.g. El  
615 | Arenosillo, FORTH Crete). The intense *DD* episodes were identified following the methodology  
616 | described in section 3, but using only *AOD* at 870 nm,  $\alpha_{440-870nm}$  (lower/equal than 0.7) and  $r_{eff}$  (higher  
617 | than 0.6) as criteria, based upon their availability from AERONET. Subsequently, the algorithm was  
618 | also operated again using satellite (MODIS-Terra, OMI-Aura, EP-TOMS) input data for the days with  
619 | available retrievals in each of the 7 AERONET stations.

Formatted: Font: Italic

620 | In Figure 74, we present the overall scatterplots between satellite and ground *AODs* when intense  
621 | *DD* episodes have been identified based on the ground (left column) and the satellite (right column)  
622 | algorithm. Colors in Figs. 74 i-a, 74 ii-a, 74 iii-a represent the associated MODIS-Terra Ångström  
623 | exponent, effective radius and day cloud fraction (*CFD*) retrievals, respectively. In Figs. 74 i-b and 74  
624 | ii-b colors represent the AERONET Ångström exponent and effective radius, respectively, while in  
625 | Figure 74 iii-b represent the day cloud fraction observations derived by MODIS-Terra. Through this  
626 | approach it is feasible to assess furthermore the performance of the satellite algorithm, specify its  
627 | drawbacks and check the validity of the defined thresholds (green boxes in Figure 42 in Gkikas et al.,  
628 | (2013)).

Formatted: Font: Italic

Formatted: Font: Italic

629 | It is apparent that the agreement between MODIS-Terra and AERONET *AODs* is better when *DD*  
630 | episodes are identified from the ground, as shown by the increased correlation coefficients (from 0.521  
631 | to 0.704), increased slopes (from 0.6 to 0.9-1.0) and decreased biases (from 0.16 to -0.03). In  
632 | particular, when *DD* episodes are identified from space, the MODIS-Terra *AOD* retrievals are  
633 | overestimated (bias=0.163) with regards to AERONET, particularly at low *AOD* values (<0.5). In both  
634 | algorithms, the highest overestimations are associated with cloud fractions higher than 0.7 due to the  
635 | possible contamination of the satellite *AODs* by clouds (Figure 74 iii-a, iii-b). Given that *DD* episodes'  
636 | identification based on AERONET retrievals is more efficient, we have used these results in order to  
637 | check the validity of the defined thresholds for  $\alpha$ , *AI*, *FF* and  $r_{eff}$  (green boxes in Figure 1) used in the  
638 | satellite algorithm. For each aerosol optical property, it has been calculated the percentage of intense  
639 | *DD* episodes for which the corresponding satellite observations are below or above the defined  
640 | thresholds, depending on the parameter. The results given in Table 2 are satisfactory, since the  
641 | percentages range from 87 to 99%, and confirm the validity of the defined thresholds.

Formatted: Font: Italic

Formatted: Font: Italic

Formatted: Font: Italic

Formatted: Font: Italic

642 | The scatterplots in Figs. 74 i-b and ii-b also reveal some weaknesses of the satellite-based  
643 | algorithm. More specifically, it is found that for few *DD* episodes identified by the satellite algorithm  
644 | the corresponding AERONET Ångström exponent and effective radius values are higher than 1 and  
645 | smaller than 0.4, respectively. These values indicate a predominance of fine particles instead of coarse  
646 | ones as it would be expected for desert dust aerosols. In order to quantify the number of misclassified  
647 | pixel level intense *DD* episodes by the satellite algorithm, we have computed the percentage of cases  
648 | for which the AERONET  $\alpha$  values are higher than 1 (15%) and  $r_{eff}$  values are lower than 0.4 (17.7%).  
649 | Also, we have repeated these calculations for all *DD* episodes (Section 4.2.1.1) and the corresponding  
650 | percentages were found to be equal to 11.8% and 14.5%, respectively. These misclassifications of the  
651 | satellite algorithm occur in AERONET stations (e.g. Thessaloniki, Rome, Avignon) with a strong  
652 | presence of anthropogenic aerosols (Kazadzis et al., 2007; Gobbi et al., 2007; Querol et al., 2009a;  
653 | Yoon et al., 2012). Some misclassifications also occur in AERONET stations (e.g. Evora, El  
654 | Arenosillo, FORTH CRETE) with mixed (natural plus anthropogenic) aerosol loads (Fotiadi et al.,  
655 | 2006; Toledano et al., 2007b; Hatzianastassiou et al., 2009; Pereira et al., 2011). Over these areas, there  
656 | are converging air masses carrying particles of different origin, as shown by performed back-  
657 | trajectories analyses (results are not shown here) using the HYSPLIT (HYbrid Single-Particle  
658 | Lagrangian Integrated Trajectory) model (Draxler and Rolph, 2015). Nevertheless, it must be  
659 | mentioned that *DD* episodes' misclassifications can be also attributed to the lower accuracy of MODIS  
660 | aerosol size retrievals over land (Section 2.1.1).

Formatted: Font: Italic

Formatted: Font: Italic

Formatted: Font: Italic

Formatted: Font: Italic

661

662 | 4.2.2+1.2  $PM_{10}$  and dust contribution

663 The satellite algorithm's outputs, apart from AERONET retrievals, have been also compared  
664 against ground  $PM_{10}$  concentrations ( $\mu\text{g m}^{-3}$ ) measured in 22 Mediterranean stations (green triangles in  
665 Figure 41).

666 First, for each station, the number of intense  $DD$  episodes was calculated, for which coincident  
667 satellite and ground measurements (total  $PM_{10}$ ) are available (Figure 85-i). The number of concurrent  
668  $DD$  episodes varies from 3 to 53, being in general decreasing from southern to northern stations. For 14  
669 out of 22 stations, where at least 10 intense  $DD$  episodes were identified by the satellite-based  
670 algorithm, we have computed the correlation coefficients between satellite  $AODs$  and surface total  
671  $PM_{10}$  concentrations (Fig. 85-ii). The highest  $R$  values (up to 0.8) are recorded in the central and  
672 eastern parts of the Mediterranean while the lowest ones are found in the western stations. It must be  
673 noted that the correlation coefficients are affected by outliers, because of the limited number of  $DD$   
674 episodes in each station, highlighting the sensitiveness of the intercomparison. Such outliers can be  
675 expected when satellite-based columnar  $AODs$  and surface-based  $PM_{10}$  data are compared, since  
676 satellite  $AODs$  are representative for the whole atmospheric column in contrast to in-situ  $PM$   
677 measurements which are more representative for the lowest part of the planetary boundary layer  
678 affected also by local factors. Therefore, the vertical distribution of desert dust load, as it will be  
679 presented in the next sections, can determine the level of agreement between satellite  $AODs$  and surface  
680  $PM$  concentrations. ~~Another influencing factor can be cloud contamination of MODIS  $AOD$ .~~

681 The identification method by the satellite algorithm can be considered as correct when dust  $PM_{10}$   
682 concentrations are higher than zero (i.e. dust has been recorded at the station). According to this, the  
683 ratio between the number of non-zero dust  $PM$  observations and the number of  $DD$  episodes  
684 (coincident satellite-derived  $DD$  episodes and total  $PM_{10}$  measurements) for each station is defined as  
685 success score. The calculated success scores (Figure 85-iii) vary from 68% (Monagrega, northeastern  
686 Spain, 28 episodes) to 97% (Bocadifalco, Sicily, 33 episodes) confirming the appropriateness of the  
687  $DD$  episodes' identification. In the majority of stations, the contribution of dust particles to the total  
688 burden (Figure 85-iv) is above 50%, ranging from 44% (Zarra, Spain) to 86.8% (Ayia-Agia Marina,  
689 Cyprus). In order to complete our analysis we have also calculated the mean (Figure 85-v) and the  
690 median (Figure 85-vi) dust  $PM_{10}$  concentrations for the identified intense  $DD$  episodes in each station.  
691 The mean  $PM_{10}$  concentrations mainly vary between 20 and 50  $\mu\text{g m}^{-3}$ , being higher in the southern

Formatted: Font: Italic

Formatted: Font: Italic

Formatted: Font: Italic

Formatted: Font: Italic

Formatted: Font: Italic

Formatted: Font: Italic

Formatted: Font: Italic

Formatted: Font: Italic

Formatted: Font: Italic

Formatted: Font: Italic

Formatted: Font: Italic

Formatted: Font: Italic

Formatted: Font: Italic

Formatted: Font: Italic

Formatted: Font: Italic

Formatted: Font: Italic

Formatted: Font: Italic

Formatted: Font: Italic

Formatted: Font: Italic

Formatted: Font: Italic

692 stations, as expected. The minimum mean value ( $17 \mu\text{g m}^{-3}$ ) was recorded in Censt (Sardinia) and the  
693 maximum one ( $223 \mu\text{g m}^{-3}$ ) in Aygia Marina (Cyprus). Our values are much higher than the  
694 corresponding ones in Querol et al. (2009b), who obtained that the mean levels of mineral matter in  
695  $PM_{10}$  during dusty days range from 8 to  $23 \mu\text{g m}^{-3}$  based on ground concentrations derived by 21  
696 Mediterranean stations. These differences are reasonable since here only intense desert dust outbreaks  
697 associated with high aerosol optical depths are considered. Finally, the median  $PM_{10}$  concentrations are  
698 lower compared to the average ones, indicating that outliers (cases with extremely high AOD or  $PM_{10}$ )  
699 can alter the results, attributed to the fact that both parameters' (AOD and  $PM_{10}$ ) distributions are not  
700 Gaussians. For this reason the highest differences are found in Finokalia (Crete) and Agia Marina  
701 (Cyprus), where the maximum daily  $PM_{10}$  concentrations, equal to 690 and  $1291 \mu\text{g m}^{-3}$ , respectively,  
702 were recorded during an intense dust outbreak affected the eastern Mediterranean on 24 and 25  
703 February 2006.

Formatted: Font: Italic

Formatted: Font: Italic

Formatted: Font: Italic

Formatted: Font: Italic

Formatted: Font: Italic

#### 704 4.12 2D geographical distributions of desert dust episodes' frequency and intensity

705 The mean geographical distributions of strong and extreme  $DD$  episodes' frequency of occurrence  
706 (episodes  $\text{yr}^{-1}$ ) are presented in Figure 26. Results are given separately as obtained from MODIS-Terra  
707 and Aqua for the periods Mar. 2000 – Feb. 2013 and 2003 – 2012, corresponding to local late morning-  
708 to-noon (Terra) and afternoon (Aqua) conditions, respectively. It is evident a gradual reduction of  
709 frequencies from south to north, while for the strong  $DD$  episodes also appears a west to east  
710 decreasing gradient. The decreasing south-to-north gradient of intense  $DD$  episodes' frequency, which  
711 is also in agreement with previous studies based on ground  $PM$  measurements (Querol et al., 2009b;  
712 Pey et al., 2013), model simulations (Papayannis et al., 2008; 2014) and AERONET AOD retrievals  
713 (Basart et al., 2009), can be attributed to the increasing distance from the major dust sources and to the  
714 higher precipitation amounts at the northern parts of the basin (e.g. Marrioti et al., 2002; Mehta and  
715 Yang, 2008).

Formatted: Font: Italic

Formatted: Font: Italic

Formatted: Font: Italic

Formatted: Font: Italic

716 The maximum frequencies ( $9.9 \text{ episodes yr}^{-1}$ ) of strong  $DD$  episodes are observed in the western  
717 parts of the study region, for both periods and datasets, while the corresponding values for the extreme  
718 ones ( $3.3 \text{ episodes yr}^{-1}$ ) are observed over the central Mediterranean Sea for MODIS-Terra (Mar. 2000  
719 – Feb. 2013). In general, there is similar spatial variability between Terra and Aqua, though slightly  
720 lower maximum frequencies are found for Aqua. Although dust episodes occur rarely across the  
721 northern parts of the study region ( $< 1$  and  $0.5 \text{ episode yr}^{-1}$  for strong and extreme episodes), their  
722 occurrence proves that dust particles can be transported far away from their sources, up to the central

Formatted: Font: Italic

723 (e.g. Klein et al., 2010) or even northern (e.g. Bègue et al., 2012) European areas under favorable  
724 meteorological conditions. Our calculated frequencies are significantly lower than the corresponding  
725 ones obtained in Pey et al. (2013), who studied the African dust intrusions towards the Mediterranean  
726 basin, based on ground  $PM$  concentrations, over the period 2001 – 2011. The observed  
727 declinationsviations between the two studies are mainly attributed to the different thresholds definition  
728 and hence nature of dust episodes. Here, focus is given on the intense dust outbreaks (intensity  
729 equal/higher than  $AOD_{Mean} + 2 * Std$ ) while in Pey et al. (2013) the dust occurrences were identified  
730 even at very low concentrations ( $> 1 \mu g m^{-3}$ ). ~~Apart from the threshold definitions, other reasons which~~  
731 ~~can contribute to these aforementioned discrepancies are that the satellite retrievals are not continuous,~~  
732 ~~in contrast to  $PM$  measurements, as well as that from columnar retrievals (e.g. MODIS) the~~  
733 ~~identification of “pure” dust conditions, particularly in areas like the Mediterranean where different~~  
734 ~~aerosol types coexist, in many cases is not feasible.~~

Formatted: Font: Italic

Formatted: Font: Italic

Formatted: Font: Italic

Formatted: Superscript

Formatted: Font: Italic

735 A noticeable difference between the two study periods and platforms is that relatively high  
736 frequencies of extreme  $DD$  episodes are recorded in more northern latitudes in the Mediterranean Sea,  
737 i.e. up to  $43^\circ N$ , according to MODIS-Terra over Mar. 2000 – Feb. 2013, while they are restricted  
738 south of  $40^\circ N$  parallel for MODIS-Aqua during 2003-~~2012~~ – 2012. In order to investigate this  
739 difference in detail we have also applied the satellite algorithm, over the period 2003-~~2012~~ – 2012, i.e. that of  
740 Aqua, using MODIS-Terra retrievals as inputs. Through this analysis (~~results not shown here~~Figures  
741 ~~S345 and S456 in the supplementary material~~), it is evident that there is a very good agreement  
742 between the satellite algorithm’s outputs, for the periods Mar. 2000 – Feb. 2013 and 2003-~~2012~~ – 2012,  
743 revealing a constant dust episodes’ regime. Therefore, the discrepancy appeared between MODIS-  
744 Terra and MODIS-Aqua spatial distributions, is attributed to the diurnal variation of factors regulating  
745 the emission and transport of dust particles from the sources areas. Schepanski et al. (2009), analyzed  
746 the variation of the Saharan dust source activation throughout the day, based on MSG-SEVIRI satellite  
747 retrievals, reporting that dust mobilization is more intense in the local early morning hours after  
748 sunrise. Note, that desert dust episodes over the period Mar. 2000 – Feb. 2013 have been identified  
749 based on observations retrieved by the Terra satellite, which flies over the study region around noon in  
750 contrast to Aqua which provides aerosol measurements at early afternoon hours.

Formatted: Font: Italic

751 The analysis has been also repeated (results not shown here) considering as inputs to the satellite  
752 algorithm only  $AODs$  associated with cloud fractions lower/equal than 0.8, in order to investigate  
753 possible modifications to our results (~~Figs 2 and 3~~) due to the cloud contamination effect. As it  
754 concerns the strong  $DD$  episodes, the geographical distributions are similar with those of Fig. ~~26~~, but

Formatted: Font: Italic

755 the maximum frequencies (recorded in Morocco) are higher by up to 2 episodes yr<sup>-1</sup> and 0.3 episodes  
756 yr<sup>-1</sup> for the MODIS-Terra (Mar. 2000 – Feb. 2013) and MODIS-Aqua (2003-2012) data set,  
757 respectively. On the contrary, in the case of extreme *DD* episodes the maximum frequencies decrease  
758 to 2.5 episodes yr<sup>-1</sup> for the period 2003-~~2012~~ – 2012 –and they shift southwards, namely over the  
759 northern coasts of Africa, while over the central parts of the Mediterranean Sea are lower than 1  
760 episode yr<sup>-1</sup>.

Formatted: Font: Italic

761 The maps of intensities (in terms of  $AOD_{550nm}$ ) of *DD* episodes (Figure 37), show that for both  
762 study periods and satellite platforms, the maximum intensities are over the Gulf of Sidra and the  
763 Libyan Sea, along the northern African coasts. These intensities reach *AODs* up to about 1.5 for strong  
764 and 4.1 for extreme episodes, while the minimum ones (values down to 0.25-0.46) are recorded in the  
765 northern and western Mediterranean parts. Note that dissimilar spatial patterns appear between the  
766 geographical distributions of *DD* episodes' frequency and intensity, indicating that these two features  
767 are determined by different factors (e.g. tracks or strength of depressions). Finally, when the cloud  
768 contamination is minimized using only *AODs* associated with *CF* lower than 0.8, then the maximum  
769 intensities are shifted southwards, across the northern Africa and eastern coasts of the Mediterranean,  
770 being lower than 1 and 2 for strong and extreme *DD* episodes, respectively. Through the rejection of  
771 possibly overestimated *AODs* from the dataset, it is found that the threshold levels are decreased  
772 (mainly over the most frequently dust affected areas) since both mean and standard deviation values are  
773 lower (results not shown here). Nevertheless, even though these *AODs* can be overestimated, in the  
774 majority of the cases the collocated AERONET *AODs* are high (but lower than the satellite  
775 observations) indicating the occurrence of desert dust outbreaks as it ~~will~~has be shown in Section  
776 4.2.1.4.

Formatted: Font: Italic

Formatted: Font: Italic

Formatted: Font: Italic

777 The analysis has been also repeated applying the alternative METHOD-B described in Section 3.  
778 Just to ensure a longer temporal coverage, this analysis was done for the period Mar. 2000- - Feb.  
779 ~~2013~~Feb. 2013 using MODIS-Terra data. The obtained results for the frequency of occurrence as well  
780 as for the intensity of *DD* episodes are depicted in Figures ~~S1-S7~~ and ~~S2S8~~, respectively, in the  
781 supplementary material. The geographical patterns for the frequency of occurrence between the two  
782 methodologies are similar; however, the maximum values for the strong and extreme *DD* episodes can  
783 reach up to 13.3 episodes year<sup>-1</sup> (Fig. ~~S1S7~~-i) and 8.1 episodes year<sup>-1</sup> (Fig. ~~S1S7~~-ii), respectively. As it  
784 concerns the intensity, the geographical patterns, particularly for the strong *DD* episodes, are dissimilar  
785 and less distinct compared to the corresponding ones obtained with the primary methodology. This  
786 difference is attributed to the inclusion of more dust episodes with variable intensity, which leads to a

Formatted: Font: Italic

Formatted: Font: Italic

Formatted: Font: Italic

787 not so clear “signal” when all these episodes are averaged. Based on METHOD-B, the maximum  
788 intensities (in terms of  $AOD_{550nm}$ ) of strong  $DD$  episodes can reach up to 1 (Fig. S2S8-i) while for the  
789 extreme episodes (Fig. S2S8-ii) it can be as large as 3. The main finding, based on the intercomparison  
790 of the two methodologies for the identification of  $DD$  episodes, is that the frequency of the episodes is  
791 higher for the METHOD-B with respect to the primary methodology, while the intensity is decreased.  
792 Both facts are expected and can be explained by the lower calculated  $AOD$  thresholds with METHOD-  
793 B thus yielding more  $DD$  episodes of lower intensity.

Formatted: Font: Italic

Formatted: Font: Italic

Formatted: Font: Italic

794

#### 795 4.3 Vertical structure of the Mediterranean desert dust outbreaks

796 The ability of the developed satellite algorithm to detect intense dust episodes has been proved  
797 adequate through the comparison analysis against AERONET retrievals and  $PM_{10}$  concentrations  
798 (Section 4.1). Nevertheless, its main limitation is that it uses columnar satellite retrievals and not  
799 vertical resolved data prohibiting thus the description of the vertical structure of these dust outbreaks.  
800 In order to address this issue, the CALIOP-CALIPSO retrievals are used as a complementary tool to  
801 the satellite algorithm’s outputs. First, for the identified dust episodes by the satellite algorithm, the  
802 spatially and temporally collocated vertically resolved CALIOP lidar observations are selected. For  
803 these cases and for each  $1^\circ \times 1^\circ$  grid cell, we have divided the lower troposphere, up to 8 km, in 16  
804 layers of 500 meters height. In this way, 14400 boxes of  $1^\circ \times 1^\circ$  surface area and 500 meters height  
805 have been produced. Then, for each one of them, we have calculated the overall number of dust and  
806 polluted dust observations (hereafter named as dust) according to the aerosol subtyping scheme of the  
807 CALIOP Vertical Feature Mask ( $VFM$ ). Note that dust and polluted dust were chosen because in  
808 previous studies (Mielonen et al., 2009) they were shown to be the best two defined aerosol types  
809 among the other ones classified by the CALIOP  $VFM$ . Nevertheless, in case of polluted dust, Burton et  
810 al. (2013) reported that dust particles can be mixed with marine aerosols instead of smoke or pollution  
811 as assumed by the  $VFM$  retrieval algorithm. In our study, more than 95% of the aerosol type records  
812 were pure dust, for the collocated cases between the satellite algorithm and CALIPSO observations. In  
813 addition, in the majority of the defined boxes, the percentage of dust from the overall observations is  
814 higher than 70%, confirming furthermore the validity of the algorithm  $DD$  episodes’ identification  
815 procedure. This is an excellent proof of the successful identification of  $DD$  episodes by the satellite  
816 algorithm, since CALIOP-CALIPSO is an independent and vertically resolved platform and database.

Formatted: Font: Italic

Formatted: Font: Italic

Formatted: Font: Italic

Formatted: Font: Italic

Formatted: Font: Italic

Formatted: Font: Italic

817 Thereby, CALIOP vertical observations were subsequently used to examine the vertical structure of  
818 dust outbreaks.

819 In order to analyze the intensity of desert dust outbreaks at different altitudes in the troposphere, the  
820 CALIOP data of the total backscatter coefficient at 532 nm ( $\beta_{532nm}$ ) have been also acquired. For each  
821 box, the average  $\beta_{532nm}$  values have been calculated from all the available CALIOP measurements (day  
822 and night), for the identified intense dust episodes by the satellite algorithm. More specifically, the  
823 average  $\beta_{532nm}$  values were calculated for the dust observations based on the CALIOP *VFM* associated  
824 with *CAD* scores ranging from -100 to -20, as it has been proposed by Winker et al. (2013) for  
825 discriminating aerosol from clouds. The selection of  $\beta_{532nm}$  values instead of extinction coefficients  
826 ensures that incorrect lidar ratio assumptions in the CALIOP retrieval algorithm do not affect our  
827 results. In the literature, it has been documented that the CALIOP lidar ratio is underestimated over the  
828 northern African deserts and the surrounding areas affected by Saharan dust particles, leading to an  
829 underestimation of the columnar *AOD* compared to MODIS and AERONET retrievals (Redemann et  
830 al., 2012; Schuster et al., 2012). Amiridis et al. (2013) stated that an increase of the lidar ratio from 40  
831 to 58 sr, along with a series of post-corrections in the CALIOP retrievals and the implementation of  
832 several criteria concerning the cloud coverage and the spatial representativeness, can improve  
833 substantially the agreement between MODIS-Aqua/AERONET and CALIOP observations.

834 It should be noted that in the present work, we have analyzed all the available CALIOP overpasses  
835 (~ 10000) over the study region, during the period Jun. 2006 – Feb. 2013. For brevity reasons,  
836 however, only the obtained results based on MODIS-Terra retrievals are presented here, since similar  
837 findings are drawn for MODIS-Aqua (Jun. 2006 – Dec. 2012). Moreover, the analysis (results are not  
838 shown here) has been made separately for the identified strong and extreme *DD* episodes without  
839 revealing remarkable differences in the geometrical characteristics of dust outbreaks. Nevertheless, the  
840  $\beta_{532nm}$  values are higher for the extreme *DD* episodes being consistent with the discrimination of dust  
841 episodes' intensity (in terms of *AOD*) which is applied to the satellite algorithm. In order to facilitate  
842 the visualization of our results, for each column ( $1^\circ \times 1^\circ$  spatial resolution) and latitudinal/longitudinal  
843 zone ( $1^\circ$  degree), we have calculated the overall number of dust observations and the associated  
844 weighted averages of  $\beta_{532nm}$ , depending on the projection plane (latitudinal, longitudinal and columnar),  
845 according to dust observations in each box. For both parameters, the analysis has been made on an  
846 annual and seasonal basis and the corresponding results are discussed in Sections 4.3.1 and 4.3.2,  
847 respectively.

Formatted: Font: Italic

Formatted: Font: Italic

Formatted: Font: Italic

Formatted: Font: Italic



849 *4.3.1 Annual characteristics*

850 In Figure 98, are presented the three dimensional structures of the CALIOP overall dust  
851 observations (Fig. 98-i) and the associated total backscatter coefficients at 532 nm (Fig. 98-ii), during  
852 intense dust episodes conditions, over the broader Mediterranean area, for the period Jun. 2006 – Feb.  
853 2013. From the latitudinal projection in Fig. 98-i, it is evident that dust particles are mainly detected  
854 between 0.5 and 6 km, and more rarely up to 8 km, between the parallels 32° N and 38° N. The number  
855 of dust observations is increased at higher altitudes with increasing latitudes, up to 40° N, while the  
856 altitude range (thickness) where these records are detected is gradually reduced from 4 to 2 km. At  
857 northern latitudes, the CALIPSO dust records are drastically reduced and are mainly observed between  
858 1 and 4 km. The ascending mode of the transported mineral particles over the Mediterranean is  
859 attributed to the prevailing low pressure systems, which mobilize and uplift dust particles from the  
860 source areas across the Sahara Desert and the Arabian Peninsula. Dust aerosols are transported over the  
861 planetary boundary layer (Hamonou et al., 1999) due to the upward movement of dry and turbid air  
862 masses (Dulac et al., 1992), while the prevailing synoptic conditions determine also the spatial and  
863 temporal characteristics of desert dust outbreaks over the Mediterranean (Gkikas et al., 2014, 2015).

864 In general, our results are in agreement with previous studies, based on lidar profiles, which have  
865 been made in several Mediterranean sites. More specifically, Papayannis et al. (2008) found that dust  
866 layers, over the EARLINET Mediterranean stations, extend from 0.5 to 10 km above mean sea level,  
867 their center of mass is located between 2.5 and 3.5 km and their thickness ranges from 2.1 to 3.3 km.  
868 Hamonou et al. (1999) reported that dust layers are mainly detected between 1.5 and 5 km based on  
869 lidar measurements in the northwestern and northeastern Mediterranean. According to di Sarra et al.  
870 (2001), who studied the Saharan dust intrusions in Lampedusa (central Mediterranean) for the period  
871 May-June 1999, dust particles can be detected up to 7-8 km, which is in line with our findings for the  
872 corresponding latitudinal zones (35° N - 36 ° N). Balis (2012), analyzed 33 Raman/lidar profiles of  
873 Saharan dust intrusions over Thessaloniki (northern Greece), and found that the mean base and top of  
874 dust layers were equal to  $2.5 \pm 0.9$  and  $4.2 \pm 1.5$  km, respectively.

875 As to the variation of vertical extension with longitude (Fig. 98-i), it is revealed that the base height  
876 of dust layers is decreased towards the eastern parts of the study region. In the western Mediterranean,  
877 the mineral particles are mainly detected between 2 and 6 km while over the central and eastern  
878 Mediterranean the corresponding altitudes are equal to 0.5 and 6 km, respectively. It is well known,

879 that dust is transported over the western Mediterranean mainly in summer (e.g. Moulin et al., 1998)  
880 favored by low pressure systems located over the northwestern Africa (Gkikas et al., 2014<sup>5</sup>) and the  
881 enhanced thermal convection, uplifting effectively dust aerosols at high altitudes in the troposphere.  
882 Moreover, air masses carrying dust particles are “convected” towards higher altitudes due to the  
883 existence of the Atlas Mountains Range. Therefore, the combination of strong convective processes  
884 over North Africa along with topography can explain the identification of dust aerosols at higher  
885 tropospheric levels over the western Mediterranean. It is the presence of mineral particles at high  
886 altitudes in western Mediterranean that can explain the poor-to-moderate agreement between  $PM_{10}$   
887 concentrations and MODIS  $AODs$  found in the Iberian Peninsula (Fig. 85-ii). In order to give a better  
888 insight to how the dust outbreaks’ vertical extension can affect the level of agreement between  
889 columnar  $AOD$  satellite retrievals and ground  $PM_{10}$  concentrations, emphasis is given at specific dust  
890 events and the relevant findings will be discussed in section 4.4. In the central and eastern parts of the  
891 Mediterranean basin, air masses carrying African dust aerosols travel at lower altitudes over Africa  
892 because of absence of significant topographical objects on their route, as suggested by Pey et al.  
893 (2013).

Formatted: Font: Italic

Formatted: Font: Italic

894 Previous studies have shown that dust layers over the Mediterranean are characterized by a  
895 multilayered structure (e.g. Hamonou et al., 1999; Mona et al., 2006; Papayannis et al., 2008). This is  
896 also depicted in the longitudinal projection of Figure 98-i, where several dust layers of different  
897 base/top altitudes and geometrical thicknesses are detected. In general, the base heights vary from 0.5  
898 to 2 km, the top heights from 4 to 6 km and the thicknesses from 1 to 4 km. The majority of common  
899 observations between the CALIOP profiles and the identified intense  $DD$  episodes by the satellite  
900 algorithm are recorded over the maritime parts of the study region (bottom map of Fig. 89-i). The  
901 maximum number of CALIOP dust observations ( $\sim 19000$ ) is recorded along the Atlantic coasts of  
902 Morocco, but high numbers (about 10000 – 15000) are also found across the northern African coasts.

Formatted: Font: Italic

903 Apart from the CALIOP dust observations, we have also analyzed the associated  $\beta_{532nm}$  values at  
904 the defined altitude ranges in order to describe the variation of intensity of the desert dust episodes with  
905 height over the Mediterranean (Fig. 89-ii). The maximum backscatter coefficients (up to  $0.006 \text{ km}^{-1} \text{ sr}^{-1}$ ) are observed below 2 km, being increased towards the southern edges ( $30^\circ \text{ N} - 34^\circ \text{ N}$ ) of the study region, close to dust source areas.  
906 ~~The maximum backscatter coefficients (up to  $0.006 \text{ km}^{-1} \text{ sr}^{-1}$ ) are observed below 2 km, being increased towards the southern edges ( $30^\circ \text{ N} - 34^\circ \text{ N}$ ) of the study region, where their source areas are found.~~  
907 This is explained by the fact that dust particles due to their coarse  
908 size and large mass, are efficiently deposited and for this reason they are recorded at higher  
909

911 concentrations near to the source areas and at low altitudes. Nevertheless, the decreasing intensity with  
912 height towards the north is not so evident. Thus, high  $\beta_{532nm}$  values ( $\sim 0.004 \text{ km}^{-1} \text{ sr}^{-1}$ ) are observed  
913 between 2 and 4 km in the latitudinal zone extending from  $35^\circ \text{ N}$  to  $42^\circ \text{ N}$ . Though, the uppermost  
914 altitudes where relatively high  $\beta_{532nm}$  values gradually decrease from 6 to 4 km, moving from south to  
915 north. Any differences in the latitudinal patterns of dust observations and backscatter values (Figs 98-i  
916 and 98-ii) can be explained by the fact that  $\beta_{532nm}$  values take into account only the dust records and not  
917 the overall observations (all aerosol types).

918 The decrease of backscatter values at higher altitudes has been pointed out in previous studies  
919 where lidar profiles have been analyzed over specific Mediterranean locations (e.g. Mona et al., 2006;  
920 Papayannis et al., 2008). Nevertheless, it must be considered that in the aforementioned studies the  
921 lidar measurements are valid above the retrieved planetary boundary layer (Matthias et al., 2004) which  
922 varies depending on the location and the season (McGrath-Spangler et al., 2013). Despite the good  
923 agreement, as it concerns the vertical shape of the  $\beta_{532nm}$  curves, between our findings and the  
924 corresponding ones based on ground retrievals, in the present analysis the calculated backscatter  
925 coefficients are in general higher, which is reasonable since are considered only cases of intense desert  
926 dust outbreaks.

927 The longitudinal pattern of  $\beta_{532nm}$  profiles (Fig. 98-ii) is less distinct compared to the corresponding  
928 one resulted from the latitudinal projection. Relatively high  $\beta_{532nm}$  values ( $\sim 0.004 \text{ km}^{-1} \text{ sr}^{-1}$ ) are found  
929 between 1 and 5 km over the western Mediterranean, while over the central and eastern parts of the  
930 study region the desert dust outbreaks' intensity ( $\sim 0.006 \text{ km}^{-1} \text{ sr}^{-1}$ ) is higher below 1.5 km. Among the  
931 sub-regions, the backscatter coefficients are higher in the central and eastern Mediterranean, which is  
932 also depicted in the bottom map of Fig. 98-ii. It is reminded that higher intensities of dust episodes over  
933 the central and eastern Mediterranean have also been noticed based on MODIS retrievals (Figure 37).  
934 From the obtained longitudinal projection, it is evident a patchy structure of the total backscatter  
935 coefficient profiles, especially in the central and eastern parts, indicating the existence of several dust  
936 layers of varying intensities at different altitudes into the atmosphere.

937 The three dimensional plots of Figures 8-i and 8-ii, have been also reproduced considering all the  
938 available dust and polluted dust CALIOP-CALIPSO records, without taking into account the satellite  
939 algorithm's outputs (intense dust outbreaks). The obtained results for the number of observations and  
940  $\beta_{532nm}$  are presented in Figures S98-i and S98-ii, respectively. Note, that for each studied parameter the  
941 colorbar scales in Figure 8 and S8-S9 are not identical because the number of observations for dust

942 average conditions (Fig. S98-i) is extremely larger than the corresponding one during intense dust  
943 outbreaks (Fig. 8-i) while the opposite is found for the  $\beta_{532nm}$  values (Fig. 8-ii and Fig. S89-ii). It is  
944 apparent that the latitudinal projections calculated for the intense dust outbreaks (Fig. 8-i) and for all  
945 the available CALIOP dust records (Fig. S989-i) reveal different patterns. More specifically, when all  
946 available CALIOP dust records are considered, it is found that dust aerosols are mainly confined  
947 between 1 and 3 km in the southernmost parts of the study region while the number of observations  
948 gradually decreases at higher altitudes and towards northern latitudes (Fig. S989-i). On the contrary,  
949 during dust outbreaks, mineral particles are transported over the Mediterranean following an ascending  
950 path, as it is depicted in the latitudinal projection of Figure 8-i. Nevertheless, it must be mentioned that  
951 over the desert areas there is a full coverage (see bottom map in Fig. S989-i) when all dust CALIOP  
952 records are considered in contrast to intense dust outbreaks (see bottom map in Fig. 8-i) attributed to  
953 the absence of *DT* retrievals, used as inputs to the satellite algorithm, over bright surfaces. The  
954 comparison between the longitudinal projections during intense dust outbreaks (Figure 8-i) and during  
955 average dust conditions (Fig. S989-i) reveals less remarkable differences than for the latitudinal  
956 projections. According to the longitudinal projection of Figure S989-i, in the western Mediterranean,  
957 dust layers are confined between 1 and 6.5 km, while their base and top altitude both decrease down to  
958 0.5 and 4.5 km, respectively, for increasing longitudes. In the easternmost part of the study region, dust  
959 layers are mainly confined between 1 and 3 km, while its top height can reach up to 5 km. The intensity  
960 of dust loads (in terms of  $\beta_{532nm}$ ) is lower than  $0.003 \text{ km}^{-1} \text{ sr}^{-1}$  regardless the projection plane for  
961 average dust conditions based on CALIOP-CALIPSO lidar profiles (Fig. S989-ii). Moreover, the  
962 intensity of dust loads decreases gradually with height as well as from south to north revealing a  
963 distinct pattern in all projection planes in contrast to the corresponding ones found during desert dust  
964 outbreaks (Fig. 8-ii).

965

#### 966 4.3.2 Seasonal characteristics

967 The vertical structure of the Mediterranean desert dust outbreaks has also been analyzed separately  
968 for winter (*DJF*), spring (*MAM*), summer (*JJA*) and autumn (*SON*). The seasonal three dimensional  
969 representations of the CALIOP overall dust observations and the associated total backscatter  
970 coefficients are depicted in the left and right column of Figure 109, respectively. It must be noted, that  
971 for  $\beta_{532nm}$  the colorbars' ranges are common, depending on the projection plane. More specifically, the  
972 maximum limits have been set to  $0.012 \text{ km}^{-1} \text{ sr}^{-1}$ ,  $0.014 \text{ km}^{-1} \text{ sr}^{-1}$  and  $0.021 \text{ km}^{-1} \text{ sr}^{-1}$  for the latitudinal,

Formatted: Font: Italic

Formatted: Font: Italic

Formatted: Font: Italic

Formatted: Font: Italic

Formatted: Font: Italic

973 longitudinal and bottom map projections, respectively. It should be mentioned that  $\beta_{532nm}$  values can  
974 reach up to  $0.045 \text{ km}^{-1} \text{ sr}^{-1}$ , but are associated with a very small number of dust observations.

975 The majority (85%) of dust observations is recorded in spring and summer, attributed to the  
976 enhanced production rates of mineral particles and the prevailing atmospheric circulation over the  
977 source areas and the Mediterranean. According to the latitudinal projections, it is evident a seasonal  
978 variability of the intense Mediterranean desert dust outbreaks' geometrical characteristics. Dust  
979 particles are detected at higher altitudes (6-7 km) during warm seasons of the year while in winter are  
980 mainly detected below 3 km and in autumn are recorded between 2 and 5 km. Nevertheless, it should  
981 be mentioned that during these seasons only a small number of pixels (see bottom maps in Figs. 109 i-  
982 a, iv-a) is available considering also that clouds prohibit the satellite observations. Note that in spring,  
983 dust can be found at low tropospheric levels while in summer it is mainly observed above 1 km  
984 highlighting thus the role of topography and the enhanced thermal convection. During the first half of  
985 the year, the maximum dust observations are confined between the parallels  $31^\circ \text{ N}$  and  $37^\circ \text{ N}$  while  
986 during the second one, are shifted northwards in the latitudinal zone extending from  $34^\circ \text{ N}$  to  $40^\circ \text{ N}$ .  
987 Similar latitudinal projections were also presented by Luo et al. (2015), for the same zonal areas of the  
988 study region, who developed a new algorithm to improve CALIOP's ability to detect optically thin dust  
989 layers. From the longitudinal projections as well as from the bottom maps, it is evident that the  
990 maximum dust records are found in different Mediterranean sub-regions, depending on the season. The  
991 geometrical characteristics, in longitudinal terms, of intense *DD* episodes affecting the western, central  
992 and eastern parts of the Mediterranean are similar to those presented in the annual three dimensional  
993 structure (Fig. 98-i) being more frequent in the eastern and central Mediterranean in winter, spring and  
994 autumn and in the western and central Mediterranean in summer.

Formatted: Font: Italic

995 The seasonal patterns of  $\beta_{532nm}$  latitudinal projections are different than those for the dust  
996 observations, while they also differ among the four seasons. The intensity of winter *DD* episodes is  
997 stronger (up to  $0.012 \text{ km}^{-1} \text{ sr}^{-1}$ ) below 2 km and at the southern parts of the study region. According to  
998 the longitudinal and bottom map projections, these episodes take place over the central and eastern  
999 Mediterranean Sea but the number of grid cells with coincident CALIOP observations and *DD* episodes  
1000 is limited. In spring, the highest  $\beta_{532nm}$  values (up to  $0.006 \text{ km}^{-1} \text{ sr}^{-1}$ ) are recorded between the parallels  
1001  $31^\circ \text{ N}$  and  $35^\circ \text{ N}$  and below 2 km, although, relatively high  $\beta_{532nm}$  values (up to  $0.004 \text{ km}^{-1} \text{ sr}^{-1}$ ) are  
1002 found up to 6-5 km (Fig. 109 ii-b). Moving northwards, over the Mediterranean, dust layers are mainly  
1003 confined between 2 and 4 km, associated with high  $\beta_{532nm}$  values (up to  $0.004 \text{ km}^{-1} \text{ sr}^{-1}$ ) in the  
1004 latitudinal zone extending from  $35^\circ \text{ N}$  to  $43^\circ \text{ N}$ . The existence of these elevated dust layers, has been

Formatted: Font: Italic

Formatted: Font: Italic

1005 also confirmed by model simulations through specific (Papayannis et al., 2008; 2014) or averaged  
1006 (Alpert et al., 2004) cross sections of dust concentrations in the central sector of the Mediterranean.  
1007 This is in accordance with our longitudinal projection (Fig. 40-9 ii-b), where  $\beta_{532nm}$  is high varying from  
1008 0.004 to 0.008  $\text{km}^{-1} \text{sr}^{-1}$  at these altitude ranges.

1009 In summer, the intensity of dust episodes is smoothly decreased at higher altitudes, where dust  
1010 layers of considerable  $\beta_{532nm}$  values are also found. More specifically, the highest backscatter  
1011 coefficients (up to 0.008  $\text{km}^{-1} \text{sr}^{-1}$ ) are recorded near to the surface but also moderate values (up to  
1012 0.006  $\text{km}^{-1} \text{sr}^{-1}$ ) are observed between 2 and 5 km, particularly over the southern parts of the study  
1013 region (Fig. 40-9 iii-b). Most of these intense *DD* episodes occur in the western Mediterranean, where  
1014 the highest  $\beta_{532nm}$  values (up to 0.005  $\text{km}^{-1} \text{sr}^{-1}$ ) are recorded between 2 and 5 km. Over the central and  
1015 eastern Mediterranean, even higher  $\beta_{532nm}$  values are found (up to 0.014  $\text{km}^{-1} \text{sr}^{-1}$ ) but at lower altitudes  
1016 (< 1 km). In autumn, the majority of the grid cells of coincident CALIOP profiles and *DD* episodes  
1017 identified by the satellite algorithm are located between the parallels 33° N and 41° N. In this  
1018 latitudinal zone, CALIOP profiles are available over the interior parts of the Iberian Peninsula and over  
1019 western and central parts of the Mediterranean Sea, near to the northern African coasts. According to  
1020 the latitudinal projection,  $\beta_{532nm}$  values mainly vary from 0.002 to 0.009  $\text{km}^{-1} \text{sr}^{-1}$ , revealing an  
1021 increasing tendency for increasing heights. On the contrary, the total backscatter coefficients do not  
1022 show a distinct spatial pattern on the longitudinal projection, due to the limited number of grid cells  
1023 participating in the calculations. Throughout the year, based on the CALIOP  $\beta_{532nm}$  retrievals, the *DD*  
1024 episodes are more intense (up to 0.018  $\text{km}^{-1} \text{sr}^{-1}$ ) in spring, when massive dust loads are transported  
1025 from the Sahara desert towards the central and eastern parts of the Mediterranean Sea (bottom map in  
1026 Fig. 40-9 ii-b).

1027

#### 1028 4.4. Intercomparison of satellite AOD and $\text{PM}_{10}$ concentrations for specific desert dust outbreaks

1029 In Section 4.21.2, it has been shown that the agreement between the satellite algorithm's outputs  
1030 and  $\text{PM}_{10}$  concentrations is better in the central and eastern Mediterranean with regards to the western  
1031 parts (Figure 85-ii). This discrepancy has been mainly attributed to the higher altitude of dust layers'  
1032 base over the western sector of the study domain (Figure 98-i), in relation to the existing areal  
1033 orography. Here, aiming at addressing how dust layers' geometrical characteristics influence the  
1034 agreement between columnar AOD satellite and ground  $\text{PM}_{10}$  measurements, specific desert dust  
1035 outbreaks that took place over the  $\text{PM}_{10}$  stations are analyzed. These outbreaks were selected based on

Formatted: Font: Italic

Formatted: Font: Italic

Formatted: Font: Italic

Formatted: Font: Italic

Formatted: Font: Italic

Formatted: Font: Italic

1036 concurrent fulfillment of the following criteria: (i) a *DD* episode must be identified by the satellite  
1037 algorithm at pixel level (at  $1^\circ \times 1^\circ$  grid cell), (ii) total  $PM_{10}$  measurement must be available at the  
1038 station which lies into the geographical limits of the corresponding grid cell and (iii) CALIPSO flies  
1039 across the grid cell. These criteria were met for 13 desert dust outbreaks, which took place over 9  $PM_{10}$   
1040 stations during the period ~~2000-2013~~ Jun. 2006 – Feb. 2013. Similarities were found among the  
1041 identified cases and therefore only the results for four desert dust outbreaks of different geometrical  
1042 characteristics are discussed in the present section. For each case, we have reproduced the cross  
1043 sections of the  $\beta_{532nm}$  vertical profiles up to 8 km above sea level (a.s.l.) along the CALIOP-CALIPSO  
1044 track when the satellite flies near the  $PM_{10}$  site (Figures ~~140-132~~). Moreover, the corresponding aerosol  
1045 subtype profiles, acquired from the CALIOP website ([http://www-  
1046 calipso.larc.nasa.gov/products/lidar/browse\\_images/production/](http://www-calipso.larc.nasa.gov/products/lidar/browse_images/production/)), are provided in the supplementary  
1047 material (Figures ~~S10S79-S9112~~). Since the  $PM_{10}$  concentrations are available only as daily averages,  
1048 the optimum solution would be to have the maximum number (2) of CALIOP overpasses near  $PM_{10}$   
1049 site throughout the day, in order to reduce the temporal inconsistencies between satellite vertical  
1050 resolved retrievals and ground data. However, in 8 out of 13 desert dust outbreaks this was not feasible.

Formatted: Font: Italic

Formatted: Font: Italic

Formatted: Font: Italic

Formatted: Font: Italic

Formatted: Font: Italic

Formatted: Font: Italic

1051

#### 1052 4.4.1 Case 1: ~~Censt~~ (26<sup>th</sup> May 2008)

1053 The first study case refers to a desert dust outbreak that took place on 26<sup>th</sup> May 2008 and affected  
1054 the station Censt (Lat: 39.064, Lon: 8.457) located in southern Sardinia. At the ground, the measured  
1055 mean daily total  $PM_{10}$  concentration was  $19 \mu\text{g m}^{-3}$  whereas 68% (or  $13 \mu\text{g m}^{-3}$ ) of the load consisted of  
1056 dust particles indicating thus their strong presence in the lowest troposphere. Based on MODIS-Terra  
1057 retrievals, representative for the whole atmospheric column and grid cell, the aerosol optical depth at  
1058 550 nm was equal to 0.81. In order to investigate the vertical distribution of the dust outbreak, the cross  
1059 sections of the  $\beta_{532nm}$  vertical profiles along CALIOP track, near the station, during daytime and  
1060 nighttime have been reproduced and depicted in Figures ~~140-i~~ and ~~140-ii~~, respectively. In addition, the  
1061 corresponding aerosol subtype profiles are provided in Figures ~~S710109-i~~ and ~~S710109-ii~~ in the  
1062 supplementary material. During night, it is evident the predominance of a well-developed dust layer  
1063 mixed with polluted aerosols (Figure ~~S7109-i~~) extending from surface up to 5 km a.s.l. between the  
1064 parallels  $33^\circ$  N and  $38^\circ$  N, while near the station its top is lowered down to 3 km (left side of Figure  
1065 ~~140-i~~). Moreover, the  $\beta_{532nm}$  values range mainly from 0.002 to  $0.003 \text{ km}^{-1} \text{ sr}^{-1}$  without revealing  
1066 remarkable variations, thus indicating a rather compact dust layer. According to the daytime CALIOP

Formatted: Font: Italic

1067 | overpass (Figure 140-ii), a pure dust layer (Figure S710-ii) is confined between surface and 4 km,  
1068 | affecting the surrounding area of the station, while its intensity (in terms of  $\beta_{532nm}$ ) varies slightly from  
1069 | 0.0015 to 0.002  $\text{km}^{-1} \text{sr}^{-1}$ . Nevertheless, due to the background solar illumination, leading thus to a  
1070 | lower signal-to-noise ratio (Nowotnick et al., 2015), the “borders” of the dust plume during daytime  
1071 | are not so distinct in contrast to nighttime. According to the obtained results, the ground-based  
1072 | measurements are able to capture satisfactorily the dust event when its load is equally distributed in the  
1073 | lowest tropospheric levels, resulting thus to a good agreement between MODIS and  $PM_{10}$  observations.

Formatted: Font: Italic

1074

#### 1075 | 4.4.2 Case 2 and 3: ~~Els Torms (16<sup>th</sup> July 2008)~~ and ~~San Pablo (12<sup>th</sup> September 2007)~~

1076 | Two dust events that affected Els Torms (NE Spain, Lat: 41.395, Lon: 0.721) and San Pablo  
1077 | (central Spain, Lat: 39.525, Lon: -4.353) on 16<sup>th</sup> July 2008 and 12<sup>th</sup> September 2007, respectively, are  
1078 | studied here. The daily averages of the total  $PM_{10}$  concentrations were equal to 16 and 30  $\mu\text{g m}^{-3}$ ,  
1079 | respectively, whereas the dust particles' contribution (dust  $PM_{10}$ ) to the total amount was zero in Els  
1080 | Torms and 33 % in San Pablo. On the contrary, the MODIS-Terra level 3 AOD retrievals were high and  
1081 | equal to 0.56 (Els Torms) and 0.64 (San Pablo), indicating the existence of dust aerosols according to  
1082 | the satellite algorithm's classification method. In order to give a better insight, aiming at describing the  
1083 | discrepancies between MODIS-Terra AOD and  $PM_{10}$  concentrations, we have reproduced the cross  
1084 | sections of the total backscatter at 532 nm when CALIPSO flies, during daytime, near Els Torms  
1085 | (Figure 1211-i) and San Pablo (Figure 1211-ii). The corresponding profiles of the CALIOP aerosol  
1086 | classification scheme are also available in Figures S811101-i and S811101-ii. In Els Torms, where the  
1087 | dust  $PM_{10}$  concentration was zero, a dust layer (Figure S811101-i) with its base at 3.5 km a.s.l. and its  
1088 | top at 5 km a.s.l., is recorded by the CALIOP lidar between the parallels 41° N and 43° N. The  
1089 | intensity of the elevated dust layer, in terms of  $\beta_{532nm}$ , varies from 0.002 to 0.004  $\text{km}^{-1} \text{sr}^{-1}$  (Figure 1211-  
1090 | i). Through CALIOP lidar profiles, it is confirmed the existence of a dust layer aloft, which cannot be  
1091 | captured by the  $PM_{10}$  measurements in contrast to the MODIS spectroradiometer. In San Pablo, where  
1092 | the dust particles' contribution to the total  $PM_{10}$  load was equal to 33 %, a dust layer abuts the ground  
1093 | extending up to 5-6 km ~~ASLa.s.l.~~, whereas the dust plume covers a wide range, in latitudinal terms,  
1094 | from the sub-Sahel to the Celtic Sea, affecting the Iberian Peninsula (Figure S811-ii). Nevertheless, the  
1095 | intensity of the dust layer, over the surrounding area of the station, differs with altitude being higher  
1096 | between 2.5 and 5 km a.s.l. (0.004 to 0.007  $\text{km}^{-1} \text{sr}^{-1}$ ) and lower between ground and 2 km a.s.l. (<  
1097 | 0.003  $\text{km}^{-1} \text{sr}^{-1}$ ), as it is depicted in the middle of Figure 112-ii. The two studied cases here differ from

Formatted: Font: Italic

Formatted: Font: Italic

Formatted: Font: Italic

Formatted: Font: Italic

Formatted: Font: Italic

Formatted: Font: Italic



1098 Case 1 (Section 4.4.1) either with regards to the position of the elevated dust layer (Els Torms) or to its  
1099 vertical distribution (San Pablo), which explains the poor agreement between satellite columnar *AOD*  
1100 retrievals (MODIS) and ground *PM*<sub>10</sub> concentrations.

Formatted: Font: Italic

#### 1102 4.4.3 Case 4: ~~Agia Marina (25<sup>th</sup> February 2007)~~

1104 The case studied here, namely the desert dust outbreak recorded in Agia Marina (Cyprus, Lat:  
1105 35.039, Lon: 33.058) on 25<sup>th</sup> February 2007, is the strongest one among the selected cases. More  
1106 specifically, the daily average of the dust *PM*<sub>10</sub> concentration was equal to 134 µg m<sup>-3</sup> accounting for  
1107 the 92 % of the total *PM*<sub>10</sub> measured amount at the station, which is indicative of the strong  
1108 predominance of dust particles in the lowest troposphere. The MODIS-Terra level 3 *AOD* value for the  
1109 grid cell to which the station it is ~~found~~ found is high and equal to 1.04. According to the CALIOP  
1110 aerosol classification scheme, during nighttime, a shallow low-elevated dust layer mixed with polluted  
1111 or marine aerosols is heading towards the station, whereas above the *PM*<sub>10</sub> site (Agia Marina) extends  
1112 from close to the ground up to 9 km a.s.l., comprising only pure dust aerosols (Figure ~~S9+12~~). The  
1113 main part of the dust layer, in the surrounding area of the station, is confined between 2.5 and 4 km  
1114 a.s.l. where the maximum  $\beta_{532nm}$  values (up to 0.006 km<sup>-1</sup> sr<sup>-1</sup>) are observed (Figure ~~132~~). Also, similar  
1115  $\beta_{532nm}$  values are recorded below 1 km a.s.l.; however, the dust layer is not well represented in the cross  
1116 section of the CALIOP  $\beta_{532nm}$  vertical profiles due to the total attenuation of the lidar beam by clouds  
1117 (located between 3 and 4 km a.s.l.) superimposed to the low-elevated dust layer.

Formatted: Font: Italic

Formatted: Font: Italic

Formatted: Font: Italic

## 1119 5. Summary and conclusions

1120 This study aims at describing the vertical structure of intense desert dust outbreaks affecting the  
1121 broader Mediterranean basin. To achieve this target, an updated version of an objective and dynamic  
1122 algorithm, which has been introduced by Gkikas et al. (2009; 2013), has been applied for the  
1123 identification of strong and extreme desert dust episodes, over the period Mar. 2000 – Feb. 2013. For  
1124 its operation, a group of optical properties, retrieved by satellite sensors (MODIS-Terra/Aqua, EP-  
1125 TOMS and OMI-Aura) on a daily basis, is used, providing information about aerosols' load, size and  
1126 nature. Briefly, the satellite algorithm consists of three parts; at the first one are computed the mean  
1127 *AOD* value (*Mean*) and the associated standard deviation (*Std*) for the whole study period in each grid

1128 cell of  $1^\circ \times 1^\circ$  spatial resolution, at the second one the identified aerosol episodes are classified based  
1129 on their intensity to strong and extreme ones. Finally, at the third part the identified aerosol episodes  
1130 are categorized as desert dust episodes, separately over land and sea. Through this approach the  
1131 selected dataset consists only of intense desert dust episodes since their intensity (expressed in terms of  
1132  $AOD_{550nm}$ ) is higher/equal than  $Mean + 2*Std$ . The *DD* episodes have also been determined by  
1133 applying an alternative second methodology (METHOD-B) which excludes dust-affected cases  
1134 identified based on the criteria set concerning the aerosol size/nature related optical properties.

Formatted: Font: Italic

1135 Through the comparison of the [default version of the](#) satellite algorithm against surface  
1136 measurements derived from 109 AERONET and 22  $PM_{10}$  stations, it is found that:

Formatted: Font: Italic

#### 1137 AERONET

- 1138 ➤ The correlation coefficient between MODIS and AERONET  $AODs$  is increased from 0.505 to  
1139 0.750 when level 3 grid cells with higher sub-grid spatial representativeness and homogeneity  
1140 are considered.
- 1141 ➤ According to the AERONET volume size distributions, it is evident the predominance of the  
1142 coarse mode with a peak ( $\sim 0.25 \mu m^3 \mu m^{-2}$ ) for particles radii between 1.70 and 2.24  $\mu m$ , in  
1143 case of intense *DD* episodes.
- 1144 ➤ The appropriateness of *DD* episodes' identification method applied to the satellite algorithm is  
1145 confirmed since the majority ( $> 75\%$ ) of AERONET  $\alpha_{440-870nm}$  and  $r_{eff}$  values are lower than  
1146 0.54 and higher than 0.55  $\mu m$ , respectively.
- 1147 ➤ About 15% of the pixel level intense *DD* episodes are misclassified by the satellite algorithm  
1148 and these drawbacks are encountered in AERONET stations where the aerosol load is  
1149 dominated either by fine particles or by complex aerosol types.

Formatted: Font: Italic

Formatted: Font: Italic

Formatted: Font: Italic

#### 1150 $PM_{10}$ and dust contribution

- 1151 ➤ The agreement between surface and satellite measurements is better over the central and eastern  
1152 Mediterranean stations.
- 1153 ➤ On a station level, the percentage of the intense *DD* episodes, for which a dust contribution to  
1154  $PM_{10}$  surface concentration has been recorded, varies from 68% (Monagrega, northeastern  
1155 Spain) to 97% (Boccadifalco, Sicily).
- 1156 ➤ In the majority of stations, dust particles contribute more than 50% of the total amount reaching  
1157 up to 86.8% (Agia Marina, Cyprus).

Formatted: Font: Italic

Formatted: Font: Italic

1158 | ➤ The mean  $PM_{10}$  concentration levels mainly vary from 20 to 50  $\mu\text{g m}^{-3}$  reaching up to 223  $\mu\text{g m}^{-3}$   
1159 | in Agia Marina (Cyprus).

Formatted: Font: Italic

1160 | Based on the satellite algorithm's outputs, an overall view about the regime of Mediterranean desert  
1161 | dust outbreaks is presented for the periods Mar. 2000 – Feb. 2013 (MODIS-Terra) and 2003-2012  
1162 | (MODIS-Aqua). The main findings concerning the intense  $DD$  episodes' frequency (in terms of  
1163 | episodes  $\text{yr}^{-1}$ ) and intensity (in terms of  $AOD$  at 550nm) are the following:

Formatted: Font: Italic

1164 | ➤ Strong  $DD$  episodes occur more frequently (up to 9.9 episodes  $\text{yr}^{-1}$ ) in the western  
1165 | Mediterranean while the extreme ones occur more frequently (up to 3.3 episodes  $\text{yr}^{-1}$ ) over the  
1166 | central parts of the Mediterranean Sea, when the satellite algorithm operates with MODIS-Terra  
1167 | retrievals.

Formatted: Font: Italic

1168 | ➤ The intensity of strong and extreme  $DD$  episodes, in  $AOD$  terms, can reach to 1.5 and 3-4,  
1169 | respectively, over the central and eastern parts of the Mediterranean Sea, near off the northern  
1170 | African coasts.

Formatted: Font: Italic

1171 | ➤ Slightly lower frequencies and higher intensities are found for the period 2003-2012, when the  
1172 | satellite algorithm operates with MODIS-Aqua retrievals.

1173 | ➤ Through the intercomparison between the two applied methodologies, it is revealed that the  
1174 | geographical patterns of frequency of occurrence are similar both for strong and extreme  $DD$   
1175 | episodes; however, higher frequencies are found based on METHOD-B.

Formatted: Font: Italic

1176 | ➤ Based on METHOD-B, the  $DD$  episodes' intensities are decreased whereas the geographical  
1177 | patterns for the strong  $DD$  episodes are not so distinct compared to the corresponding results  
1178 | obtained by the default version of the satellite algorithm.

Formatted: Font: Italic

Formatted: Font: Italic

1179 | ➤ The similarity between the outputs of the algorithm using the two methodologies shows the  
1180 | consistency of the algorithm and the validity of its concept.

1181

1182 | In order to describe the vertical structure of the intense Mediterranean dust outbreaks, the CALIOP  
1183 | vertical profiles of aerosol subtyping and total backscatter coefficient at 532 nm, are used as a  
1184 | complementary tool to the identified intense  $DD$  episodes by the satellite algorithm. Through this  
1185 | synergistic approach it is found that:

Formatted: Font: Italic

1186 | ➤ Dust particles are mainly detected between 0.5 and 6 km, following an ascending mode, up to  
1187 | 40° N, leaving from the source areas and transported towards the Mediterranean.

- 1188 ➤ Over the western Mediterranean, the dust layers are mainly observed between 2 and 6 km while  
1189 their base height is decreased down to 0.5 km for increasing longitudes.
- 1190 ➤ During the warm period of the year, dust particles are uplifted at higher altitudes (up to 8 km).
- 1191 ➤ In summer, the transported dust loads over the western Mediterranean are recorded above 1 km  
1192 and in spring at lower altitudes over the central and eastern parts of the study region. This  
1193 behavior underlies the role of topography (e.g. Atlas Mountains) and the enhanced thermal  
1194 convection.
- 1195 ➤ The intensity of dust outbreaks, in terms of  $\beta_{532nm}$ , is maximized (up to  $0.006 \text{ km}^{-1} \text{ sr}^{-1}$ ) below 2  
1196 km and at the southern parts ( $30^\circ \text{ N} - 34^\circ \text{ N}$ ) of the study region.
- 1197 ➤ In spring, considerably high  $\beta_{532nm}$  values ( $\sim 0.004 \text{ km}^{-1} \text{ sr}^{-1}$ ) are observed between 2 and 4 km  
1198 in the latitudinal zone extending from  $35^\circ \text{ N}$  to  $42^\circ \text{ N}$ .
- 1199 ➤ Moderate-to-high  $\beta_{532nm}$  values are observed up to 6 km, near to the source areas, while the top  
1200 of dust layers is gradually decreased down to 4 km towards northern latitudes.
- 1201 ➤ From the longitudinal projection of  $\beta_{532nm}$ , it is evident that *DD* episodes are more intense ( $\sim$   
1202  $0.004 \text{ km}^{-1} \text{ sr}^{-1}$ ) between 1 and 5 km in the western Mediterranean, while over the central and  
1203 eastern sectors, the maximum intensities ( $\sim 0.006 \text{ km}^{-1} \text{ sr}^{-1}$ ) are recorded below 1.5 km.
- 1204 ➤ On a seasonal basis, *DD* episodes are found to be more intense (up to  $0.018 \text{ km}^{-1} \text{ sr}^{-1}$ ) in spring,  
1205 when dust is transported towards the central and eastern parts of the Mediterranean region.

Formatted: Font: Italic

Formatted: Font: Italic

1206 At the last part of the present study, it is investigated how the desert dust outbreaks' vertical  
1207 distribution can affect the level of agreement between columnar satellite *AOD* retrievals (MODIS) and  
1208 ground *PM*<sub>10</sub> concentrations. For this purpose, four intense Mediterranean desert dust outbreaks of  
1209 different geometrical characteristics that took place across the Mediterranean, namely in Spain  
1210 (western), *Sardinia-Italy* (central) and Cyprus (eastern), are studied when satellite algorithm's outputs,  
1211 ground *PM*<sub>10</sub> concentrations and CALIOP-CALIPSO lidar profiles are available concurrently. Our  
1212 analysis clearly shows that when a well-developed and compact dust layer is located in the lowest  
1213 tropospheric levels, then the level of agreement between MODIS-*PM*<sub>10</sub> is high. On the contrary, when  
1214 the dust layer is aloft or its load is not equally distributed in vertical terms then a poor agreement  
1215 between MODIS-*PM*<sub>10</sub> is found.

Formatted: Font: Italic

Formatted: Font: Italic

Formatted: Font: Italic

Formatted: Font: Italic

1216 This study attempts to highlight the importance of the synergistic use of satellite observations and  
1217 the usage of surface-based measurements, targeting to the representation of the 3D structure of dust  
1218 outbreaks and the description of their spatial and temporal features. For this reason, the further  
1219 development of the satellite algorithm is an ongoing process by our group, aiming at extending the

1220 study domain from regional to global scale, considering the latest version of MODIS retrievals  
1221 (Collection 006) as well as the Deep Blue Algorithm retrievals, available over the major dust sources of  
1222 the planet.

1223

## 1224 **Acknowledgements**

1225 The MDRAF project has received funding from the European Union's Seventh Framework  
1226 Programme for research, technological development and demonstration under grant agreement no  
1227 622662. The Collection 051 MODIS-Terra and MODIS-Aqua data were obtained from NASA's Level  
1228 1 and Atmosphere Archive and Distribution System (LAADS) website  
1229 (<ftp://ladsweb.nascom.nasa.gov/>). The Earth Probe (TOMS) and OMI aerosol climatology is available  
1230 from the Mirador ftp server (<http://mirador.gsfc.nasa.gov/>). The CALIPSO retrievals have been derived  
1231 from NASA's Earth Observing System Data and Information System (<http://reverb.echo.nasa.gov/>).  
1232 We would like to thank the principal investigators maintaining the AERONET sites used in the present  
1233 work. We would like to acknowledge the EMEP Programme and the public European databases  
1234 Airbase and ACTRIS, which supplied  $PM_{10}$  data used in this study. J. Pey benefits from a Ramón y  
1235 Cajal Research Grant (RYC-2013-14159) from the Spanish Ministry of Economy and Competitiveness.  
1236 S. Basart, O. Jorba, S. Gassó and J.M. Baldasano acknowledge the CICYT project CGL2013-46736  
1237 and Severo Ochoa (SEV-996 2011-00067) programme of the Spanish Government. The publication  
1238 was supported by the European Union Seventh Framework Programme (FP-7-REGPOT-2012-2013-1),  
1239 in the framework of the project BEYOND, under Grant Agreement No. 316210 (BEYOND – Building  
1240 Capacity for a Centre of Excellence for EO-based monitoring of Natural Disasters. The figures 140,  
1241 121 and 132 have been produced with ccplot (<http://ccplot.org/>). This work is contributing to the  
1242 Chemistry-Aerosol Mediterranean Experiment (ChArMEx) coordinated effort for the long-term  
1243 Mediterranean aerosol characterization using available remote sensing datasets.

1244

## 1245 **References**

1246 Adams, A. M., Prospero, J. M., and Zhang, C.: CALIPSO-derived three-dimensional structure of  
1247 aerosol over the Atlantic Basin and adjacent continents, *J. Climate*, 25, 6862–6879, doi:10.1175/JCLI-  
1248 D-11-00672.1, 2012.

1249 Alados-Arboledas, A., Alcántara, A., Olmo, F. J., Martínez-Lozano, J. A., Estellés, V., Cachorro, V.,  
1250 Silva, A. M., Horvath, H., Gangl, A., Díaz, A., Pujadas, M., Lorente, J., Labajo, A., Sorribas, M., and

40

Formatted: Subscript

1251 Pavese, G.: Aerosol columnar properties retrieved from Cimel radiometers during VELETA 2002,  
1252 *Atmos. Environ.*, 42, 2630–2642, [doi:10.1016/j.atmosenv.2007.10.006](https://doi.org/10.1016/j.atmosenv.2007.10.006), 2008.

1253 Alam, K., Trautmann, T., Blaschke, T., Subhan, F.: Changes in aerosol optical properties due to dust  
1254 storms in the Middle East and Southwest Asia, *Remote Sens. Environ.* 143, 216–227,  
1255 [doi:10.1016/j.rse.2013.12.021](https://doi.org/10.1016/j.rse.2013.12.021), 2014.

1256 Alpert, P., Kishcha, P., Shtivelman, A., Krichak, S.O., Joseph, J.H.: Vertical distribution of Saharan  
1257 dust based on 2.5-year model predictions, *Atmos. Res.*, 70, 109-130,  
1258 [doi:10.1016/j.atmosres.2003.11.001](https://doi.org/10.1016/j.atmosres.2003.11.001), 2004.

1259 Amiridis, V., Kafatos, M., Pérez, C., Kazadzis, S., Gerasopoulos, E., Mamouri, R. E., Papayannis, A.,  
1260 Kokkalis, P., Giannakaki, E., Basart, S., Daglis, I., and Zerefos, C.: The potential of the synergistic use  
1261 of passive and active remote sensing measurements for the validation of a regional dust model, *Ann.*  
1262 *Geophys.*, 27, 3155-3164, [doi:10.5194/angeo-27-3155-2009](https://doi.org/10.5194/angeo-27-3155-2009), 2009.

1263 Amiridis, V., Wandinger, U., Marinou, E., Giannakaki, E., Tsekeri, A., Basart, S., Kazadzis, S.,  
1264 Gkikas, A., Taylor, M., Baldasano, J. M., and Ansmann, A.: Optimizing CALIPSO Saharan dust  
1265 retrievals, *Atmos. Chem. Phys.*, 13, 12089-12106, [doi:10.5194/acp-13-12089-2013](https://doi.org/10.5194/acp-13-12089-2013), 2013.

1266 Ångström, A.K.: On the atmospheric transmission of sun radiation and on the dust in the air, *Geogr.*  
1267 *Ann.*, 12, 130-159, [doi: 10.2307/519399](https://doi.org/10.2307/519399), 1929.

1268 Balis, D., Amiridis, V., Kazadzis, S., Papayannis, A., Tsaknakis, G., Tzortzakis, S., Kalivitis, N.,  
1269 Vrekoussis, M., Kanakidou, M., Mihalopoulos, N., Chourdakis, G., Nickovic, S., Pérez, C.,  
1270 Baldasano, J. M., and Drakakis, M.: Optical characteristics of desert dust over the East Mediterranean  
1271 during summer: a case study, *Ann. Geophys.*, 24, 807-821, [doi:10.5194/angeo-24-807-2006](https://doi.org/10.5194/angeo-24-807-2006), 2006.

1272 Balis, D.: Geometrical characteristics of desert dust layers over Thessaloniki estimated with  
1273 backscatter/Raman lidar and the BSC/DREAM model, *Remote Sens. Lett.*, 353-362, [doi:](https://doi.org/10.1080/01431161.2011.597793)  
1274 [10.1080/01431161.2011.597793](https://doi.org/10.1080/01431161.2011.597793), 2012.

1275 Barkan, J., Alpert, P., Kutiel, H., and Kishcha, P.: Synoptics of dust transportation days from Africa  
1276 toward Italy and central Europe, *J. Geophys. Res.*, 110, D07208, [doi:10.1029/2004JD005222](https://doi.org/10.1029/2004JD005222), 2005.

1277 Barnaba, F. and Gobbi, G. P.: Aerosol seasonal variability over the Mediterranean region and relative  
1278 impact of maritime, continental and Saharan dust particles over the basin from MODIS data in the year  
1279 2001, *Atmos. Chem. Phys.*, 4, 2367-2391, [doi:10.5194/acp-4-2367-2004](https://doi.org/10.5194/acp-4-2367-2004), 2004.

1280 Basart, S., Pérez, C., Cuevas, E., Baldasano, J. M., and Gobbi, G. P.: Aerosol characterization in  
1281 Northern Africa, Northeastern Atlantic, Mediterranean Basin and Middle East from direct-sun  
1282 AERONET observations, *Atmos. Chem. Phys.*, 9, 8265-8282, doi:10.5194/acp-9-8265-2009, 2009.

1283 Basart, S., Pay, M. T., Jorba, O., Pérez, C., Jiménez-Guerrero, P., Schulz, M., and Baldasano, J. M.:  
1284 Aerosols in the CALIOPE air quality modelling system: evaluation and analysis of PM levels, optical  
1285 depths and chemical composition over Europe, *Atmos. Chem. Phys.*, 12, 3363-3392, doi:10.5194/acp-  
1286 12-3363-2012, 2012.

1287 Ben-Ami, Y., Koren, I., and Altaratz, O.: Patterns of North African dust transport over the Atlantic:  
1288 winter vs. summer, based on CALIPSO first year data, *Atmos. Chem. Phys.*, 9, 7867-7875,  
1289 doi:10.5194/acp-9-7867-2009, 2009.

1290 Ben-Ami, Y., Koren, I., Rudich, Y., Artaxo, P., Martin, S. T., and Andreae, M. O.: Transport of North  
1291 African dust from the Bodélé depression to the Amazon Basin: a case study, *Atmos. Chem. Phys.*, 10,  
1292 7533-7544, doi:10.5194/acp-10-7533-2010, 2010.

1293 Bègue, N., Tulet, P., Chaboureau, J. P., Roberts, G., Gomes, L., and Mallet, M.: Long-range transport  
1294 of Saharan dust over north-western Europe during EUCAARI 2008 campaign: Evolution of dust  
1295 optical properties by scavenging, *J. Geophys. Res.*, 117,D17201, doi:10.1029/2012JD017611, 2012.

1296 Berthier, S., Chazette, P., Couvert, P., Pelon, J., Dulac, F., Thieuleux, F., Moulin, C., and Pain, T.:  
1297 Desert dust aerosol columnar properties over ocean and continental Africa from Lidar in-Space  
1298 Technology Experiment (LITE) and Meteosat synergy. *J. Geophys. Res.*, 111, D21202,  
1299 doi:10.1029/2005JD006999, 2006.

1300 Bollasina, M. A., Ming, Y., and Ramaswamy, V.: Anthropogenic Aerosols and the Weakening of the  
1301 South Asian Summer Monsoon, *Science*, 334, 502-505, doi:10.1126/science.1204994, 2011.

1302 Bösenberg, J., Matthias, V., Amodeo, A., Amoiridis, V., Ansmann, A., Baldasano, J. M., Balin, I.,  
1303 Balis, D., Böckmann, C., Boselli, A., Carlsson, G., Chaikovsky, A., Chourdakis, G., Comerón, A., De  
1304 Tomasi, F., Eixmann, R., Freudenthaler, V., Giehl, H., Grigorov, I., Hågård, A., Iarlori, M., Kirsche,  
1305 A., Kolarov, G., Komguem, L., Kreipl, S., Kumpf, W., Larchevêque, G., Linné, H., Matthey, R.,  
1306 Mattis, I., Mekler, A., Mironova, I., Mitev, V., Mona, L., Müller, D., Music, S., Nickovic, S.,  
1307 Pandolfi, M., Papayannis, A., Pappalardo, G., Pelon, J., Pérez, C., Perrone, R. M., Persson, R.,  
1308 Resendes, D. P., Rizi, V., Rocadenbosch, F., Rodrigues, J. A., Sauvage, L., Schneidenbach, L.,  
1309 Schumacher, R., Shcherbakov, V., Simeonov, V., Sobolewski, P., Spinelli, N., Stachlewska, I.,

1310 Stoyanov, D., Trickl, T., Tsaknakis, G., Vaughan, G., Wandinger, U., Wang, X., Wiegner, M.,  
1311 Zavrtnik, M. and Zerefos, C.: A European aerosol research lidar network to establish an aerosol  
1312 climatology, MPI-Rep. 317, Max-Planck Inst. für Meteorol., Hamburg, Germany, 2003.  
1313 [http://www.mpimet.mpg.de/fileadmin/publikationen/Reports/max\\_scirep\\_348.pdf](http://www.mpimet.mpg.de/fileadmin/publikationen/Reports/max_scirep_348.pdf)  
1314

1315 Burton, S. P., Ferrare, R. A., Vaughan, M. A., Omar, A. H., Rogers, R. R., Hostetler, C. A., and  
1316 Hair, J. W.: Aerosol classification from airborne HSRL and comparisons with the CALIPSO vertical  
1317 feature mask, *Atmos. Meas. Tech.*, 6, 1397-1412, doi:10.5194/amt-6-1397-2013, 2013.  
1318

1319 Cachorro, V. E., Vergaz, R., de Frutos, A. M., Vilaplana, J. M., Henriques, D., Laulainen, N., and  
1320 Toledano, C.: Study of desert dust events over the southwestern Iberian Peninsula in year 2000: two  
1321 case studies, *Ann. Geophys.*, 24, 1493-1510, doi:10.5194/angeo-24-1493-2006, 2006.  
1322

1323 Cao, C. X., Zheng, S., and Singh, R. P.: Characteristics of aerosol optical properties and meteorological  
1324 parameters during three major dust events (2005–2010) over Beijing, China, *Atmos. Res.*, 150, 129–  
1325 142, doi:10.1016/j.atmosres.2014.07.022, 2014.  
1326

1327 Córdoba-Jabonero, C., Sorribas, M., Guerrero-Rascado, J. L., Adame, J. A., Hernández, Y.,  
1328 Lyamani, H., Cachorro, V., Gil, M., Alados-Arboledas, L., Cuevas, E., and de la Morena, B.:  
1329 Synergetic monitoring of Saharan dust plumes and potential impact on surface: a case study of dust  
1330 transport from Canary Islands to Iberian Peninsula, *Atmos. Chem. Phys.*, 11, 3067-3091,  
1331 doi:10.5194/acp-11-3067-2011, 2011.  
1332

1333 Di Sarra, A., Di Iorio, T., Cacciani, M., Fiocco, G., and Fuà, D.: Saharan dust profiles measured by  
1334 lidar at Lampedusa, *J. Geophys. Res.*, 106, 10 335–10 348, doi:10.1029/2000JD900734, 2001.  
1335

1336 Díaz, J., Tobías A., and Linares, C.: Saharan dust and association between particulate matter and case-  
1337 specific mortality: a case crossover analysis in Madrid (Spain), *Environ. Health*, doi:10.1186/1476-  
1338 069X-11-11, 2012.  
1339

Formatted: English (U.S.)



1340 Draxler, R.R. and Rolph, G.D., 2015. HYSPLIT (HYbrid Single-Particle Lagrangian Integrated  
1341 Trajectory) Model access via NOAA ARL READY Website (<http://ready.arl.noaa.gov/HYSPLIT.php>).  
1342 NOAA Air Resources Laboratory, Silver Spring, MD.  
1343  
1344 Dubovik, O., Smirnov, A., Holben, B. N., King, M. D., Kaufman, Y. J., and Slutsker, I.: Accuracy  
1345 assessments of aerosol optical properties retrieved from AERONET sun and sky radiance  
1346 measurements, *J. Geophys. Res.*, 105, 9791–9806, doi: 10.1029/2000JD900040, 2000.  
1347  
1348 Dubovik, O. and King, M. D.: A flexible inversion algorithm for retrieval of aerosol optical properties  
1349 from Sun and sky radiance measurements, *J. Geophys. Res.*, 105, 20673-20696, doi:  
1350 10.1029/2000JD900282, 2000.  
1351  
1352 Dulac, F., Moulin, C., Lambert, C.E., Guillard, F., Poitou, J., Guelle, W., Quétel, C.R., Schneider, X.,  
1353 Ezat, U., and Buat-Ménard, P.: Dry deposition of mineral aerosol particles in the atmosphere:  
1354 Significance of the large size fraction, in *Precipitation Scavenging and Atmosphere-Surface Exchange*,  
1355 edited by S. E. Schwartz and W.G. N. Slinn, pp. 841-854, Hemisphere. Richland, Wash., 1992.  
1356  
1357 Eck, T. F., Holben, B. N., Reid, J. S., Dubovik, O., Smirnov, A., O’Neill, N. T., Slutsker, I., and Kinne,  
1358 S.: Wavelength dependence of optical depth of biomass burning, urban and desert dust aerosols, *J.*  
1359 *Geophys. Res.*, 104, 31333–31350, doi: 10.1029/1999JD900923, 1999.  
1360  
1361 Eguchi, K., Uno, I., Yumimoto, K., Takemura, T., Shimizu, A., Sugimoto, N., and Liu, Z.: Trans-  
1362 pacific dust transport: integrated analysis of NASA/CALIPSO and a global aerosol transport model,  
1363 *Atmos. Chem. Phys.*, 9, 3137-3145, doi:10.5194/acp-9-3137-2009, 2009.  
1364  
1365 Escudero, M., Querol, X., Pey, J., Alastuey, A., Pérez, N., Ferreira, F., Alonso, S., Rodríguez, S., and  
1366 Cuevas, E.: A methodology for the quantification of the net African dust load in air quality monitoring  
1367 networks, *Atmos. Environ.*, 41, 5516–5524, doi:10.1016/j.atmosenv.2007.04.047, 2007.  
1368  
1369 Fotiadi, A., Hatzianastassiou, N., Drakakis, E., Matsoukas, C., Pavlakakis, K.G., Hatzidimitriou, D.,  
1370 Gerasopoulos, E., Mihalopoulos, N., and Vardavas, I.: Aerosol physical and optical properties in the

1371 Eastern Mediterranean Basin, Crete, from Aerosol Robotic Network data, *Atmos. Chem. Phys.*, 6,  
1372 5399–5413, doi:10.5194/acp-6-5399-2006, 2006.

1373

1374 Ginoux, P., Prospero, J. M., Gill, T. E., Hsu, N. C., and Zhao, M.: Global-scale attribution of  
1375 anthropogenic and natural dust sources and their emission rates based on MODIS Deep Blue aerosol  
1376 products, *Rev. Geophys.*, 50, RG3005, doi:10.1029/2012rg000388, 2012.

1377

1378 Gkikas, A., Hatzianastassiou, N., and Mihalopoulos, N.: Aerosol events in the broader Mediterranean  
1379 basin based on 7-year (2000–2007) MODIS C005 data, *Ann. Geophys.*, 27, 3509-3522,  
1380 doi:10.5194/angeo-27-3509-2009, 2009.

1381

1382 Gkikas, A., Hatzianastassiou, N., Mihalopoulos, N., Katsoulis, V., Kazadzis, S., Pey, J., Querol, X.,  
1383 and Torres, O.: The regime of intense desert dust episodes in the Mediterranean based on contemporary  
1384 satellite observations and ground measurements, *Atmos. Chem. Phys.*, 13, 12135-12154,  
1385 doi:10.5194/acp-13-12135-2013, 2013.

1386 Gkikas, A., Houssos, E. E., Lolis, C. J., Bartzokas, A., Mihalopoulos, N. and Hatzianastassiou, N.:  
1387 Atmospheric circulation evolution related to desert-dust episodes over the Mediterranean. *Q.J.R.*  
1388 *Meteorol. Soc.*, 141: 1634–1645. doi: 10.1002/qj.2466, 2015.

1389 [Gkikas, A., Hatzianastassiou, N., Mihalopoulos, N., Torres, O.: Characterization of aerosols episodes  
1390 in the greater Mediterranean Sea area from satellite observations \(2000 – 2007\), \*Atmos. Environ.\*, 128,  
1391 286 – 304, doi:10.1016/j.atmosenv.2015.11.056, 2016.](#)

1392 Gobbi, G.P., Barnaba, F., Giorgi, R., Santacasa, A.: Altitude-resolved properties of a Saharan dust  
1393 event over the Mediterranean, *Atmos. Environ.*, 34, 5119-5127, doi:10.1016/S1352-2310(00)00194-1,  
1394 2000.

1395 Gobbi, G. P., Kaufman, Y. J., Koren, I., and Eck, T. F.: Classification of aerosol properties derived  
1396 from AERONET direct sun data, *Atmos. Chem. Phys.*, 7, 453-458, doi:10.5194/acp-7-453-2007, 2007.

1397 Gobbi, G. P., Angelini, F., Barnaba, F., Costabile, F., Baldasano, J. M., Basart, S., Sozzi, R., and  
1398 Bolignano, A.: Changes in particulate matter physical properties during Saharan advections over Rome  
1399 (Italy): a four-year study, 2001–2004, *Atmos. Chem. Phys.*, 13, 7395–7404, doi:10.5194/acp-13-7395-  
1400 2013, 2013.

**Formatted:** Font: (Default) Times New Roman, 12 pt

**Formatted:** Font: (Default) Times New Roman, 12 pt

1401 Hamonou, E., Chazette, P., Balis, D., Dulac, F., Schneider, X., Galani, E., Ancellet, G., and  
1402 Papayannis, A.: Characterization of the vertical structure of Saharan dust export to the Mediterranean  
1403 basin, *J. Geophys. Res.*, 104, 22 257–22 270, doi:10.1029/1999JD900257, 1999.

1404 Hara, Y., Yumimoto, K., Uno, I., Shimizu, A., Sugimoto, N., Liu, Z., and Winker, D. M.: Asian dust  
1405 outflow in the PBL and free atmosphere retrieved by NASA CALIPSO and an assimilated dust  
1406 transport model, *Atmos. Chem. Phys.*, 9, 1227-1239, doi:10.5194/acp-9-1227-2009, 2009.

1407 Hatzianastassiou, N., Gkikas, A., Mihalopoulos, N., Torres, O., and Katsoulis, B. D.: Natural versus  
1408 anthropogenic aerosols in the eastern Mediterranean basin derived from multiyear TOMS and MODIS  
1409 satellite data, *J. Geophys. Res.*, 114, D24202, doi:10.1029/2009JD011982, 2009.

1410 Heinold, B., Helmert, J., Hellmuth, O., Wolke, R., Ansmann, A., Marticorena, B., Laurent, B. and  
1411 Tegen, I.: Regional modeling of Saharan dust events using LM-MUSCAT: Model description and case  
1412 studies, *J. Geophys. Res.*, 112, D11204, doi:10.1029/2006JD007443, 2007.

1413 Heinold, B., Tegen, I., Schepanski, K., and Hellmuth, O.: Dust Radiative feedback on Saharan  
1414 boundary layer dynamics and dust mobilization. *Geophys. Res. Lett.*, 35, L20817,  
1415 doi:10.1029/2008GL035319, 2008.

1416 Herman, J. R., Bhartia, P. K., Torres, O., Hsu, N.C., Sefstor, C. J., and Celarier E.: Global distribution of  
1417 UV-absorbing aerosols from Nimbus-7/ TOMS data, *J. Geophys. Res.*, 102, 16911– 16923, doi:  
1418 10.1029/96JD03680, 1997.

1419 Holben, B. N., Eck, T. F., Slutsker, I., Tanré, D., Buis, J. P., Setzer, A., Vermote, E., Reagan, J. A.,  
1420 Kaufman, Y. J., Nakajima, T., Lavenu, F., Jankowiak, I., and Smirnov, A.: AERONET – A federated  
1421 instrument network and data archive for aerosol characterization, *Remote Sens. Environ.*, 66, 1–16,  
1422 doi:10.1016/S0034-4257(98)00031-5, 1998.

1423 Huang, J., Minnis, P., Lin, B., Wang, T., Yi, Y., Hu, Y., Sun-Mack, S. and Ayers, K.: Possible influences  
1424 of Asian dust aerosols on cloud properties and radiative forcing observed from MODIS and CERES,  
1425 *Geophys. Res. Lett.*, 33, L06824, doi:10.1029/2005GL024724, 2006.

1426 Huang, J., Zhang, C., and Prospero, J. M.: African dust outbreaks: a satellite perspective of temporal  
1427 and spatial variability over the tropical Atlantic Ocean, *J. Geophys. Res.*, 115, D05202,  
1428 doi:10.1029/2009JD012516, 2010.

1429 Hubanks, P. A., King, M. D., Platnick, S. A., and Pincus, R. A.: MODIS Atmosphere L3 Gridded  
1430 Product Algorithm Theoretical Basis Document, MODIS Algorithm Theoretical Basis Document No.  
1431 ATBD-MOD-30 for Level-3 Global Gridded Atmosphere Products (08 D3, 08 E3, 08M3), online:  
1432 [http://modis-atmos.gsfc.nasa.gov/docs/L3 ATBD 2008 12 04.pdf](http://modis-atmos.gsfc.nasa.gov/docs/L3%20ATBD%202008%2012%2004.pdf), 2008.

1433 Hunt, W. H, Winker, D. M., Vaughan, M. A., Powell, K. A., Lucker, P. L., and Weimer, C.: CALIPSO  
1434 Lidar Description and Performance Assessment, *J. Atmos. Ocean. Technol.*, 26, 1214–1228,  
1435 doi:10.1175/2009JTECHA1223.1, 2009.

1436 IPCC, 2013: Summary for Policymakers. In: *Climate Change 2013: The Physical Science Basis.*  
1437 *Contribution of Working Group I to the Fifth Assessment Report of the Intergovernmental Panel on*  
1438 *Climate Change* [Stocker, T.F., D. Qin, G.-K. Plattner, M. Tignor, S. K. Allen, J. Boschung, A. Nauels,  
1439 Y. Xia, V. Bex and P.M. Midgley (eds.)]. Cambridge University Press, Cambridge, United Kingdom  
1440 and New York, NY, USA.

1441 Kalivitis, N., Gerasopoulos, E., Vrekoussis, M., Kouvarakis, G., Kubilay, N., Hatzianastassiou, N.,  
1442 Vardavas, I., and Mihalopoulos, N.: Dust transport over the eastern Mediterranean derived from  
1443 TOMS, AERONET and surface measurements, *J. Geophys. Res.*, 112, D03202,  
1444 doi:10.1029/2006JD007510, 2007.

1445 Karanasiou, A., Moreno, N., Moreno, T., Viana, M., de Leeuw, F., Querol, X.: Health effects from  
1446 Sahara dust episodes in Europe: literature review and research gaps, *Environ. Int.*, 15, 107–  
1447 114, doi:10.1016/j.envint.2012.06.012, 2012.

1448 Karyampudi, V. M., Palm, S. P., Reagen, J. A., Fang, H., Grant, W. B., Hoff, R. M., Moulin, C.,  
1449 Pierce, H. F., Torres, O., Browell, E. V., and Melfi, S. H.: Validation of the Saharan dust plume  
1450 conceptual model using lidar, Meteosat and ECMWF, *B. Am. Meteorol. Soc.*, 80, 1045–1075, doi:  
1451 10.1175/1520-0477(1999)080<1045:VOTSDP>2.0.CO;2, 1999.

1452 Kaufman, Y. J., Tanré, D., Remer, L. A., Vermote, E. F., Chu, A., and Holben, B. N.: Operational  
1453 remote sensing of tropospheric aerosol over land from EOS Moderate-resolution Imaging  
1454 Spectroradiometer, *J. Geophys. Res.*, 102, 17051–17065, doi: 10.1029/96JD03988, 1997.

1455 Kaufman, Y. J., Smirnov, A., Holben, B. N., and Dubovik, O.: Baseline maritime aerosol: methodology  
1456 to derive the optical thickness and the scattering properties, *Geophys. Res. Lett.*, 28, 3251– 3254, doi:  
1457 10.1029/2001GL013312, 2001.

1458 Kaufman, Y. J., Tanre, D., Holben, B. N., Mattoo, S., Remer, L. A., Eck, T. F., Vaughan, J., and  
1459 Chatenet, B.: Aerosol radiative impact on spectral solar flux at the surface, derived from principal-  
1460 plane sky measurements, *J. Atmos. Sci.*, 59, 635–646, doi: 10.1175/1520-  
1461 0469(2002)059<0635:AROSS>2.0.CO;2, 2002.

1462 Kazadzis, S., Bais, A., Amiridis, V., Balis, D., Meleti, C., Kouremeti, N., Zerefos, C. S.,  
1463 Rapsomanikis, S., Petrakakis, M., Kelesis, A., Tzoumaka, P., and Kelektoglou, K.: Nine years of UV  
1464 aerosol optical depth measurements at Thessaloniki, Greece, *Atmos. Chem. Phys.*, 7, 2091-2101,  
1465 doi:10.5194/acp-7-2091-2007, 2007.

1466 Kishcha, P., Barnaba, F., Gobbi, G. P., Alpert, P., Shtivelman, A., Krichak, S. O., and Joseph, J. H.:  
1467 Vertical distribution of Saharan dust over Rome (Italy): Comparison between 3-year model predictions  
1468 and lidar soundings, *J. Geophys. Res.*, 110, D06208, doi:10.1029/2004JD005480, 2005.

1469

1470 Klein, H., Nickovic, S., Haunold, W., Bundke, U., Nillius, B., Ebert, M., Weinbruch, S., Schuetz, L.,  
1471 Levin, Z., Barrie, L. A., and Bingemer, H.: Saharan dust and ice nuclei over Central Europe, *Atmos.*  
1472 *Chem. Phys.*, 10, 10211–10221, doi:10.5194/acp-10-10211-2010, 2010.

1473

1474 Kubilay, N., Cokacar, T., and Oguz, T.: Optical properties of mineral dust outbreaks over the  
1475 northeastern Mediterranean, *J. Geophys. Res.*, 108, 4666, doi:10.1029/2003JD003798, 2003.

1476 Lau, K. M., Kim, M. K., and Kim, K. M.: Asian summer monsoon anomalies induced by direct forcing:  
1477 The role of the Tibetan plateau, *Clim. Dynam.*, 26, 855–864, doi: 10.1007/s00382-006-0114-z, 2006.

1478 Levy, R. C., Remer, L. A., Tanré, D., Kaufman, Y. J., Ichoku, C., Holben, B. N., Livingston, J. M.,  
1479 Russell, P. B., and Maring, H.: Evaluation of the Moderate-Resolution Imaging Spectroradiometer  
1480 (MODIS) retrievals of dust aerosol over the ocean during PRIDE, *J. Geophys. Res.*, 108, 8594,  
1481 doi:10.1029/2002JD002460, 2003.

1482 Levy, R. C., Remer, L. A., Kleidman, R. G., Mattoo, S., Ichoku, C., Kahn, R., and Eck, T. F.: Global  
1483 evaluation of the Collection 5 MODIS dark-target aerosol products over land, *Atmos. Chem. Phys.*, 10,  
1484 10399–10420, doi:10.5194/acp-10-10399-2010, 2010.

1485 Liu, D., Wang, Z., Liu, Z., Winker, D., and Trepte, C.: A height resolved global view of dust aerosols  
1486 from the first year CALIPSO lidar measurements, *J. Geophys. Res.*, 113, D16214,  
1487 doi:10.1029/2007JD009776, 2008.

1488 Liu, Z., Vaughan, M., Winker, D., Kittaka, C., Getzewich, B., Kuehn, R., Omar, A., Powell, K., Trepte,  
1489 C., and Hostetler, C.: The CALIPSO Lidar Cloud and Aerosol Discrimination: Version 2 Algorithm  
1490 and Initial Assessment of Performance, *J. Atmos. Ocean. Technol.*, 26, 1198–1213,  
1491 doi:10.1175/2009jtecha1229.1, 2009.

1492 Luo, T., Wang, Z., Zhang, D., Liu, X., Wang, Y., and Yuan, R.: Global dust distribution from improved  
1493 thin dust layer detection using A-train satellite lidar observations, *Geophys. Res. Lett.*, 42,  
1494 doi:10.1002/2014GL062111, 2015.

1495 Lyamani, H., Olmo, F. J., and Alados-Arboledas, L.: Saharan dust outbreak over southeastern Spain as  
1496 detected by sun photometer, *Atmos. Environ.*, 39, 7276–7284,  
1497 doi:10.1016/j.atmosenv.2005.09.011, 2005.

1498 Mallet, M., Tulet, P., Serça, D., Solmon, F., Dubovik, O., Pelon, J., Pont, V., and Thouron, O.: Impact  
1499 of dust aerosols on the radiative budget, surface heat fluxes, heating rate profiles and convective  
1500 activity over West Africa during March 2006, *Atmos. Chem. Phys.*, 9, 7143-7160, doi:10.5194/acp-9-  
1501 7143-2009, 2009.

1502 Mallet, M., Dubovik, O., Nabat, P., Dulac, F., Kahn, R., Sciare, J., Paronis, D., and Léon, J. F.:  
1503 Absorption properties of Mediterranean aerosols obtained from multi-year ground-based remote  
1504 sensing observations, *Atmos. Chem. Phys.*, 13, 9195-9210, doi:10.5194/acp-13-9195-2013, 2013.

1505 Marriotti, A., Struglia, M.V., Zeng, N., Lau, K.-M.: The Hydrological Cycle in the Mediterranean  
1506 Region and Implications for the Water Budget of the Mediterranean Sea, *J. Clim.*, 15, 1674-1690, doi:  
1507 10.1175/1520-0442(2002)015<1674:THCITM>2.0.CO;2, 2002.

1508 Matthias, V., Balis, D., Bösenberg, J., Eixmann, R., Iarlori, M., Komguem, L., Mattis, I., Papayannis,  
1509 A., Pappalardo, G., Perrone, M. R., and Wang, X.: Vertical aerosol distribution over Europe: Statistical  
1510 analysis of Raman lidar data from 10 European Aerosol Research Lidar Network (EARLINET)  
1511 stations, *J. Geophys. Res.*, 109, D18201, doi:10.1029/2004JD004638, 2004.

1512 McGrath-Spangler, E. L. and Denning, A. S.: Global Seasonal Variations of Midday Planetary  
1513 Boundary Layer Depth from CALIPSO Space-borne LIDAR, *J. Geophys. Res. Atmos.*, 118, 1226–  
1514 1233, doi: 10.1002/jgrd.50198, 2013.

1515 Mehta, A. V. and Yang, S.: Precipitation climatology over Mediterranean Basin from ten years of  
1516 TRMM measurements, *Adv. Geosci.*, 17, 87-91, doi:10.5194/adgeo-17-87-2008, 2008.

1517 Meloni, D., di Sarra, A., Biavati, G., DeLuisi, J. J., Monteleone, F., Pace, G., Piacentino, S., and  
1518 Sferlazzo, D. M.: Seasonal behavior of Saharan dust events at the Mediterranean island of Lampedusa  
1519 in the period 1999–2005, *Atmos. Environ.*, 41, 3041–3056, [doi:10.1016/j.atmosenv.2006.12.001](https://doi.org/10.1016/j.atmosenv.2006.12.001), 2007.  
1520

1521 Meloni, D., di Sarra, A., Monteleone, F., Pace, G., Piacentino, S., and Sferlazzo, D. M.: Seasonal  
1522 transport patterns of intense Saharan dust events at the Mediterranean island of Lampedusa, *Atmos.*  
1523 *Res.*, 88, 134–148, [doi:10.1016/j.atmosres.2007.10.007](https://doi.org/10.1016/j.atmosres.2007.10.007), 2008.

1524 Middleton, N. J. and Goudie, A. S.: Saharan dust: sources and trajectories, *Trans. Inst. Br. Geogr.*, 26,  
1525 165–181, doi: 10.1111/1475-5661.00013, 2001.

1526 Mielonen, T., Arola, A., Komppula, M., Kukkonen, J., Koskinen, J., de Leeuw, G., and Lehtinen, K. E.  
1527 J.: Comparison of CALIOP level 2 aerosol subtypes to aerosol types derived from AERONET  
1528 inversion data, *Geophys. Res. Lett.*, 36, L18804, [doi:10.1029/2009gl039609](https://doi.org/10.1029/2009gl039609), 2009.

1529 Mona, L., Amodeo, A., Pandolfi, M. and Pappalardo, G.: Saharan dust intrusions in the Mediterranean  
1530 area: Three years of Raman lidar measurements, *J. Geophys. Res.*, 111, D16203,  
1531 [doi:10.1029/2005JD006569](https://doi.org/10.1029/2005JD006569), 2006.

1532 Mona, L., Liu, Z., Müller, D., Omar, A., Papayannis, A., Pappalardo, G., Sugimoto, N., and  
1533 Vaughan, M.: Lidar Measurements for Desert Dust Characterization: An Overview, *Adv. Meteorol.*,  
1534 2012, 356265, [doi:10.1155/2012/356265](https://doi.org/10.1155/2012/356265), 2012.

1535 Mona, L., Papagiannopoulos, N., Basart, S., Baldasano, J. M., Biniotoglou, I., Cornacchia, C., and  
1536 Pappalardo, G.: EARLINET dust observations vs. BSC-DREAM8b modeled profiles: 12-year-long  
1537 systematic comparison at Potenza, Italy, *Atmos. Chem. Phys.*, 14, 8781–8793, [doi:10.5194/acp-14-](https://doi.org/10.5194/acp-14-8781-2014)  
1538 8781-2014, 2014.

1539 Moulin, C., Lambert, C. E., Dulac, F., and Dayan, U.: Control of atmospheric export of dust from  
1540 North Africa by the North Atlantic Oscillation, *Nature*, 387, 691–694, 1997.

1541 Moulin, C., Lambert, C., Dayan, U., Masson, V., Ramonet, M., Bousquet, P., Legrand, M., Balkanski,  
1542 Y., Guelle, W., Marticorena, B., Bergametti, G., and Dulac, F.: Satellite climatology of African dust  
1543 transport in the Mediterranean atmosphere, *J. Geophys. Res.*, 103, 13137–13144, doi:  
1544 10.1029/98JD00171, 1998.

1545 Nabat, P., Somot, S., Mallet, M., Chiapello, I., Morcrette, J. J., Solmon, F., Szopa, S., Dulac, F.,  
1546 Collins, W., Ghan, S., Horowitz, L. W., Lamarque, J. F., Lee, Y. H., Naik, V., Nagashima, T., Shindell,  
1547 D., and Skeie, R.: A 4-D climatology (1979–2009) of the monthly tropospheric aerosol optical depth  
1548 distribution over the Mediterranean region from a comparative evaluation and blending of remote  
1549 sensing and model products, *Atmos. Meas. Tech.*, 6, 1287–1314, doi:10.5194/amt-6-1287-2013, 2013.

1550 Nowotnick, E. P., Colarco, P. R., Welton, E. J., and da Silva, A.: Use of the CALIOP vertical feature  
1551 mask for evaluating global aerosol models, *Atmos. Meas. Tech.*, 8, 3647–3669, doi:10.5194/amt-8-  
1552 3647-2015, 2015.

1553 Omar, A. H., Winker, D. M., Kittaka, C., Vaughan, M. A., Liu, Z. Y., Hu, Y. X., Treppe, C. R., 20  
1554 Rogers, R. R., Ferrare, R. A., Lee, K. P., Kuehn, R. E., and Hostetler, C. A.: The CALIPSO automated  
1555 aerosol classification and lidar ratio selection algorithm, *J. Atmos. Ocean. Technol.*, 26, 1994–2014,  
1556 doi:10.1175/2009jtech1231.1, 2009.

1557 O’Neill, N. T., Eck, T. F., Smirnov, A., Holben, B. N., and Thulasiraman, S.: Spectral discrimination of  
1558 coarse and fine mode optical depth, *J. Geophys. Res.-Atmos.*, 108, 4559, doi:10.1029/2002JD002975,  
1559 2003.

1560 Pace, G., di Sarra, A., Meloni, D., Piacentino, S., and Chamard, P.: Aerosol optical properties at  
1561 Lampedusa (Central Mediterranean). 1. Influence of transport and identification of different aerosol  
1562 types, *Atmos. Chem. Phys.*, 6, 697–713, doi:10.5194/acp-6-697-2006, 2006.

1563 Papadimas, C. D., Hatzianastassiou, N., Mihalopoulos, N., Querol, X., and Vardavas, I.: Spatial and  
1564 temporal variability in aerosol properties over the Mediterranean basin based on 6-year (2000–2006)  
1565 MODIS data, *J. Geophys. Res.*, 113, D11205, doi:10.1029/2007JD009189, 2008.

1566 Papadimas, C. D., Hatzianastassiou, N., Mihalopoulos, N., Kanakidou, M., Katsoulis, B. D., and  
1567 Vardavas, I.: Assessment of the MODIS Collections C005 and C004 aerosol optical depth products  
1568 over the Mediterranean basin, *Atmos. Chem. Phys.*, 9, 2987– 2999, doi:10.5194/acp-9-2987-2009,  
1569 2009.

1570 Papayannis, A., Balis, D., Amiridis, V., Chourdakis, G., Tsaknakis, G., Zerefos, C., Castanho, A.D.A.,  
1571 Nickovic, S., Kazadzis, S., and Grabowski, J.: Measurements of Saharan dust aerosols over the Eastern  
1572 Mediterranean using elastic backscatter-Raman lidar, spectrophotometric and satellite observations in  
1573 the frame of the EARLINET project, *Atmos. Chem. Phys.*, 5, 2065–2079, doi:10.5194/acp-5-2065-  
1574 2005, 2005.



1575 Papayannis, A., Amiridis, V., Mona, L., Tsaknakis, G., Balis, D., Bösenberg, J., Chaikovski, A., De  
1576 Tomasi, F., Grigorov, I., Mattis, I., Mitev, V., Müller, D., Nickovic, S., Pérez, C., Pietruczuk, A.,  
1577 Pisani, G., Ravetta, F., Rizi, V., Sicard, M., Trickl, T., Wiegner, M., Gerding, M., Mamouri, R. E.,  
1578 D'Amico, G., and Pappalardo, G.: Systematic lidar observations of Saharan dust over Europe in the  
1579 frame of EARLINET (2000–2002), *J. Geophys. Res.*, 113, D10204, doi:10.1029/2007JD009028, 2008.

1580 Papayannis, A., Mamouri, R. E., Amiridis, V., Kazadzis, S., Pérez, C., Tsaknakis, G., Kokkalis, P., and  
1581 Baldasano, J. M.: Systematic lidar observations of Saharan dust layers over Athens, Greece in the  
1582 frame of EARLINET project (2004–2006), *Ann. Geophys.*, 27, 3611–3620, doi:10.5194/angeo-27-  
1583 3611-2009, 2009.

1584 Papayannis, A., Nicolae, D., Kokkalis, P., Biniotoglou, I., Talianu, C., Belegante, L., Tsaknakis, G.,  
1585 Cazacu, M.M., Vetres, I., Ilic, L.: Optical, size and mass properties of mixed type aerosols in Greece  
1586 and Romania as observed by synergy of lidar and sunphotometers in combination with model  
1587 simulations: A case study, *Sci. Total Environ.*, Volumes: 500-501, 277–294,  
1588 doi:10.1016/j.scitotenv.2014.08.101, 2014.

1589 Pereira, S. N., Wagner, F., and Silva, A. M.: Seven years of measurements of aerosol scattering  
1590 properties, near the surface, in the southwestern Iberia Peninsula, *Atmos. Chem. Phys.*, 11, 17–29,  
1591 doi:10.5194/acp-11-17-2011, 2011.

1592 Pérez, C., Nickovic, S., Pejanovic, G., Baldasano, J.M. and Özsoy, E.: Interactive dust-radiation  
1593 modeling: A step to improve weather forecasts, *J. Geophys. Res.*, 111, D16206,  
1594 doi:10.1029/2005JD006717, 2006.

1595 Pérez García-Pando, C., Stanton, M. C., Diggle, P. J., Trzaska, S., Miller, R. L., Perlwitz, J. P.,  
1596 Baldasano, J. M., Cuevas, E., Ceccato, P., Yaka, P., and Thomson, M. C.: Soil Dust Aerosols and Wind  
1597 as Predictors of Seasonal Meningitis Incidence in Niger, *Environ. Health Perspect.*, 122, 679–686,  
1598 doi:10.1289/ehp.1306640, 2014.

1599 Pey, J., Querol, X., Alastuey, A., Forastiere, F., and Stafoggia, M.: African dust outbreaks over the  
1600 Mediterranean Basin during 2001–2011: PM10 concentrations, phenomenology and trends, and its  
1601 relation with synoptic and mesoscale meteorology, *Atmos. Chem. Phys.*, 13, 1395–1410, doi:  
1602 10.5194/acp-13-1395-2013, 2013.

1603 Pisani, G., Boselli, A., Spinelli, N., Wang, X.: Characterization of Saharan dust layers over Naples  
1604 (Italy) during 2000–2003 EARLINET project, *Atmos. Res.* 102, 286 – 299,  
1605 doi:10.1016/j.atmosres.2011.07.012, 2011.

1606 Prospero, M. J., Ginoux, P., Torres, O., Nicholson, S. E., and Gill, T. E.: Environmental  
1607 characterization of global sources of atmospheric soil dust identified with the Nimbus 7 Total Ozone  
1608 Mapping Spectrometer (TOMS) absorbing aerosol product, *Rev. Geophys.*, 40, 1002,  
1609 doi:10.1029/2000RG000095, 2002.

1610 Prospero, J. M. and Lamb, P. J.: African droughts and dust transport to the Caribbean: climate change  
1611 implications, *Science*, 302, 1024–1027, doi:10.1126/science.1089915, 2003.

1612 Querol, X., Alastuey A., Lopez-Soler A., Plana F. Puigercus J.A, Mantilla E., Miro J.V.; Artiñano B.:  
1613 Seasonal evolution of atmospheric suspended particles around a coal-fired power station: Particulate  
1614 levels and sources, *Atmos. Environ.*, 32, 11, 1963-1978, doi: 10.1016/S1352-2310(97)00504-9, 1998.

1615 Querol, X., Alastuey, A., Pey, J., Cusack, M., Pérez, N., Mihalopoulos, N., Theodosi, C.,  
1616 Gerasopoulos, E., Kubilay, N., and Koçak, M.: Variability in regional background aerosols within the  
1617 Mediterranean, *Atmos. Chem. Phys.*, 9, 4575-4591, doi:10.5194/acp-9-4575-2009, 2009a.

1618 Querol, X., Pey, J., Pandolfi, M., Alastuey, A., Cusack, M., Pérez, N., Moreno, T., Viana, N.,  
1619 Mihalopoulos, N., Kallos, G. and Kleanthous, S.: African dust contributions to mean ambient PM10  
1620 mass-levels across the Mediterranean basin, *Atmos. Environ.*, 43, 4266–4277,  
1621 doi:10.1016/j.atmosenv.2009.06.013, 2009b.

1622 Redemann, J., Vaughan, M. A., Zhang, Q., Shinozuka, Y., Russell, P. B., Livingston, J. M.,  
1623 Kacenelenbogen, M., and Remer, L. A.: The comparison of MODIS-Aqua (C5) and CALIOP (V2 &  
1624 V3) aerosol optical depth, *Atmos. Chem. Phys.*, 12, 3025–3043, doi:10.5194/acp-12-3025-2012, 2012.

1625 Remer, L. A., Tanré, D., Kaufman, Y. J., Ichoku, C., Mattoo, S., Levy, R., Chu, D. A., Holben, B.,  
1626 Dubovik, O., Smirnov, A., Martins, J. V., Li, R.-R., and Ahman, Z.: Validation of MODIS aerosol  
1627 retrieval over ocean, *Geophys. Res. Lett.*, 29, 8008, doi:10.1029/2001GL013204, 2002.

1628 Remer, L. A., Kaufman, Y. J., Tanré, D., Mattoo, S., Chu, D. A., Martins, J. V., Li, R. R., Ichoku, C.,  
1629 Levy, R. C., Kleidman, R. G., Eck, T. F., Vermote, E., and Holben, B. N.: The MODIS aerosol  
1630 algorithm, products and validation, *J. Atmos. Sci.*, 62, 947–973,  
1631 doi: <http://dx.doi.org/10.1175/JAS3385.1>, 2005.

1632 Remer, L. A., Kleidman, R. G., Levy, R. C., Kaufman, Y. J., Tanré, D., Mattoo, S., Martins, J. V.,  
1633 Ichoku, C., Koren, I., Yu, H., and Holben, B. N.: Global aerosol climatology from the MODIS satellite  
1634 sensors, *J. Geophys. Res.*, 113, D14S07, doi:10.1029/2007JD009661, 2008.

1635 Rodríguez, S., Querol, X., Alastuey, A., Kallos, G., Kakaliagou, O.: Saharan dust contributions to  
1636 PM10 and TSP levels in Southern and Eastern Spain, *Atmos. Environ.*, 35, 2433–2447,  
1637 doi:10.1016/S1352-2310(00)00496-9, 2001.

1638 Salvador, P., Alonso-Pérez, S., Pey, J., Artñano, B., de Bustos, J. J., Alastuey, A., and Querol, X.:  
1639 African dust outbreaks over the western Mediterranean Basin: 11-year characterization of atmospheric  
1640 circulation patterns and dust source areas, *Atmos. Chem. Phys.*, 14, 6759–6775, doi:10.5194/acp-14-  
1641 6759-2014, 2014.

1642 Schepanski, K., Tegen, I., Todd, M. C., Heinold, B., Bönisch, G., Laurent, B., and Macke, A.:  
1643 Meteorological processes forcing Saharan dust emission inferred from MSG-SEVIRI observations of  
1644 subdaily dust source activation and numerical models, *J. Geophys. Res.*, 114, D10201,  
1645 doi:10.1029/2008jd010325, 2009.

1646 Schuster, G. L., Vaughan, M., MacDonnell, D., Su, W., Winker, D., Dubovik, O., Lapyonok, T., and  
1647 Trepte, C.: Comparison of CALIPSO aerosol optical depth retrievals to AERONET measurements, and  
1648 a climatology for the lidar ratio of dust, *Atmos. Chem. Phys.*, 12, 7431–7452, doi:10.5194/acp-12-  
1649 7431-2012, 2012.

1650 Smirnov, A., Holben, B. N., Eck, T. F., Dubovik, O. and Slutsker, I.: Cloud screening and quality  
1651 control algorithms for the AERONET database, *Remote Sens. Environ.*, 73, 337–349,  
1652 doi:10.1016/S0034-4257(00)00109-7, 2000.

1653 Solmon, F., Mallet, M., Elguindi, N., Giorgi, F., Zakey, A. and Konaré, A.: Dust aerosol impact on  
1654 regional precipitation over western Africa, mechanisms and sensitivity to absorption properties,  
1655 *Geophys. Res. Lett.*, 35, L24705, doi:10.1029/2008GL035900, 2008.

1656 Stephens, G. L., Vane, D. G., Boain, R. J., Mace, G. G., Sassen, K., Wang, Z., Illingworth, A. J.,  
1657 O’Conner, E. J., Rossow, W. G., Durden, S. L., Miller, S. D., Austin, R. T., Benedetti, A., and  
1658 Mitrescu, C.: The CloudSat mission and the A-Train, *Bull. Amer. Meteorol. Soc.*, 83, 1771–1790, doi:  
1659 10.1175/BAMS-83-12-1771, 2002.

1660 Tafuro, A.M., Barnaba, F., De Tomassi, F., Perrone, M.R., Gobbi, G.P.: Saharan dust particle  
1661 properties over the Central Mediterranean, *Atmos. Res.*, 81, 67-93,  
1662 [doi:10.1016/j.atmosres.2005.11.008](https://doi.org/10.1016/j.atmosres.2005.11.008), 2006.

1663 Tanré, D., Kaufman, Y. J., Herman, M., and Mattoo, S.: Remote sensing of aerosol properties over  
1664 oceans using the MODIS/EOS spectral radiances, *J. Geophys. Res.*, 102, 16971–16988, doi:  
1665 10.1029/96JD03437, 1997.

1666 Tegen, I.: Modelling the mineral dust aerosol cycle in the climate system, *Quat. Sci. Rev.*, 22, 1821–  
1667 1834, doi:10.1016/S0277-3791(03)00163-X, 2003.

1668 Toledano, C., Cachorro, V. E., de Frutos, A. M. Sorribas, M., Prats, N., and de la Morena, B. A.:  
1669 Inventory of African desert dust events over the southwestern Iberian Peninsula in 2000–2005 with an  
1670 AERONET Cimel Sun Photometer, *J. Geophys. Res.*, 112, D21201, doi:10.1029/2006JD008307,  
1671 2007a.

1672

1673 Toledano, C., Cachorro, V.E., Sorribas, M., Berjón, A., de la Morena, B.A., de Frutos, A.M. and  
1674 Gouloub, P.: Aerosol optical depth and Ångström exponent climatology at El Arenosillo AERONET  
1675 site (Huelva, Spain), *Q. J. R. Meteorol. Soc.*, 133, 795–807, doi:10.1002/qj.54, 2007b.

1676

1677 Torres, O., Bhartia, P.K., Herman, J.R., Ahmad, Z. and Gleason, J.: Derivation of aerosol properties  
1678 from a satellite measurements of backscattered ultraviolet radiation: Theoretical basis, *J. Geophys.*  
1679 *Res.*, 103, 17099–17110, doi: 10.1029/98JD00900, 1998.

1680

1681 Torres, O., Bhartia, P. K., Herman, J. R., Sinyuk A., Holben, B.: A long term record of aerosol optical  
1682 thickness from TOMS observations and comparison to AERONET measurements, *J. Atmos. Sci.*,  
1683 59398-413, doi: 10.1175/1520-0469(2002)059<0398:ALTROA>2.0.CO;2, 2002.

1684

1685 Torres, O., Bhartia, P.K., Sinyuk, A., Welton, E.J., and Holben, D.: Total Ozone Mapping  
1686 Spectrometer measurements of aerosol absorption from space: Comparison to SAFARI 2000 ground-  
1687 based observations, *J. Geophys. Res.*, 110, D10S18, doi:10.1029/2004JD004611, 2005.

1688

1689 Torres, O., A. Tanskanen, B. Veihelman, C. Ahn, R. Braak, P. K. Bhartia, P. Veefkind, and P. Levelt,  
1690 Aerosols and Surface UV Products from OMI Observations: An Overview, *J. Geophys. Res.*, 112,  
1691 D24S47, doi:10.1029/2007JD008809, 2007.

1692

1693 Trigo, I. F., Bigg, G. R., and Davies, T. D.: Climatology of cyclogenesis in the Mediterranean, *Mon.*  
1694 *Weather Rev.*, 130, 549–569, doi: 10.1175/1520-0493(2002)130<0549:COCMIT>2.0.CO;2, 2002.

1695 Tsamalis, C., Chédin, A., Pelon, J., and Capelle, V.: The seasonal vertical distribution of the Saharan  
1696 Air Layer and its modulation by the wind, *Atmos. Chem. Phys.*, 13, 11235-11257, doi:10.5194/acp-13-  
1697 11235-2013, 2013.

1698 Varga, G., Újvári, G., Kovács, J.: Spatiotemporal patterns of Saharan dust outbreaks in the  
1699 Mediterranean Basin, *Aeolian Res.*, Vol. 15, 151-160, doi:10.1016/j.aeolia.2014.06.005, 2014.

1700 Vaughan, M. A., Powell, K. A., Kuehn, R. E., Young, S. A., Winker, D. M., Hostetler, C. A., Hunt, W.  
1701 H., Liu, Z. Y., McGill, M. J., and Getzewich, B. J.: Fully automated detection of cloud and aerosol  
1702 layers in the CALIPSO lidar measurements, *J. Atmos. Ocean. Tech.*, 26, 2034–2050,  
1703 doi:10.1175/2009jtecha1228.1, 2009.

1704 Winker, D., Vaughan, M., Omar, A., Hu, Y., Powell, K., Liu, Z., Hunt, W., and Young, S.: Overview  
1705 of the CALIPSO mission and CALIOP data processing algorithm, *J. Atmos. Ocean. Technol.*, 26,  
1706 2310–2323, doi: <http://dx.doi.org/10.1175/2009JTECHA1281.1>, 2009.

1707 Winker, D. M., Tackett, J. L., Getzewich, B. J., Liu, Z., Vaughan, M. A., and Rogers, R. R.: The global  
1708 3-D distribution of tropospheric aerosols as characterized by CALIOP, *Atmos. Chem. Phys.*, 13, 3345-  
1709 3361, doi:10.5194/acp-13-3345-2013, 2013.

1710 Yoon, J., von Hoyningen-Huene, W., Kokhanovsky, A. A., Vountas, M., and Burrows, J. P.: Trend  
1711 analysis of aerosol optical thickness and Ångström exponent derived from the global AERONET  
1712 spectral observations, *Atmos. Meas. Tech.*, 5, 1271-1299, doi:10.5194/amt-5-1271-2012, 2012.

1713 Zhang, J. L., Reid, J. S., and Holben, B. N.: An analysis of potential cloud artifacts in MODIS over  
1714 ocean aerosol optical thickness products, *Geophys. Res. Lett.*, 32, L15803,  
1715 doi:10.1029/2005GL023254, 2005.

1716 Zhang, L., Li, Q. B., Gu, Y., Liou, K. N., and Meland, B.: Dust vertical profile impact on global  
1717 radiative forcing estimation using a coupled chemical-transport–radiative-transfer model, *Atmos.*  
1718 *Chem. Phys.*, 13, 7097-7114, doi:10.5194/acp-13-7097-2013, 2013.

1719

1720

1721

1722

1723

1724

1725

1726

1727

1728

1729

1730

1731

1732

1733

1734

1735

1736

1737

1738

1739 **Table 1:** AERONET stations, depicted with cyan colors in Figure 41, which have been used for the identification of desert  
1740 dust (*DD*) episodes based on ground retrievals.

Formatted: Font: Italic

Stations	Latitude	Longitude	Study period
<b>Blida</b>	N 36° 30' 28"	E 02° 52' 51"	7 Nov. 2003 – 18 Feb. 2012
<b>El Arenosillo</b>	N 37° 06' 18"	W 06° 43' 58"	1 Mar. 2000 – 21 Feb. 2010
<b>Evora</b>	N 38° 34' 04"	W 07° 54' 43"	4 Jul. 2003 – 28 Feb. 2013
<b>FORTH CRETE</b>	N 35° 19' 58"	E 25° 16' 55"	23 Jan. 2003 – 6 Aug. 2011
<b>IMC Oristano</b>	N 39° 54' 36"	E 08° 30' 00"	30 May 2000 – 28 Feb. 2003
<b>IMS METU Erdemli</b>	N 36° 33' 54"	E 34° 15' 18"	1 Mar. 2000 – 28 Feb. 2013
<b>Nes Ziona</b>	N 31° 55' 19"	E 34° 47' 20"	1 Feb. 2000 – 28 Feb. 2013

1741

1742 **Table 2:** Percentages of the satellite Ångström exponent, Fine fraction, Effective Radius and Aerosol Index retrievals  
1743 satisfying the defined thresholds in the satellite algorithm for the identification of desert dust episodes.

Formatted: Font: Italic

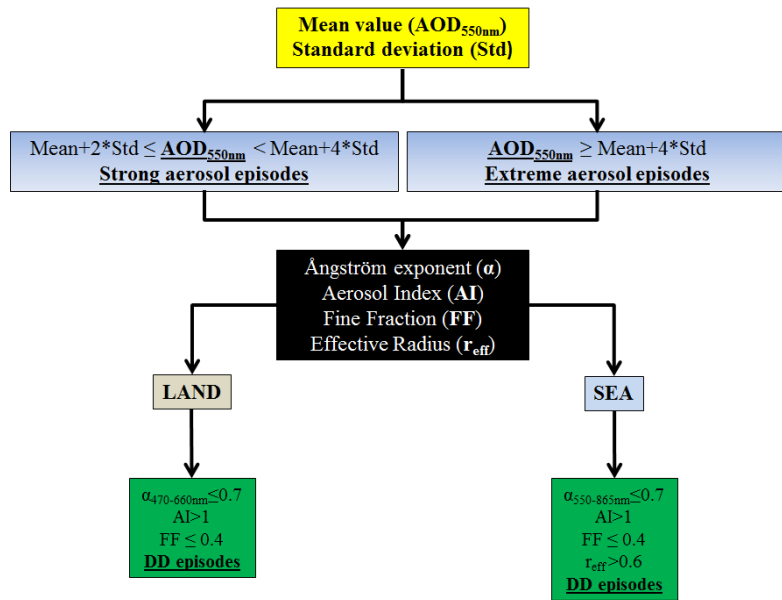
Parameter	Valid	Invalid	Number of <i>DD</i> episodes
<b>Ångström exponent</b>	97.8%	2.2%	232
<b>Fine fraction</b>	98.7%	1.3%	232
<b>Effective radius</b>	94.5%	5.5%	117
<b>Aerosol Index</b>	86.9%	13.1%	206

1744

1745

1746

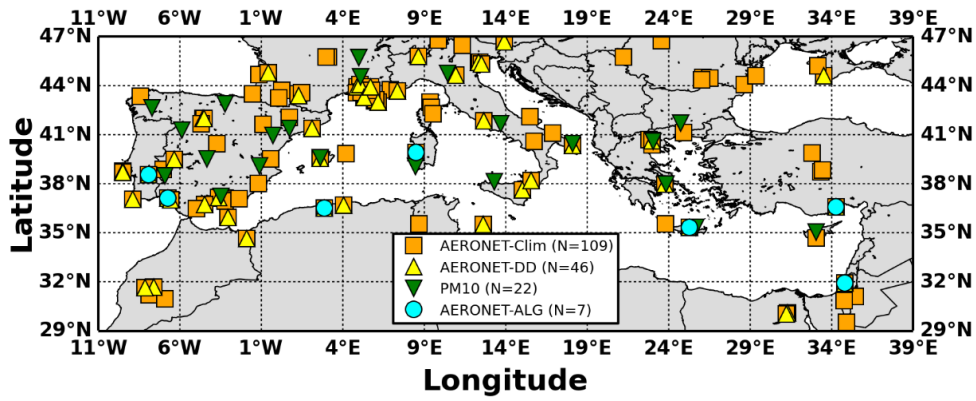
1747



1748  
1749  
1750  
1751  
1752  
1753  
1754

**Figure 1:** Methodology applied to each 1° x 1° grid cell for the identification of the intense Mediterranean desert dust outbreaks.





1755

1756 | **Figure 41:** Locations of the AERONET and  $PM_{10}$  stations which have been used for the evaluation of the algorithm's  
 1757 outputs. More specifically, with orange squares are denoted the AERONET stations located into the study region, with the  
 1758 yellow triangles the AERONET stations with coincident satellite and ground retrievals under dust episodes conditions, with  
 1759 the cyan circles the AERONET stations which have been used for the evaluation of the defined algorithm thresholds and  
 1760 with the green triangles are depicted the  $PM_{10}$  stations.

**Formatted:** English (U.S.)

**Formatted:** Font: Italic

**Formatted:** Font: Italic

1761

1762

1763

1764

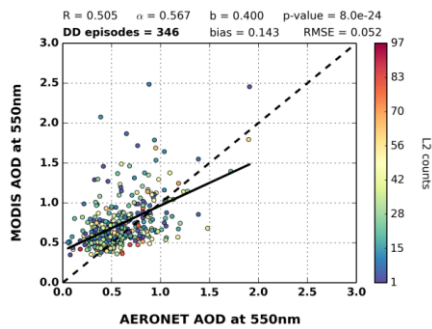
1765

1766

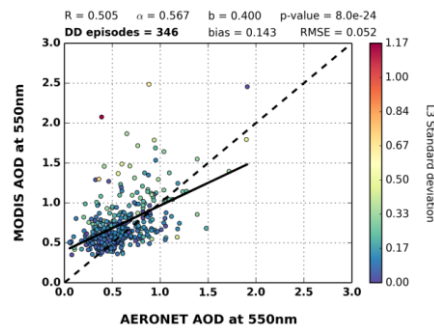
1767

1768

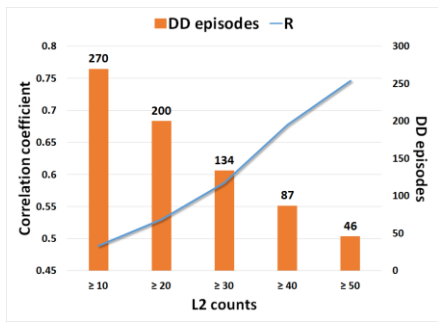
1769



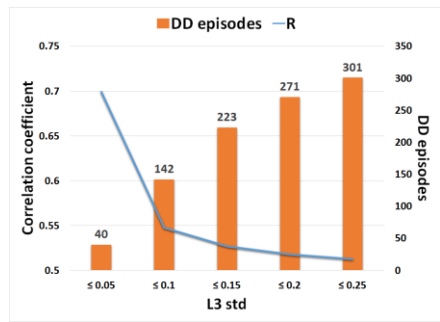
(i-a)



(i-b)



(ii-a)

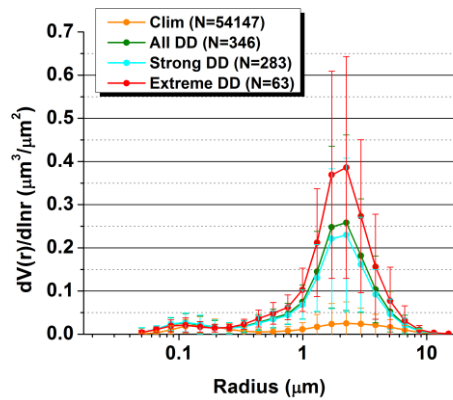


(ii-b)

1770 | **Figure 52:** (i) Scatterplots between MODIS-Terra and AERONET aerosol optical depths at 550 nm under intense desert  
 1771 dust episodes conditions related to the: (a) number of level 2 counts which are used for the calculation of the level 3  
 1772 retrievals and (b) spatial standard deviation inside the  $1^\circ \times 1^\circ$  grid cells (level 3 retrievals). (ii) Sensitivity analysis for the  
 1773 calculated correlation coefficients between satellite and ground  $AOD_s$ , depending on the: (a) number of level 2 retrievals  
 1774 and (b) sub-grid standard deviation of level 3 retrievals.

Formatted: English (U.S.)

1775  
 1776  
 1777  
 1778  
 1779  
 1780  
 1781  
 1782  
 1783  
 1784



1785

1786 | **Figure 36:** AERONET size distributions averaged for all available retrievals (orange curve) as well as for the total (green  
 1787 curve), strong (cyan curve) and extreme (red curve) desert dust episodes, occurred over the broader area of the  
 1788 Mediterranean basin, during the period Mar. 2000 – Feb. 2013. The error bars represent the calculated standard deviation.

Formatted: English (U.S.)

1789

1790

1791

1792

1793

1794

1795

1796

1797

1798

1799

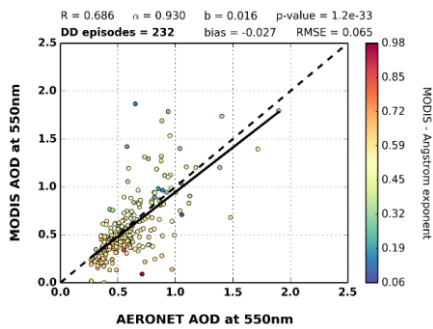
1800

1801

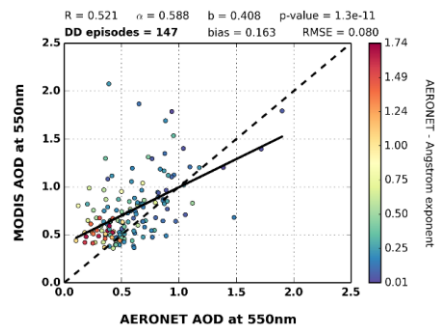
1802

1803

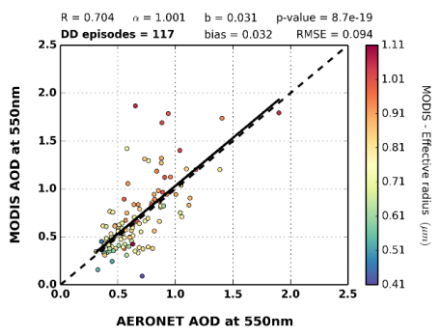
1804



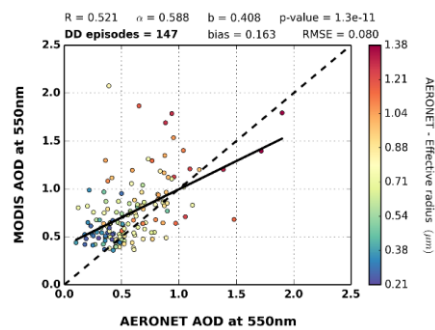
(i-a)



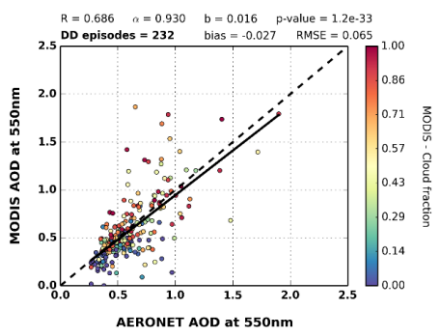
(i-b)



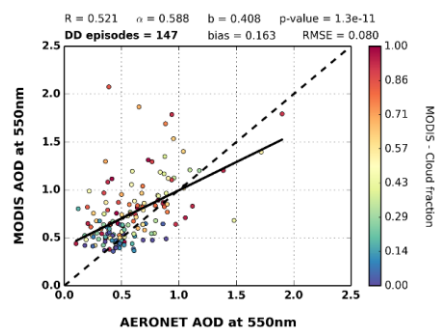
(ii-a)



(ii-b)



(iii-a)



(iii-b)

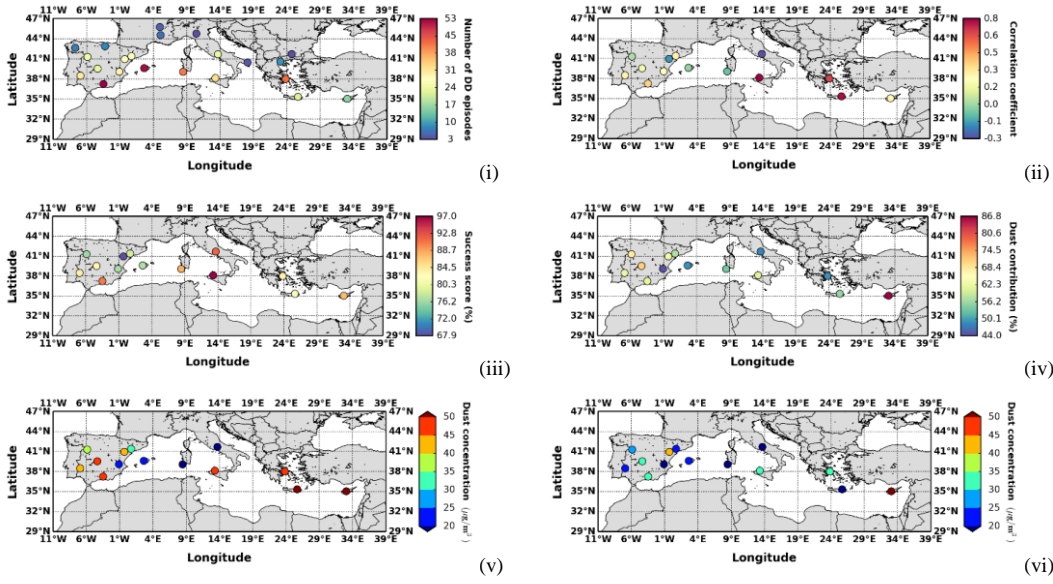
1805 | **Figure 74:** Scatterplots of MODIS-Terra and AERONET aerosol optical depths at 550 nm when intense dust episodes have  
 1806 been identified based on: (a) AERONET retrievals and (b) satellite algorithm, respectively. In the left column, colormaps  
 1807 indicate the corresponding values of: (i) Ångström exponent, (ii) Effective radius and (iii) Day cloud fraction derived by  
 1808 MODIS-Terra retrievals. In the right column, colormaps indicate the corresponding values of: (i) AERONET Ångström  
 1809 exponent, (ii) AERONET Effective radius and (iii) MODIS day cloud fraction retrievals. For each scatterplot, are provided  
 1810 the correlation coefficient ( $R$ ), slope ( $\alpha$ ), intercept ( $b$ ), p-value, number of  $DD$  episodes, bias ( $MODIS - AERONET$ ) and  
 1811 root mean square error ( $RMSE$ ).

Formatted: English (U.S.)

Formatted: Font: Italic

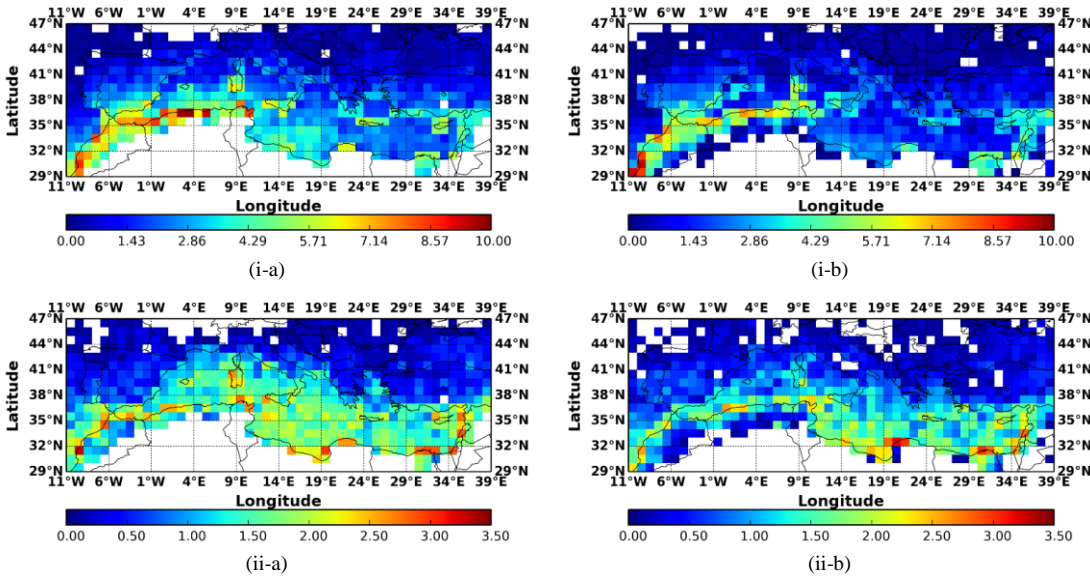
1812

1813



1814 **Figure S8:** (i) Number of concurrent intense *DD* episodes where total  $PM_{10}$  concentrations and MODIS-Terra *AOD*  
 1815 retrievals are available, (ii) Computed correlation coefficient values between total  $PM_{10}$  concentrations and MODIS-Terra  
 1816 *AOD* retrievals in stations where at least 10 *DD* episodes have been recorded, (iii) Percentage of intense *DD* episodes where  
 1817 dust particles have been identified by the ground stations, (iv) Dust contribution percentages (%) to the total  $PM_{10}$   
 1818 concentrations, (v) Calculated mean and (vi) median dust concentrations ( $\mu\text{g m}^{-3}$ ), based on ground measurements for the  
 1819 identified intense *DD* episodes by the satellite algorithm.

- Formatted: English (U.S.)
- Formatted: Font: Italic
- Formatted: Font: Italic
- Formatted: Font: Italic
- Formatted: Font: Italic
- Formatted: Font: Italic
- Formatted: Font: Italic
- Formatted: Font: Italic



1831 | **Figure 26:** Geographical distributions of the occurrence frequency (episodes<sub>year<sup>-1</sup></sub>) of: (i) strong and (ii) extreme desert  
 1832 dust episodes, averaged for the periods: (a) Mar. 2000 – Feb. 2013 (MODIS-Terra) and (b) 2003 – 2012 (MODIS-Aqua),  
 1833 over the broader area of the Mediterranean basin.

Formatted: English (U.S.)

Formatted: Superscript

1834

1835

1836

1837

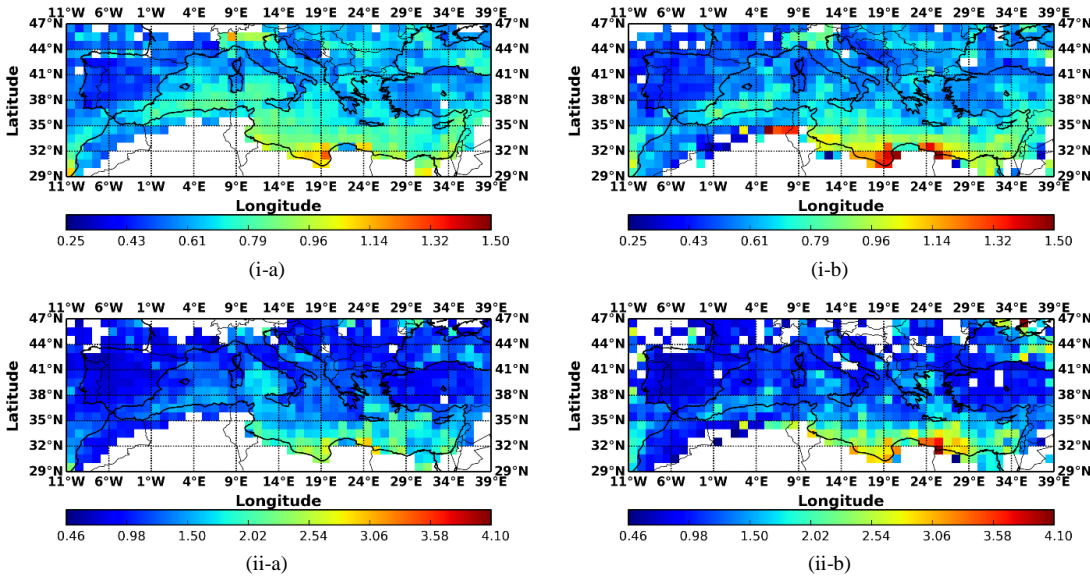
1838

1839

1840

1841

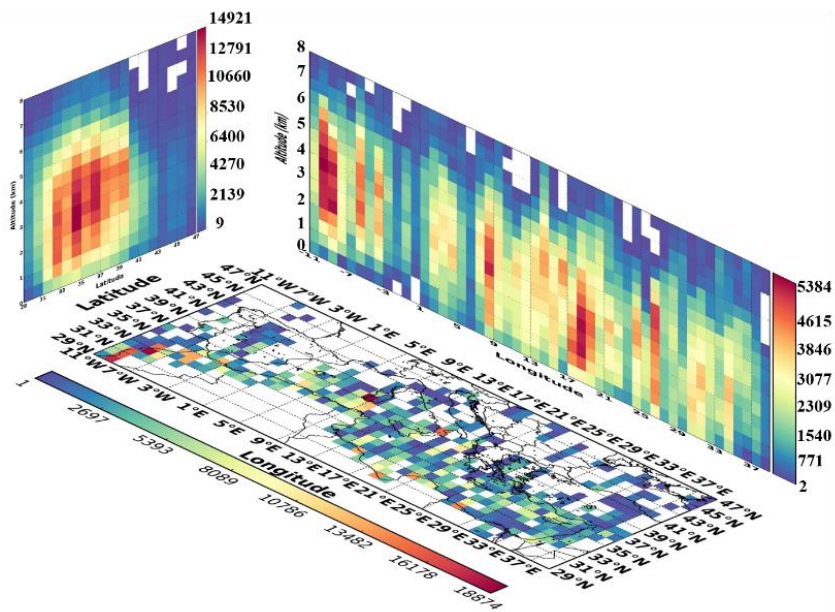
1842



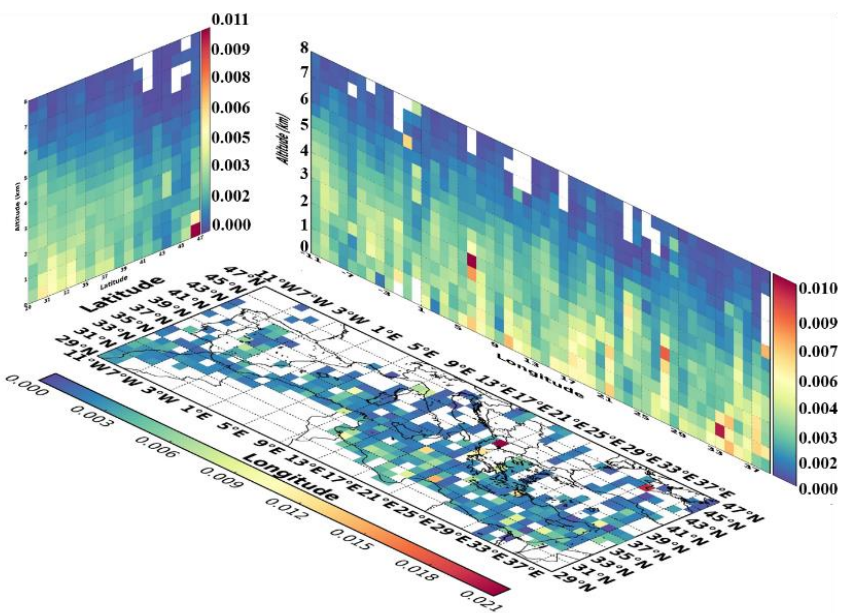
1843 **Figure 37:** Geographical distributions of the intensity (in terms of  $AOD_{550nm}$ ) of: (i) strong and (ii) extreme desert dust  
 1844 episodes, averaged for the periods: (a) Mar. 2000 – Feb. 2013 (MODIS-Terra) and (b) 2003 – 2012 (MODIS-Aqua), over  
 1845 the broader area of the Mediterranean basin. (a) 2000 – 2013 and (b) 2003 – 2012, over the broader area of the  
 1846 Mediterranean basin.

Formatted: English (U.S.)

1847  
 1848  
 1849  
 1850  
 1851  
 1852  
 1853  
 1854  
 1855  
 1856  
 1857  
 1858  
 1859



(i)



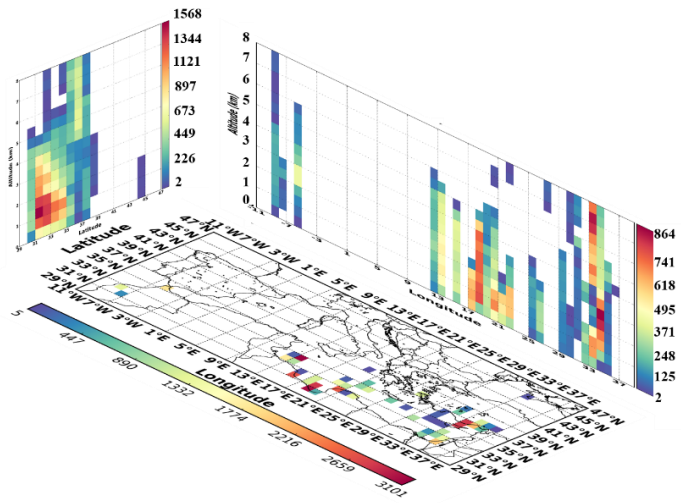
(ii)

**Figure 89:** Three dimensional structure of the: (i) overall number of dust and polluted dust observations and (ii) total backscatter coefficient at 532 nm (in  $\text{km}^{-1} \text{sr}^{-1}$ ), over the broader Mediterranean basin under *DD* episodes conditions, based on CALIOP-CALIPSO vertical resolved retrievals for the period Jun. 2006 – Feb. 2013.

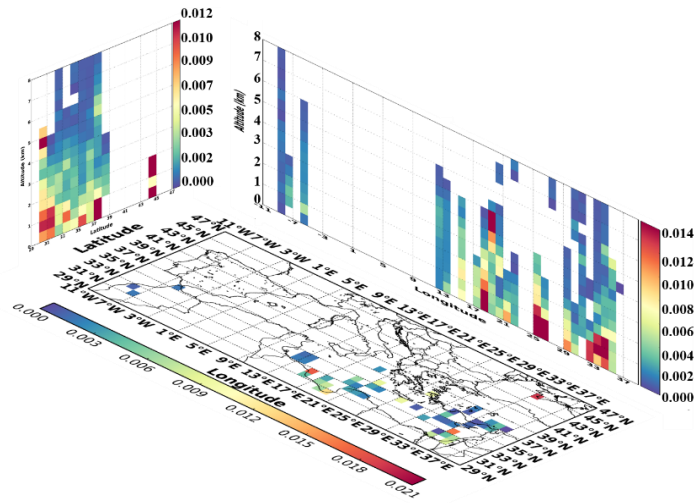
Formatted: English (U.S.)

Formatted: Font: Italic

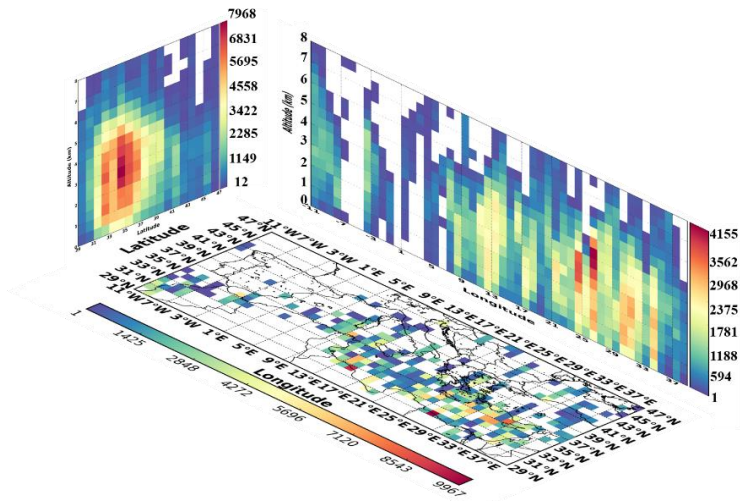




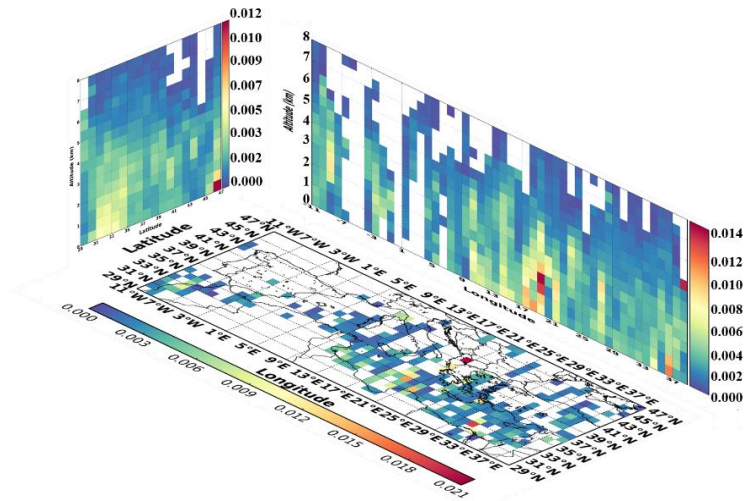
(i-a)



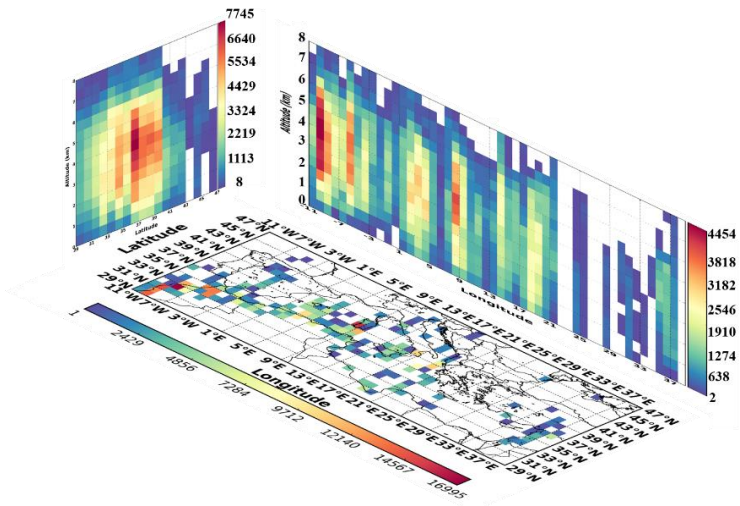
(i-b)



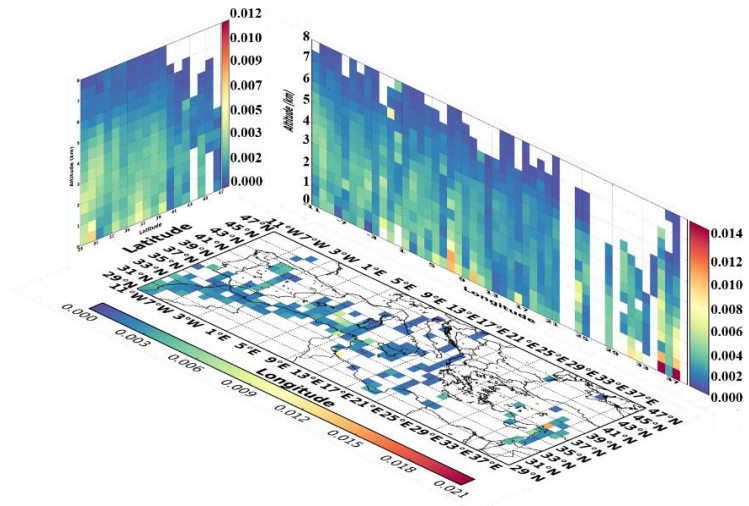
(ii-a)



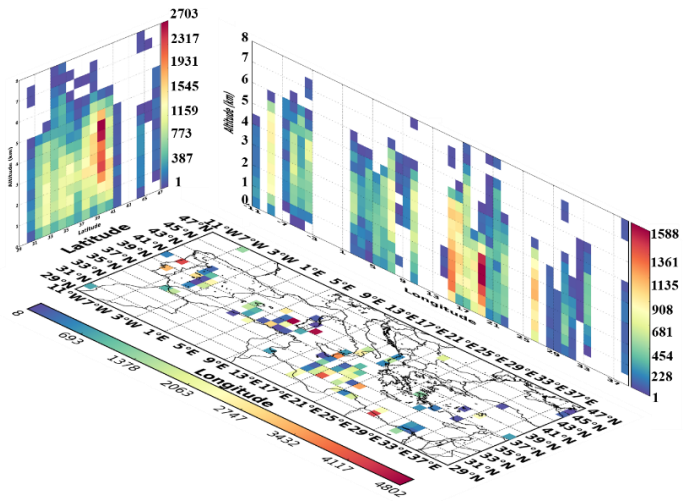
(ii-b)



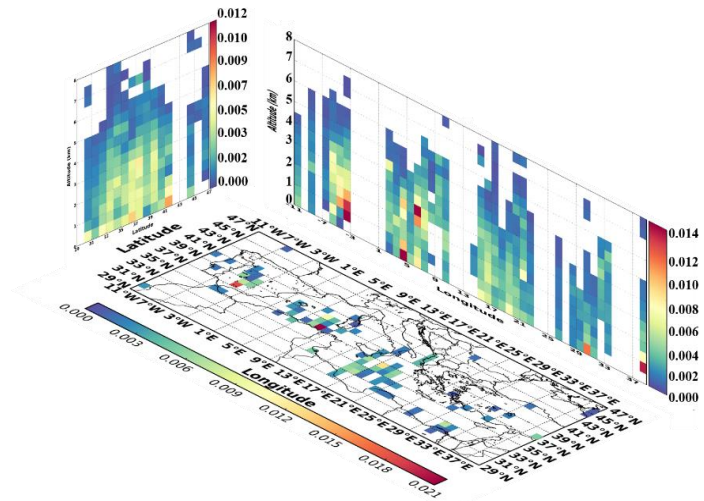
(iii-a)



(iii-b)



(iv-a)

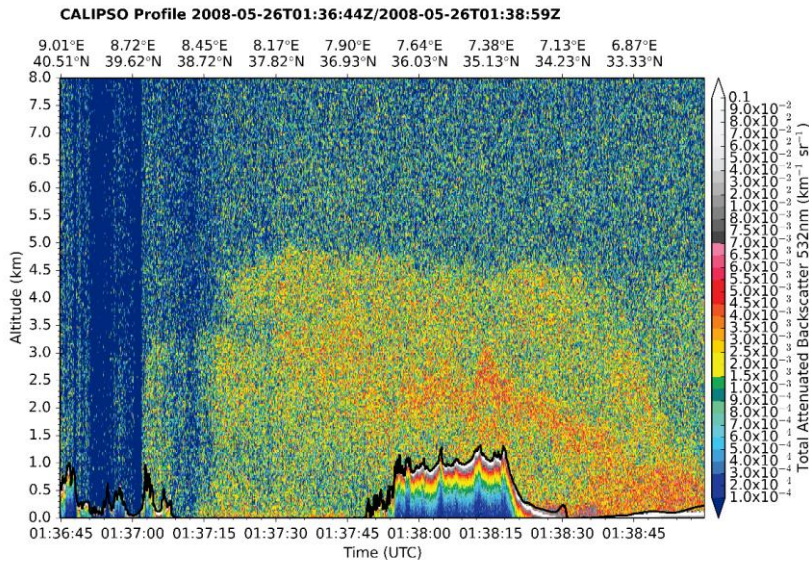


(iv-b)

**Figure 210:** Three dimensional representation of the: (a) overall number of dust and polluted dust observations and (b) total backscatter coefficient at 532 nm (in  $\text{km}^{-1} \text{sr}^{-1}$ ), over the broader Mediterranean basin, under *DD* episodes conditions, for: (i) winter, (ii) spring, (iii) summer and (iv) autumn based on CALIOP-CALIPSO vertical resolved retrievals, over the period Jun. 2006 – Feb. 2013.

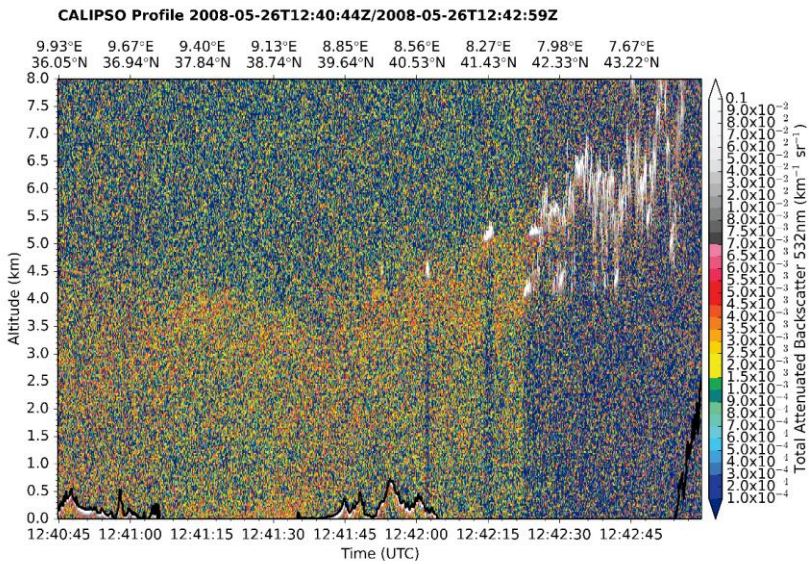
**Formatted:** English (U.S.)

**Formatted:** Font: Italic



1866

(i)

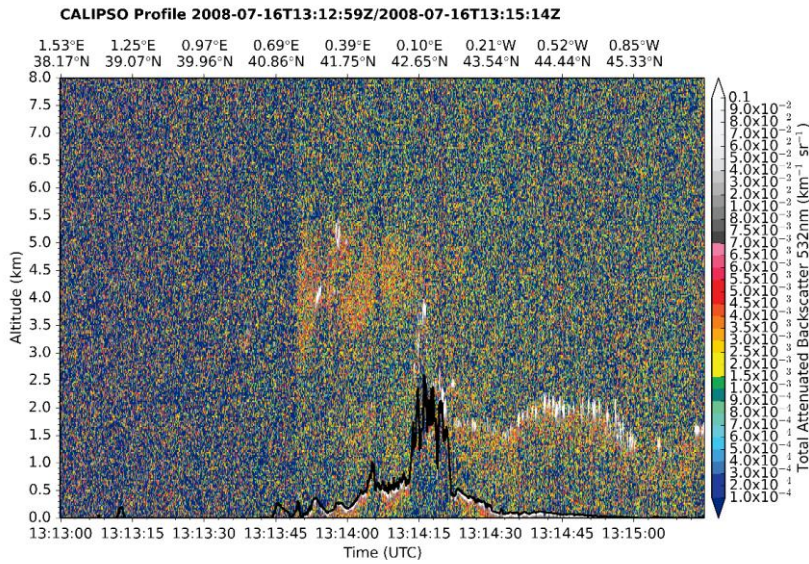


1867

(ii)

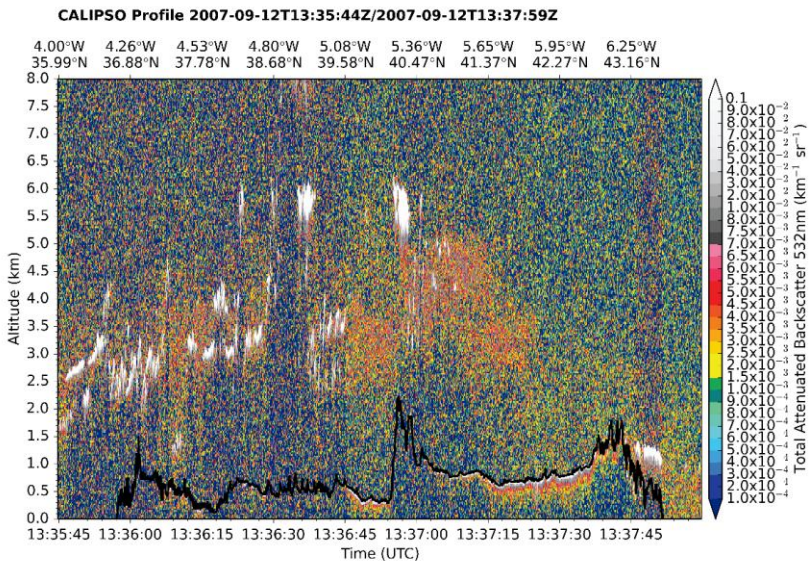
1868 **Figure 104:** Cross sections of the total backscatter coefficient at 532 nm (in  $\text{km}^{-1} \text{sr}^{-1}$ ) vertical profiles along the CALIOP-  
 1869 CALIPSO track during: (i) nighttime and (ii) daytime, on 26<sup>th</sup> May 2008, over the station Censt (Lat: 39.064, Lon: 8.457).  
 1870 The black thick solid line represents the surface elevation.

Formatted: English (U.S.)



1871

(i)

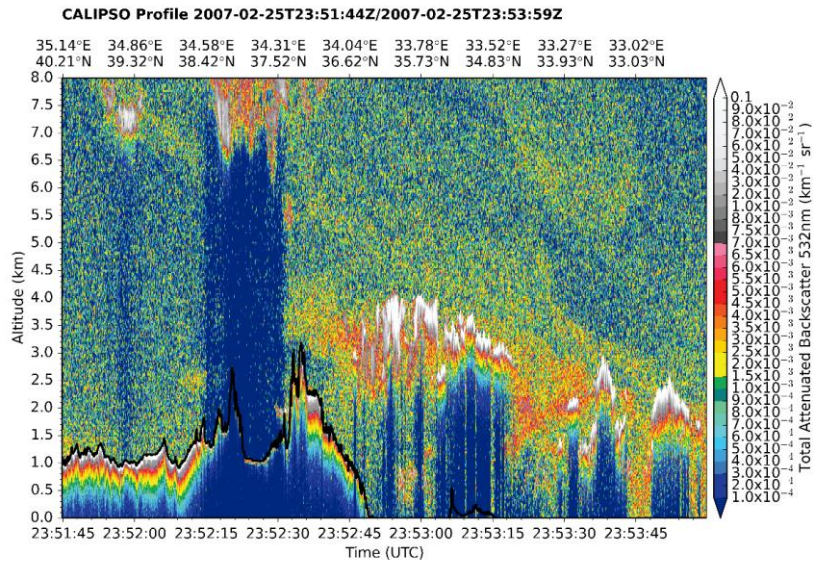


1872

(ii)

1873 | **Figure 112:** Cross sections of the total backscatter coefficient at 532 nm (in  $\text{km}^{-1} \text{sr}^{-1}$ ) vertical profiles along the CALIOP-  
 1874 CALIPSO track during daytime over the stations: (i) Els Torms (Lat: 41.395, Lon: 0.721) on 16<sup>th</sup> July 2008 and (ii) San  
 1875 Pablo (Lat: 39.525, Lon: -4.353) on 12<sup>th</sup> September 2007. The black thick solid line represents the surface elevation.

Formatted: English (U.S.)



1876

1877 **Figure 123:** Cross section of the total backscatter coefficient at 532 nm (in  $\text{km}^{-1} \text{sr}^{-1}$ ) vertical profiles along the CALIOP-  
 1878 CALIPSO track during daytime nighttime over the station Agia Marina (Lat: 35.039, Lon: 33.058) on 25<sup>th</sup> February 2007.  
 1879 The black thick solid line represents the surface elevation.

Formatted: English (U.S.)

1880

1881

1882

1883

1884

1885

1886

1887